Toward a mathematical modelling of white blood cells filtration

Mohamed Belhadj

Thèse de Doctorat présentée par

Mohamed BELHADJ

pour obtenir les titres de :

DOCTEUR DE L'UNIVERSITÉ PIERRE ET MARIE CURIE - PARIS VI
&
DOCTEUR DE L'ÉCOLE NATIONALE D'INGÉNIEURS DE TUNIS

Spécialité : **Mathématiques Appliquées**

Sujet : *Vers une modélisation mathématique de la filtration des globules blancs du sang*

Soutenue le 11 mars 2005 devant le jury composé de :

Président :	Olivier PIRONNEAU
Directeurs de thèse :	Jean-Frédéric GERBEAU Benoît PERTHAME
Rapporteurs :	Robert EYMARD Danielle HILHORST
Responsable de la cotutelle	Taïeb HADHRI

À la mémoire de mon frère,
à mes parents,
à mes frères.

Everything is more simple than one thinks but at the same time more complex than one can understand.
Johann Wolfgang von Goethe

To reach the point that is unknown to you, you must take the road that is unknown to you.
St. John of the Cross

Remerciements

J'ai été profondément marqué par les qualités humaines et scientifiques de Jean-Frédéric Gerbeau qui a dirigé ma thèse avec beaucoup d'énergie. Je lui suis extrêmement redevable du temps qu'il m'a consacré. Je le remercie infiniment pour avoir su se rendre toujours disponible, pour sa patience, son sens de la pédagogie et pour l'enthousiasme qu'il sait communiquer.

Benoît Perthame a orienté et suivi mon travail pendant ces trois années. C'est une chance immense de l'avoir comme directeur de thèse et je tiens à lui témoigner mon profond respect ainsi que toute ma gratitude.

Taïeb Hadhri m'a accueilli dans le laboratoire qu'il dirige à l'École polytechnique de Tunisie. Ses qualités scientifiques et humaines sont pour beaucoup au bon fonctionnement du laboratoire. Je tiens à lui exprimer ma gratitude pour la confiance qu'il m'a témoignée en acceptant de diriger cette thèse dans le cadre d'une cotutelle entre l'Université Pierre et Marie Curie et l'École Nationale d'Ingénieurs de Tunis.

Je présente mes remerciements les plus sincères à Olivier Pironneau pour m'avoir fait l'honneur de présider le jury de ma thèse. Robert Eymard et Danielle Hilhorst m'ont fait un grand honneur en acceptant de rédiger un rapport sur mon travail et je tiens à leur exprimer toute ma gratitude.

Une partie des études présentées ici est le fruit des collaborations avec d'autres chercheurs. Je remercie ainsi Jean Luc Wautier et Laurent Barbe de l'Institut National de la transfusion sanguine qui m'ont aidé pendant la phase de modélisation ainsi que pendant les expériences. Je remercie également Eric Cancès et Andro Mikelić dont l'enthousiasme et le sérieux apportent beaucoup d'efficacité à notre travail commun.

Je me fais aussi un plaisir de remercier les membres des projets Bang et Reo, entre autres Emmanuel Audusse, Paola Causin, Vincent Martin, Nuno Dos Santos, Astrid Décoene, Maryse Desnous. Une pensée particulière s'adresse à Americo Marrocco et marie-Odile Bristeau.

Il m'est également très agréable d'évoquer la chance d'avoir fait partie du Laboratoire d'Ingénierie Mathématique de l'École polytechnique de Tunisie. Je remercie tous ses membres. Une pensée particulière se tourne vers Lassaad El Asmi, Hatem Hamda et Latifa Belhadj.

Merci à mes amis sans qui cette thèse ne serait pas tout à fait ce qu'elle est. Une pensée particulière à Angy, Mourad, Singrid et Abdelaaziz.

Résumé

Cette thèse concerne l'étude de modèles mathématiques et méthodes numériques motivés par la filtration des globules blancs du sang.

Dans la première partie, nous définissons des modèles mathématiques qui réprésentent les principaux phénomènes physiques qui entrent en jeu dans le procédé de la filtration.

La deuxième partie est dédiée à l'étude théorique de systèmes d'équations aux dérivées partielles modélisant le procédé de la filtration. Dans le *chapitre 2*, nous considérons un système d'équations semi-linéaires de type hyperbolique-parabolique avec une diffusion anisotrope dégénérée. Nous étudions ce problème avec une théorie L^1 ; nous considérons en particulier l'existence et l'unicité de solutions faibles ainsi que d'autres propriétés comme le principe du maximum ; puis nous établissons la limite quand la constante de réaction devient grande. Nous montrons que le système converge vers une équation non linéaire parabolique-hyperbolique qui généralise le problème de Stefan. Dans le *chapitre 3*, nous étudions, par des techniques de l'homogénéisation, la filtration au travers de milieux poreux fibrés. Le réseau des fibres étudié est celui utilisé par M. Briane dans le cadre d'une étude sur la conduction thermique des tissus biologiques. Nous dérivons et justifions l'équation de Darcy ainsi que la forme du tenseur de perméabilité pour un tel milieu fibreux. Les résultats théoriques concernant la perméabilité sont illustrés par quelques simulations numériques. Finalement, nous considérons le cas où le diamètre des fibres tend vers zéro. En appliquant des résultats de G. Allaire à notre cas, nous justifions rigoureusement la forme du terme dominant dans les formules de perméabilité efficace utilisées en ingénierie. Ces résultats sont également confirmés par un calcul numérique direct de la perméabilité, dans lequel la petitesse du diamètre des fibres rend nécessaire le recours à des approximations de précision élevée.

La définition des méthodes numériques efficaces pour approximer la solution des modèles mathématiques est envisagée dans la troisième partie. Précisément, concernant les équations de Darcy, nous avons utilisé la méthode des éléments finis mixtes hybrides. Pour la résolution de l'équation du transport, nous avons implémenté une méthode numérique utilisant des volumes finis pour la discrétisation du terme convection/réaction associé à une approximation mixte hybride pour la discrétisation du terme dispersif.

Abstract

The aim of this work is to set up mathematical tools (mathematical models and numerical methods) to investigate the white blood cells filtration.

In the first part, we set up specific mathematical models to represent the physical phenomena that are involved in the filtration process.

The second part is devoted to the theoretical study of partial differential equations modelling the filtration. In *chapter 2*, we consider a semilinear parabolic-hyperbolic system with a degenerate and anisotropic diffusion. We study the well-posedness of the system using a L^1 theory ; we consider in particular the existence and the uniqueness of a solution and we investigate other mathematical properties such as maximum principle. Then, we establish the relaxation limit as the reaction constant becomes large. We prove that the system converges to a nonlinear parabolic-hyperbolic equation that generalizes the Stefan problem. In *chapter 3*, we study the flow through fibrous media using homogenization techniques. The fiber network under study is the one already used by M. Briane in the context of heat conduction of biological tissues. We derive and justify the effective Darcy equation and the permeability tensor for such fibrous media. The theoretical results on the permeability are illustrated by some numerical simulations. Finally, the low solid fraction limit is considered. Applying results by G. Allaire to our setting, we justify rigorously the leading order term in the empirical formulas for the effective permeability used in engineering. The results are also confirmed by a direct numerical calculation of the permeability, in which the small diameter of the fibers requires high accuracy approximations.

In part 3 we present the construction of suitable numerical methods to compute solutions of the considered models. Precisely, we discuss the mixed hybrid finite element formulation for the space discretization of the Darcy problem. For the discretization of the transport equation, we use a splitting technique for the space discretization and the Euler method for the time discretization.

Table des matières

Introduction

Afin de limiter les risques de réactions néfastes chez les receveurs, diverses techniques ont été mises au point pour réduire le nombre des globules blancs (leucocytes) dans les préparations destinées à la transfusion [33]. A l'heure actuelle, la déleucocytation par filtration est la plus répandue. C'est dès 1926 qu'Alexandre Fleming décrit une méthode de déplétion des leucocytes du sang par la filtration sur la ouate [48]. Ses recherches n'étaient pas appliquées à la transfusion et il fallut attendre 1962 pour que cette idée fut appliquée à la filtration du sang pour les banques du sang [51]. La modélisation de la filtration du sang conduit à considérer une grande variété de phénomènes physiques, réaction physico-chimique, colmatage, etc. Les hypothèses avancées par plusieurs auteurs proposent que la filtration des leucocytes soit gouvernée par deux principaux mécanismes : le tamisage et l'adhésion [92, 83].
Cette thèse concerne l'étude avec modèles mathématiques et méthodes d'approximation numérique de la filtration des globules blancs du sang.
La première partie de ce travail consiste en une présentation de la filtration ainsi qu'à la définition des modèles mathématiques qui représentent les phénomènes physiques que nous considérons. Cette phase de modélisation a été menée en collaboration avec J.-L. Wautier et L. Barbe (Institut National de la Transfusion Sanguine). Dans le cadre de cette collaboration, nous avons contribué à une campagne de mesures effectuée à l'Institut National de la Transfusion Sanguine.
La deuxième partie est dédiée à l'étude théorique de systèmes d'équations aux dérivées partielles modélisant le procédé de la filtration. Dans le *chapitre 2*, nous considérons un système d'équations semi-linéaires de type hyperbolique-parabolique avec une diffusion anisotrope dégénérée. Nous étudions ce problème avec une théorie L^1 ; nous considérons en particulier l'existence et l'unicité de solutions faibles ainsi que d'autres propriétés comme le principe du maximum ; puis nous établissons la limite quand la constante de réaction devient grande. Nous montrons que le système converge vers une équation non linéaire parabolique-hyperbolique qui généralise le problème de Stefan.
Dans le *chapitre 3*, Nous étudions, par des techniques de l'homogénéisation, la filtration au travers de milieux poreux fibrés. Le réseau des fibres étudié est celui utilisé par M. Briane dans le cadre d'une étude sur la conduction

thermique des tissus biologiques. Nous dérivons et justifions l'équation de Darcy ainsi que la forme du tenseur de perméabilité pour un tel milieu fibreux. Les résultats théoriques concernant la perméabilité sont illustrés par quelques simulations numériques. Finalement, nous considérons le cas où le diamètre des fibres tend vers zéro. En appliquant des résultats de G. Allaire à notre cas, nous justifions rigoureusement la forme du terme dominant dans les formules de perméabilité efficace utilisées en ingénierie. Ces résultats sont également confirmés par un calcul numérique direct de la perméabilité, dans lequel la petitesse du diamètre des fibres rend nécessaire le recours à des approximations de précision élevée.
La présentation des méthodes numériques efficaces pour approximer la solution des modèles mathématiques est envisagée dans la troisième partie. Précisément, concernant les équations de Darcy, nous avons utilisé la méthode des éléments finis mixtes hybrides. Pour la résolution de l'équation du transport, nous avons implémenté une méthode numérique utilisant des volumes finis pour la discrétisation du terme convection/réaction associé à une approximation mixte hybride pour la discrétisation du terme dispersif.

Signalons enfin que les références bibliographiques spécifiques au procédé de la filtration sont situées à la fin de la première partie (p. 45) et que celles correspondant aux autres chapitres sont regroupées à la fin de la thèse (p. 121).

1 Présentation de la déleucocytation par filtration

Le sang destiné à être transfusé subit une filtration systématique afin d'en retirer les globules blancs. La déleucocytation permet en effet d'améliorer la sécurité transfusionnelle en

- diminuant des complications observées chez certains receveurs de produits sanguins tels la fièvre, certains troubles pulmonaires et éventuellement certaines infections post-opératoires.
- prévenant la transmission d'agents infectieux vectorisés par les leucocytes (virus, bactéries).

Environ 3 millions de poches de sang de près d'un demi litre sont ainsi traitées en France chaque année. Le procédé actuel de la déleucocytation par filtration consiste à faire passer par gravité le sang total à travers plusieurs couches de fibres destinées à retenir les globules blancs [24].
L'intérieur des filtres à déleucocyter n'est pas homogène et consiste en une série de couches de fibres non tissées, compactées entre elles, à travers lesquelles le sang doit circuler. Au fur et à mesure, la taille des pores de chaque couche diminue. Ainsi, les feuilles des filtres présentent un gradient de porosité : les premiers pores sont très larges (diamètre d'environ 60 μm), les derniers ont une taille légèrement inférieure à celle des globules blancs et légèrement supérieure à celle des globules rouges (environ 7 μm).

Les mécanismes de capture des leucocytes pour la filtration du sang sont de nature complexe et regroupent différents types d'interactions que l'on désignera par interactions mécaniques et interactions biologiques. Le premier type correspond au tamisage des cellules, discriminées par des critères de diamètre cellulaire et des critères de déformabilité cellulaire. Dans ce type d'interaction intervient un paramètre géométrique inhérent au filtre, c'est-à-dire sa porosité et le diamètre des fibres entre autres. Les interactions biologiques quant à elles font appel d'une part aux propriétés adhésives des différents types cellulaires et des caractéristiques physico-chimiques qui peuvent influencer cette adhésion.
L'adhérence aux fibres est la conséquence d'une interaction entre les molécules d'adhésion leucocytaires et des molécules chimiques présentes sur les fibres. Si la nature de l'adhésion est essentiellement chimique, il semble néanmoins clair que les caractéristiques de l'écoulement l'influencent fortement. La rétention cellulaire est dépendante de la surface totale du contact : en effet, quand il fut constaté que la déplétion des leucocytes était accomplie en partie par l'adhésion des cellules sur les fibres, la solution a été d'utiliser des fibres de faible diamètre. Les fibres de petit diamètre sont préférées car elles offrent une plus grande surface de contact pour un volume donné de boîtier de filtre. Il a été montré que le taux de rétention de leucocytes passe de 20%, pour un réseau de fibres de $10\mu m$ de diamètre, à 90%, pour des fibres de $3\mu m$ de diamètre [41].
Des recherches ont été menées à l'Institut National de la Transfusion Sanguine (INTS) pour mieux comprendre les mécanismes impliquées dans l'adhésion leucocytaire au cours de la filtration sanguine (thèse de L. Barbe sous la direction de J. -L. Wautier [14]). Une bonne compréhension et une bonne maîtrise de l'adhésion est une des clés de l'amélioration de la filtration.

Nous allons à présent établir un modèle mathématique macroscopique décrivant le procédé de la filtration qui pourrait enrichir la compréhension des phénomènes impliqués dans la filtration du sang.
On note $\mathbf{u}$ la vitesse de Darcy, p la pression, c la concentration en leucocytes dans le sang, s la fraction surfacique occupée par les leucocytes ayant adhéré (surface occupée divisée par surface totale initialement libre sur les fibres, *cf.* Fig. 1).
On se donne a l'aire occupée sur la fibre par un leucocyte ayant adhéré, f la surface spécifique du filtre, *i.e.* surface des fibres par unité de volume dans le filtre, $\mathbf{K}$ le tenseur de conductivité hydraulique, μ la viscosité dynamique, $\mathbf{D}$ le tenseur de dispersion, ω la porosité.

L'écoulement est gouverné par les équations de Darcy :

$$\mathbf{u} + \frac{\mathbf{K}}{\mu}(\nabla p - \mathbf{f}) = 0, \tag{1}$$

$$\operatorname{div} \mathbf{u} = 0. \tag{2}$$

où $\mathbf{f}$ représente les forces de pesanteur. L'adhésion des leucocytes est décrite par :

$$\frac{\partial}{\partial t}(\omega c) + \operatorname{div}(\mathbf{u}c - \omega \mathbf{D}(\mathbf{u})\nabla c) = -\frac{f}{a}\frac{\partial s}{\partial t} \quad (3)$$

$$\frac{\partial s}{\partial t} = ak(\mathbf{u})cB(s) \quad (4)$$

Les équations (1)-(4) sont à compléter par des conditions aux limites et initiales.
La fonction B est la *fonction de blocage dynamique*, le choix le plus simple est la fonction de blocage de Langmuir :

$$B(s) = 1 - \frac{s}{s_{max}} \quad (5)$$

où s_{max} est la fraction maximale de surface de fibre pouvant accueillir des leucocytes. La fonction $k(\mathbf{u})$ mesure la vitesse de réaction.

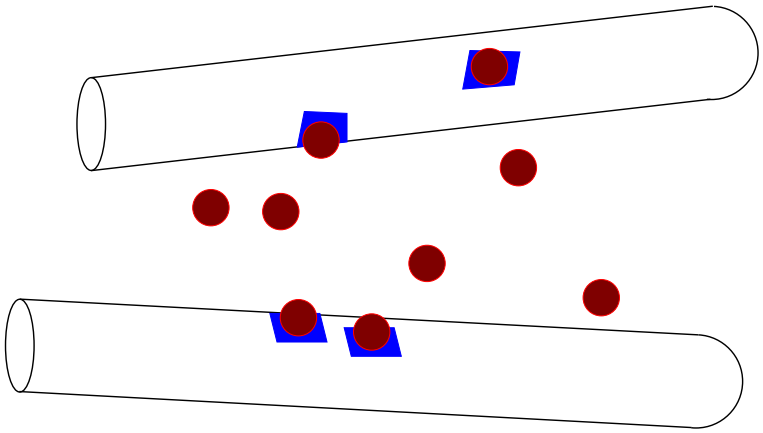

FIG. 1: Des leucocytes en solution et sur des fibres. La variable s est le rapport entre la surface occupée par les leucocytes et la surface libre sur les fibres

Le modèle que nous avons proposé (ou des variations de celui-ci) a été utilisé dans d'autres applications. On trouve par exemple dans [47] une étude de la pénétration d'anticorps dans des tissus tumoraux et de leur réaction avec des antigènes. Dans ce modèle, les anticorps sont l'analogue des leucocytes et les antigènes des sites libres sur les fibres du filtre. Ce type de modèle est également très utilisé dans l'étude du transport de colloïdes (virus, bactéries, $\cdots$) dans les aquifères sableux [93], [18].
Plusieurs modèles de filtration ont été proposés (par exemple le modèle de

filtration de colloïdes 1D de Herzig *et al.* [77]). Il y a également le modèle de A. Bruil *et al.* [24], qui est l'étude la plus récente que nous connaissions sur la modélisation de la filtration des leucocytes.
Afin de tester notre modèle de filtration, une série d'expériences a été effectuée à l'Institut National de la Transfusion Sanguine (INTS). Malheureusement, elles ne nous ont pas permis de tirer des conclusions intéressantes du point de vu de la modélisation.

2 Etudes mathématiques

2.1 Analyse d'un modèle de transport de colloïdes avec diffusion dégénérée anisotrope (Chapitre 2)

Nous présenterons dans le Chapitre 2 une analyse mathématique d'une variante du modèle (3)-(4) qui complète des résultats établis par D. Hilhorst, R. van der Hout et L.A. Peletier [55, 56, 57]. On considère en particulier le cas où la diffusion dégénère complètement, et on étudie la limite quand la vitesse de réaction tend vers l'infini. Plus précisemment, nous avons effectué une analyse mathématique (existence, unicité et analyse asymptotique) de la solution d'un système faiblement couplé d'équations semi-linéaires de type hyperbolique-parabolique dégénéré : Trouver la solution (c, s) définie sur $\mathbb{R}^d \times (0,T)$ (avec $T > 0$ et $d \leq 3$), par

$$(P_k) \begin{cases} \partial_t c + \operatorname{div} \mathbf{A}(c) - \displaystyle\sum_{i,j=1}^{d} \frac{\partial^2 \phi_{ij}(c)}{\partial x_i \partial x_j} &= -k\,c\,s \quad \text{dans } \mathcal{D}'((0,T)\times\mathbb{R}^d), \\ \partial_t s &= -k\,c\,s \quad \text{dans } \mathcal{D}'((0,T)\times\mathbb{R}^d), \\ c(0,x) &= c_0(x) \geq 0 \quad \text{p.p. dans } \mathbb{R}^d, \\ s(0,x) &= s_0(x) \geq 0 \quad \text{p.p. dans } \mathbb{R}^d, \end{cases}$$

où k est une constante positive.
Ce système se rencontre dans la modélisation de l'évolution d'un traceur chimique ou biologique dans un milieu poreux. Nous avons étudié ce problème avec une théorie L^1.
Concernant la théorie mathématique, D. Hilhorst et al. ont déja proposé diverses études mathématiques sur des systèmes de même type. En [55], ils ont étudié le comportement asymptotique lorsque $k \to \infty$ d'une version 1D de ce problème avec $\mathbf{A} = 0$ et $\phi(c) = c$. En [56], ils ont considéré également le cas 1D avec $\mathbf{A} = 0$ et $\phi(c) = c$, mais ils ont pris plusieurs termes généraux de réaction. En [57], ils ont gardé $\mathbf{A} = 0$ mais ils ont étendu leurs travaux aux cas multidimensionnels avec diffusion non-linéaire. Plus précisément, ils supposent que $\phi(c) = \int_0^c D(\xi)\,d\xi$ avec $D(\xi) > 0$ pour tout $\xi > 0$.
Dans le présent travail, nous considérons une équation plus générale dans la mesure où nous traitons une diffusion dégénérée et non-isotrope. De plus,

nous ajoutons le terme de convection div $\mathbf{A}(c)$, et traitant ainsi le cas hyperbolique-parabolique.

L'idée essentielle est de commencer par prouver l'existence d'une unique solution régulière pour le problème approché suivant :

$$\left\{ \begin{array}{rcl} \partial_t c_\varepsilon + \operatorname{div} \mathbf{A}_\varepsilon(c_\varepsilon) - \operatorname{div}\left(\phi'_\varepsilon(c_\varepsilon)\nabla c_\varepsilon\right) & = & -k\, c_\varepsilon\, s_\varepsilon, \\ \partial_t s_\varepsilon & = & -k\, c_\varepsilon\, s_\varepsilon. \end{array} \right. \tag{6}$$

où ϕ_ε (resp. $\mathbf{A}_\varepsilon$) est une régularisation de ϕ (resp. $\mathbf{A}$), en particulier, nous supposons que $\phi'_\varepsilon \geq \varepsilon Id$.
En utilisant un résultat de compacité de Kolmogorov-Ascoli, nous prouvons ensuite que la solution de ce problème régularisé tend vers une solution du problème initial quand ε tend vers zéro.

Sous des hypothèses de régularité des données que l'on précisera au Chapitre 2, nous établissons ainsi le résultat suivant :

Théorème 1
Le problème (P_k) admet une unique solution $(c,s) \in \mathcal{C}(\mathbb{R}^+; L^1(\mathbb{R}^d))^2$. De plus, on a les propriétés suivantes :

(i) Principe du maximum :

$$0 \leq c(t,x) \leq \|c_0\|_{L^\infty(\mathbb{R}^d)}, \quad \text{p.p. dans } \mathbb{R}^+ \times \mathbb{R}^d, \tag{7}$$

$$0 \leq s(t,x) \leq \|s_0\|_{L^\infty(\mathbb{R}^d)}, \quad \text{p.p. dans } \mathbb{R}^+ \times \mathbb{R}^d. \tag{8}$$

(ii) Propriété de contraction : soient (c,s) et $(\overline{c},\overline{s})$ deux solutions correspondant respectivement aux données initiales (c_0,s_0) et $(\overline{c}_0,\overline{s}_0)$. Alors pour tout $t \geq 0$,

$$\|c(t)-\overline{c}(t)\|_{L^1(\mathbb{R}^d)}+\|s(t)-\overline{s}(t)\|_{L^1(\mathbb{R}^d)} \leq \|c_0-\overline{c}_0\|_{L^1(\mathbb{R}^d)}+\|s_0-\overline{s}_0\|_{L^1(\mathbb{R}^d)}. \tag{9}$$

(iii) Propriété de comparaison : soient (c,s) et $(\overline{c},\overline{s})$ deux solutions correspondant respectivement aux données initiales (c_0,s_0) et $(\overline{c}_0,\overline{s}_0)$.
Si $c_0 \leq \overline{c}_0$ et $s_0 \leq \overline{s}_0$ alors pour tout $t \geq 0$,

$$c(t) \leq \overline{c}(t) \quad \text{et} \quad s(t) \leq \overline{s}(t) \quad \text{p.p. dans } \mathbb{R}^d. \tag{10}$$

(iv) Inégalité d'entropie : pour deux fonctions régulières, croissantes S et Σ , avec S convexe, et avec les notations $(\mathbf{A}^{\mathbf{S}})' = \mathbf{A}'S'$, $(\phi_{ij}^S)' = \phi'_{ij}\, S'$, $(\psi_{ik}^S)' = S''^{1/2}\, \phi_{ik}'^{1/2}$, nous avons

$$\nabla \cdot \psi^S(c) \in \left(L^2(\mathbb{R}^+ \times \mathbb{R}^d\right)^d \quad \text{où} \quad \nabla \cdot \psi^S(c) = \Big(\sum_{i=1}^d \frac{\partial \psi_{ik}^S(c)}{\partial x_i}\Big)_{k=1,\dots d}$$

$$\partial_t[S(c)+\Sigma(s)] + div\, \mathbf{A}^{\mathbf{S}}(c) - \sum_{i,j=1}^d \frac{\partial^2 \phi_{ij}^S(c)}{\partial x_i \partial x_j} + \sum_{k=1}^d |\nabla \cdot \psi^S(c)|^2 \leq 0. \tag{11}$$

2.1.1 Comportement asymptotique

Nous avons établi la limite quand la constante de réaction k devient grande. Sous des hypothèses de régularité des données que l'on précisera au Chapitre 2, nous avons obtenu le résultat suivant :

Théorème 2
Quand k tend vers l'infini, la solution (c_k, s_k) de (P_k), admet une limite dans $L^1((0,T)\times\mathbb{R}^d)^2$ notée par $(c,s)\in L^\infty(\mathbb{R}^+;L^1(\mathbb{R}^d))^2$ qui satisfait

$$(P_\infty)\begin{cases} \partial_t(c-s)+div\,\mathbf{A}(c)-\displaystyle\sum_{i,j=1}^{d}\frac{\partial^2\phi_{ij}(c)}{\partial x_i\partial x_j} &= 0, \quad \text{dans } \mathcal{D}'((0,T)\times\mathbb{R}^d),\\ c\geq 0,\ s\geq 0,\ c\,s &= 0, \quad \text{p.p. dans } (0,T)\times\mathbb{R}^d,\\ c(0,x)-s(0,x) &= c_0(x)-s_0(x) \quad \text{p.p. dans } \mathbb{R}^d. \end{cases}$$

De plus, (c,s) est l'unique solution entropique du système (P_∞) i.e. pour deux fonctions régulières, croissantes S et Σ , avec S convexe, et avec les notations $(\mathbf{A^S})'=\mathbf{A}'S'$, $(\phi^S_{ij})'=\phi'_{ij}\,S'$, $(\psi^S_{ik})'=S''^{1/2}\,\phi'^{1/2}_{ik}$, nous avons

$$\nabla\cdot\phi'^{1/2}(c)\in(L^2(\mathbb{R}^+\times\mathbb{R}^d))^d,\quad \nabla\cdot\psi^S(c)=(S'')^{1/2}\phi'^{1/2}(c),$$

$$\partial_t[S(c)+\Sigma(s)]+div\,\mathbf{A^S}(c)-\sum_{i,j=1}^{d}\frac{\partial^2\phi^S_{ij}(c)}{\partial x_i\partial x_j}+\sum_{k=1}^{d}|\nabla\cdot\psi^S(c)|^2\leq 0. \qquad (12)$$

Nous avons montré ensuite que le système (P_∞) est équivalent à une équation non linéaire parabolique-hyperbolique de type Stefan.

$$(Q_\infty)\begin{cases} \partial_t w+\operatorname{div}\mathbf{A}(w_+)-\displaystyle\sum_{i,j=1}^{d}\frac{\partial^2\phi_{ij}(w_+)}{\partial x_i\partial x_j} &= 0 \quad \text{dans } \mathcal{D}'((0,T)\times\mathbb{R}^d),\\ w(0,x) &= c_0(x)-s_0(x) \quad \text{p.p. dans } \mathbb{R}^d. \end{cases}$$

où $w=c-s\in\mathcal{C}(\mathbb{R}^+;L^1(\mathbb{R}^d))$ est l'unique solution entropique du système (Q_∞).

Ces résultats ont été publiés dans *Asymptotic Analysis*.

2.2 Perméabilité d'un milieu fibreux non périodique (Chapitre 3)

Les filtres servant à la déleucocytation sont constitués de feuilles de fibres d'orientations variables. Ceci a motivé l'étude présentée dans le chapitre 3.

2.2.1 Homogénéisation : calcul de la perméabilité

Nous considérons un milieu fibreux correspondant à une structure localement stratifiéé inspiré des travaux de M. Briane pour le laplacien [22]. La géométrie considérée par M. Briane est un milieu poreux Ω de $\mathbb{R}^3$ composé de couches $\Omega^{\varepsilon,n}$ perpendiculaire à l'axe x_1 et d'épaisseur ε^r $(0 < r < 1)$. Dans chaque couche $\Omega^{\varepsilon,n}$, il y a un réseau périodique, de périodicité ε, de fibres cylindriques de rayon $\mathcal{R}\varepsilon$, dont les axes sont perpendiculaires à x_1 et font avec l'axe x_2 un angle $\gamma_{\varepsilon,n}$. Il y a ε^{r-1} rangées de fibres dans chaque couche. Nous sommes alors amenés à résoudre un problème d'homogénéisation à deux échelles dans lequel l'échelle la plus fine est celle des fibres et la moins fine celle des couches. Pour obtenir le résultat, nous homogénéisons couche par couche en imposant une condition sur les deux échelles. Plus précisemment, nous considérons un écoulement lent visqueux et incompressible décrit par le système de Stokes suivant pour la vitesse $\mathbf{u}^\varepsilon$ et la pression p^ε :

$$-\nu \triangle \mathbf{u}^\varepsilon + \nabla p^\varepsilon = \mathbf{f} \qquad \text{dans } \Omega^\varepsilon, \tag{13}$$

$$\operatorname{div} \mathbf{u}^\varepsilon = 0 \qquad \text{dans } \Omega^\varepsilon, \tag{14}$$

$$\mathbf{u}^\varepsilon = 0 \qquad \text{sur } \partial\Omega^\varepsilon. \tag{15}$$

Ensuite, nous allons étudier le système de Stokes (13)-(15) localement, i.e. dans chaque couche $\Omega^{\varepsilon,n}$.
Afin de pouvoir homogénéiser, nous admettons les développements suivants (voir [17]) :

$$\mathbf{u}^\varepsilon(x) = \varepsilon^2 \mathbf{u}^0\left(x, \frac{\rho(x_1^{\varepsilon,n}, x)}{\varepsilon}\right) + \dots \tag{16}$$

$$p^\varepsilon(x) = p^0\left(x, \frac{\rho(x_1^{\varepsilon,n}, x)}{\varepsilon}\right) + \varepsilon p^1\left(x, \frac{\rho(x_1^{\varepsilon,n}, x)}{\varepsilon}\right) + \dots \tag{17}$$

Pour trouver l'expression pour la perméabilité, nous introduisons une transformation $\varphi_{\varepsilon,n}$ d'un élément de référence $\hat{\Omega}^{\varepsilon,n}$ dans $\Omega^{\varepsilon,n}$ définie par

$$(\hat{x}_1, \hat{x}_2, \hat{x}_3) = \varphi_{\varepsilon,n}^{-1}(x_1, x_2, x_3) = \left| \begin{array}{l} x_1 \\ -x_2 \sin\gamma_{\varepsilon,n} + x_3 \cos\gamma_{\varepsilon,n} \\ -x_2 \cos\gamma_{\varepsilon,n} - x_3 \sin\gamma_{\varepsilon,n} \end{array} \right. \tag{18}$$

Dans l'élément de référence, $\hat{\Omega}^{\varepsilon,n}$, les fonctions $\hat{\mathbf{u}}$ and $\hat{p}$ admettent les développements suivants

$$\hat{\mathbf{u}}^\varepsilon(\hat{x}) = \varepsilon^2 \hat{\mathbf{u}}^0\left(\hat{x}, \frac{\hat{x}_1}{\varepsilon}, \frac{\hat{x}_2}{\varepsilon}\right) + \dots \tag{19}$$

$$\hat{p}^\varepsilon(\hat{x}) = \hat{p}^0(\hat{x}, \frac{\hat{x}_1}{\varepsilon}, \frac{\hat{x}_2}{\varepsilon}) + \varepsilon \hat{p}^1\left(\hat{x}, \frac{\hat{x}_1}{\varepsilon}, \frac{\hat{x}_2}{\varepsilon}\right) + \dots \tag{20}$$

Nous désignons par $\hat{z} = (\hat{z}_1, \hat{z}_2) = (\hat{x}_1/\varepsilon, \hat{x}_2/\varepsilon)$ l'échelle rapide et par $\mathcal{Y}_F = \{(\hat{z}_1, \hat{z}_2) \in \mathcal{Y}, \chi(\hat{z}) = 0\}$; $\mathcal{Y}$ étant la cellule unité. En injectant (19)-(20)

dans le système (13)-(15) écrit dans la configuration de référence $\hat{\Omega}^{\varepsilon,n}$, nous sommes amenés à résoudre les problèmes de cellules suivants :

$$\left\{\begin{array}{rcll} -\triangle_{\hat{z}_1,\hat{z}_2}\omega_1^j(x_1,\hat{z}_1,\hat{z}_2)+\partial_{\hat{z}_1}\pi^j &=& \delta_{1j} & \text{dans } \mathcal{Y}_F,\\ -\triangle_{\hat{z}_1,\hat{z}_2}\omega_2^j(x_1,\hat{z}_1,\hat{z}_2)-\sin\gamma(x_1)\partial_{\hat{z}_2}\pi^j &=& \delta_{2j} & \text{dans } \mathcal{Y}_F,\\ -\triangle_{\hat{z}_1,\hat{z}_2}\omega_3^j(x_1,\hat{z}_1,\hat{z}_2)+\cos\gamma(x_1)\partial_{\hat{z}_2}\pi^j &=& \delta_{3j} & \text{dans } \mathcal{Y}_F,\\ \partial_{\hat{z}_1}\omega_1^j+\partial_{\hat{z}_2}(-\sin\gamma(x_1)\omega_2^j+\cos\gamma(x_1)\omega_3^j) &=& 0 & \text{dans } \mathcal{Y}_F,\\ \omega^j(x_1,\hat{z}_1,\hat{z}_2) &=& 0 & \text{sur } \partial\mathcal{Y}_F\backslash\partial\mathcal{Y},\\ \{\omega^j,\pi^j\} \text{ est } \mathcal{Y}\text{-périodique en } (\hat{z}_1,\hat{z}_2). & & & \end{array}\right. \tag{21}$$

Proposition 1

1. Le problème (21) admet une solution unique $(\boldsymbol{\omega}^j,\pi^j)\in H^1(\mathcal{Y}_F)^3\times L^2(\mathcal{Y}_F)$.
2. La fonction $\mathbf{u}^0$ dans (16) est donnée par

$$\mathbf{u}^0(x,z_1,z_2)=\frac{1}{\nu}\sum_{j=1}^{3}\left(f_j(x)-\frac{\partial p^0}{\partial x_j}(x)\right)\boldsymbol{\omega}^j(x_1,z_1,z_2) \tag{22}$$

3. La pression efficace p^0 dans (17) depend uniquement de x et elle est solution du problème de Darcy :

$$\left\{\begin{array}{rcll} \mathbf{u}^D(x) &=& \dfrac{\boldsymbol{K}(x_1)}{\nu}\left(\mathbf{f}-\nabla p^0(x)\right) & \text{dans } \Omega,\\ \operatorname{div}\mathbf{u}^D &=& 0, & \text{dans } \Omega,\\ \mathbf{u}^D\cdot\mathbf{n} &=& 0, & \text{sur } \partial\Omega. \end{array}\right. \tag{23}$$

où le tenseur de perméabilité $\boldsymbol{K}=[K_{i,j}]_{i,j=1,2,3}$ est déterminé par

$$K_{ij}(x_1)=\frac{1}{|\mathcal{Y}|}\int_{\mathcal{Y}_F}\omega_i^j(x_1,z_1,z_2)dz_1dz_2. \tag{24}$$

Il est utile de remarquer que la formule (24) n'est pas commode du point de vue numérique puisqu'elle depend de la variable macroscopique x_1. Afin de remedier à ce problème, nous résolvons les deux problèmes des cellules suivants : soient $U_1^j(z_1,z_2)$, $U_2^j(z_1,z_2)$, $P^j(z_1,z_2)$, $j=1,2$ les solutions du problème de Stokes 2D

$$\left\{\begin{array}{rcll} -\triangle_{z_1,z_2}U_1^j+\partial_{z_1}P^j &=& \delta_{1j} & \text{dans } \mathcal{Y}_F,\\ -\triangle_{z_1,z_2}U_2^j+\partial_{z_2}P^j &=& \delta_{2j} & \text{dans } \mathcal{Y}_F,\\ \partial_{z_1}U_1^j+\partial_{z_2}U_2^j &=& 0 & \text{dans } \mathcal{Y}_F,\\ U_1^j=U_2^j &=& 0 & \text{sur } \partial\mathcal{Y}_F\backslash\partial\mathcal{Y},\\ \{U_1^j,U_2^j,P^j\} \text{ est } \mathcal{Y}\text{-périodique en } z_1,z_2, & & & \end{array}\right. \tag{25}$$

et soit $V(z_1, z_2)$ la solution du problème de Poisson 2D

$$\left\{ \begin{array}{rcll} -\triangle V & = & 1 & \text{dans } \mathcal{Y}_F, \\ V & = & 0 & \text{sur } \partial\mathcal{Y}_F \backslash \partial\mathcal{Y}, \\ V \text{ est } \mathcal{Y}\text{-périodique en } z_1, z_2. & & & \end{array} \right. \tag{26}$$

Par des calculs élémentaires, nous simplifions l'expression (24) et nous obtenons alors

$$\boldsymbol{K}(x_1) = \boldsymbol{R}(x_1)\boldsymbol{K}_0\boldsymbol{R}^{-1}(x_1) \tag{27}$$

avec $\boldsymbol{R}(x_1)$ est la matrice orthogonale définie par

$$\boldsymbol{R}(x_1) = \begin{bmatrix} 1 & 0 & 0 \\ 0 & \cos\gamma(x_1) & -\sin\gamma(x_1) \\ 0 & \sin\gamma(x_1) & \cos\gamma(x_1) \end{bmatrix}.$$

et

$$\boldsymbol{K}_0 = \frac{1}{|\mathcal{Y}|} \begin{bmatrix} \displaystyle\int_{\mathcal{Y}_F} U_1^1 & 0 & \displaystyle\int_{\mathcal{Y}_F} U_1^2 \\ 0 & \displaystyle\int_{\mathcal{Y}_F} V & 0 \\ \displaystyle\int_{\mathcal{Y}_F} U_2^1 & 0 & \displaystyle\int_{\mathcal{Y}_F} U_2^2 \end{bmatrix}. \tag{28}$$

Anisi, nous obtenons la perméabilité en variable macroscopique x_1 par simple produit matrice-matrice.

2.2.2 Limite de faible fraction solide

Nous considérons le cas où le diamètre des fibres tend vers zéro. En appliquant des résultats de G. Allaire à notre cas, nous justifions rigoureusement la forme du terme dominant dans les formules de perméabilité efficace utilisées en ingénierie. Ces résultats sont également confirmés par un calcul numérique direct de la perméabilité, dans lequel la petitesse du diamètre des fibres rend nécessaire le recours à des approximations de précision élevée.

Ces résultats ont été soumis pour publication.

3 Etudes Numériques

Les problèmes des cellules (25)-(26) sont résolus en utilisant des éléments finis Q_2 pour la vitesse et des éléments finis P_1 discontinus pour la pression. Cette paire d'éléments satisfait bien la condition inf-sup (*cf.* [50]) et préserve le bilan de masse par élément. Concernant les équations de Darcy, nous avons utilisé les méthodes des éléments finis mixtes : la vitesse est approximée par les élements de Raviart-Thomas de plus bas degré (*cf.* [85]), et la pression est

constante par maille. Ce choix assure la continuité de la composante normale de la vitesse et aussi un bilan de masse exact. Nous adoptons une formulation mixte-hybride : un système symétrique défini positif est d'abord résolu par la méthode du gradient conjugué afin de calculer la trace de la pression sur les interfaces des éléments ; puis la pression et la vitesse sont récupérées par un procédé local.
Pour la résolution de l'équation du transport, nous avons utilisé une méthode numérique utilisant des volumes finis pour la discrétisation du terme convection/réaction associé à une approximation mixte hybride pour la discrétisation du terme dispersif. Avec cette méthode, les flux convectifs et dispersifs sont continus d'un élément à l'autre.
Enfin pour résoudre une équation d'advection, nous avons proposé un schéma numérique basée sur la méthode de décentrage. L'idée principale de ce schéma suit une approche bien connue où un principe du maximum local est défini afin d'obtenir une méthode non-oscillante et qui n'ajoute pas de diffusion numérique excessive. Notre schéma est une version simplifiée de limiteurs de pente. En effet, son implémentation numérique est simple et ne demande pas la résolution d'un problème d'optimisation avec contraintes comme dans le cas des limiteurs de pentes [59].

4 Conclusions et perspectives

Dans ce travail, nous avons proposé un modèle mathématique de filtration des globules blancs du sang. Du point de vue théorique, nous nous sommes intéréssés à des questions d'existence et d'unicité pour un tel modèle en utilisant une théorie L^1. Nous avons ensuite étudié, par des techniques de l'homogénéisation, la filtration au travers de milieux poreux fibrés.

Du point de vue numérique, nous avons développé un code $3D$ basé sur la méthode des éléments finis mixtes, permettant la simulation des modèles proposés. Ce code fait partie de la bibliothèque LIFE-V développée conjointement à l'INRIA, à l'EPFL et au Politecnico de Milan (www.lifev.org). Nous ne sommes pas encore en mesure de réaliser des simulations numériques "réalistes" de la filtration du sang, les expériences effectuées à l'Institut National de la Transfusion Sanguine n'ayant malheureusement pas permis de valider notre modèle.

Néanmoins, les travaux présentés dans cette thèse pourraient s'appliquer à d'autres types d'écoulements sanguins où des modèles analogues sont utilisés :

- Modélisation de la perfusion dans le myocarde [28].
- Modélisation de la pénétration de l'oxygène et des lipoprotéines dans les parois vasculaires.

Nous envisageons de poursuivre ces études en nous intéressant à la perfusion dans le myocarde.

5 Liste des publications

- Articles :
  1. M. Belhadj, J.-F. Gerbeau, and B. Perthame, A multiscale colloid transport model with anistropic degenerate diffusion, *Rapport de recherche INRIA No 4468, 2002*, Asymptotic Analysis, Vol. 34, Num. 1, p. 41-54, 2003.
- Communication :
  1. M. Belhadj, E. Cancès, J.-F. Gerbeau, A. Mikelić, and B. Perthame, Analyse d'un modèle de filtration à travers un milieu fibreux, *36 ème Congrés National d'Analyse Numérique, 2004*. (**Ce travail a reçu le prix du meilleur poster**).
- Colloque :
  1. Perméabilté d'un milieu fibreux non périodique, *Workshop : Fluide et Structure, Mulhouse, 18–19, Nov., 2004.*
- Rapports de recherche :
  1. M. Belhadj, E. Cancès, J.-F. Gerbeau, and A. Mikelć, *Homogenization approach to filtration through a fibrous medium*, Rapport de recherche INRIA No 5277, 2004, soumis pour publication.

Part I

Model set up

Chapter 1

Model set up

L'objectif de ce chapitre est de proposer un modèle mathématique de la filtration des globules blancs du sang et quelques références bibliographiques concernant la modélisation mathématique d'autres modèles de filtration.

1 Introduction

White blood cells are the cellular components of the immune system that provide protection against foreign matter or antigens. There are several types of white blood cells, each having special functions.
Over the last several years, various studies have implicated leukocytes (white blood cells) in most of the adverse reactions to blood component therapy. Leukoreduction is the removal of leukocytes from blood in order to minimize these adverse reactions. Indeed, the removal of leukocytes from blood is effective in reducing the risk of leukocyte-associated virus transmission [14].
Over the years, a variety of techniques have been developed to prepare leukocyte depleted blood products [41]. At present, filtration is the most efficient technique with respect to the reduction or prevention of adverse transfusion reactions caused by leukocytes.
The procedure of filtration is simple and does not require expensive equipment. Most filtrations were performed with the equipment represented in the figure (*cf.* Fig. 1.1). The mechanism of leukocyte depletion by such filters is not completely understood, this fact limiting the development of improved, cost-effective, and clinically applicable filter materials. So far, these mechanisms have not been studied systematically, although it has been suggested by several investigators that leukocyte filtration is gouverned by *sieving* and *adhesion cf.* [24, 38, 33]. However, the quantitative contribution of each of these factors has never been rigorously investigated.
The aim of this chapter is to discuss the various mechanisms of leukocyte removal by filtration, as well as the mathematical models to describe the process of leukocyte filtration.

Figure 1.1: Filtration equipment.

2 The mechanisms of leukocyte removal by filtration

Several mechanisms are known to play a role in leukocytes depletion by filters. A possible approach to explain filtration is to distinguish mechanical entrapment (*sieving*) from physico-chemical entrapment (*adhesion*), which means that filtration is caused by biological and physical interaction of blood cells and fibers as well as by passive trapping due to mechanical *sieving*.
Because blood cells differ both in size and deformability, *sieving* should be considered as a possible mechanism in the filtration of leukocytes. The pore size of the filter then determines if *sieving* becomes important. Bruil et al [3] found that leukocytes were only successfully removed when the filter pore size approached the size of leukocytes ($\sim 10\mu m$). It should be noted that in addition to the pore size of the filter, the hydrostatic pressure applied also determines whether cells will flow through the pores.
The *adhesion* is mediated by specific cell adhesion molecules and specific molecules present on the fibers. *Adhesion* of particles to the filter material becomes important when the ratio of particle to pore diameter is about 10^{-4} to 10^{-1} [21]. Several mechanisms are responsible for leukocyte *adhesion* during blood filtration for leukoreduction. Indeed, the composition of the blood may influence leukocyte *adhesion* in many aspects. Red blood cells may influence leukocyte *adhesion* under conditions of flow, because these cells are known to promote the migration of leukocytes to the substrate surface. Several investigators have reported that leukocyte *adhesion* is reduced in the presence of plasma [18].
The *adhesion* of cells to the filter surface can also be influenced by a number of other factors. Firstly the capacity of the filter media for cell *adhesion*, and secondly the effect of mechanical forces, such as gravity or blood flow encouraging cells to come into contact with the surface of the fibers to which they are then able to adhere. The surface charge of the fibre material also plays a role in attracting leukocytes towards the fibre surface.
Adhesion of blood cells to filter surfaces was the objective of some works (*see.* [1, 6, 7, 8] for example).
Effective leukoreduction depends on many factors. Indeed, some importants parameters for the performance of the recents filters are given in the table 1.1. The mechanisms responsible for leukocytes depletion by filters are complicated processes, so mathematical models to describe the leukocyte filtration process, based on current knowledge of filtration mechanisms, may be helpful to explain results obtained with leukocyte filtration and to optimize filters and filtration procedures.
In the next section, we start by giving an overview on some attempts to describe mathematically the removal of the leukocytes by filtration. After which, we propose our model.

General characteristics	sectional surface (cm2) Thickness (cm) Dead volume (mL)
Interior of the filter	Material of fibres and modification of surfaces Diameter of fibres (μm) Density of fibres (mg/cm3) Total fibre surface (m2) Surface stress (dynes/cm2)
Characteristics of flow	Time of passage (sec) Pressure (Pa) Flow rate (mL/min) Shear stress (sec^{-1})

Table 1.1: Filter's specifications (*cf.* [13])

3 Mathematical models

3.1 State of the art

Only a few attempts to describe mathematically the leukocyte filtration process are known.
Diepenhorst evaluated a mathematical model, originally derived to explain the removal of ferrous hydroxide particles from ground water through sand beds, to describe the filtration of leukocytes through cotton wool filters [11]. More recently, Prins developed a computer model to explain the depletion of leukocytes in filters composed of filter segments with different leukocyte-trapping efficiencies [34]. However, according to Bruil et al [5], Diepenhorst did not succeed in explaining his experimental results; therefore the relative roles of mechanical sieving or adhesion have not been determined. Bruil et al also pointed out that a shortcoming of the model proposed by Prins was that its parameters were based on empirically derived probability factors, and therefore the theoretical value of the model is minimal. To the best of our knowledge, the more advanced model to describe the leukocyte filtration process has been proposed by Bruil et al [4]. This model consists of the following differential system:

$$\frac{\partial \sigma}{\partial t} + \omega \frac{\partial c}{\partial h} = 0, \tag{1}$$

$$-\frac{\partial c}{\partial h} = \lambda c, \tag{2}$$

$$\lambda = \lambda_0 \Big(1 - \frac{\sigma}{\sigma_{\max}}\Big). \tag{3}$$

Here c is the concentration of the particles in suspension, σ is the concentration of the particles deposited in the filter. ω is the rate of fluid flow through the filter. The filtration coefficient λ, a measure of the efficiency

of the filter, was first introduced by Iwasaki in 1937 *cf.* [23]. The filtration coefficient may be regarded as the fraction of particles, captured per unit of filter length. During filtration, λ changes as a function of time, because the amount of material already deposited in the filter, σ, influences the filtration of the other particles present. It is assumed that a limited number of retention sites ($\sigma_{\max}$) in the filter is accessible for the capture of particles. Therefore, the filter efficiency decreases on occupation of these retention sites during filtration. Hence, a linear decrease of λ with σ is often assumed [32]. In equation (3), λ_0 is the filtration coefficient of the noncontaminated filter.

Remark 3.1 *Some investigators have postulated that λ_0 is proportional to the specific surface area (S) of the filter when adhesion is the predominant mechanism for particle depletion [22]. Assuming that S is inversely proportional to the filter pore size d, it follows that:*

$$\lambda_0 \sim \frac{1}{d}$$

The above $1D$ model has various limitations:

- In the $1D$ model, the porosity is constant whereas the filter is a fibrous medium of variable porosity.
- In the $1D$ model, the dispersion is not taken into account. At the microscpopic level, the variation in the size of the pores from one layer to another, brings about a velocity variation which implies kinematic dispersion.
- Geometrically speaking, the filter consists of various fibrous layers, which makes it a $3D$ medium.

In the next section, we give a complete description of our model. It is based on mass balance that incorporate advection, dispersion, and adsorption.

3.2 A 3D model for leukocyte removal

The simulation of the flow and transport processes inside the porous medium, based on models that resolve the complex pore structure in detail, would be computationally too expensive. Hence these simulations are based on homogenized or volume-averaged equations, where the fluid and the solid are considered as a pseudohomogeneous medium.
Here a three-dimensional model, capable of simulating colloid transport, in the fibrous porous media is presented. The model consists of two equations, flow equation and colloid transport-reaction equation.
For the sake of clarity, before starting the presentation of the equations, we introduce the following physical quantities.

- $\mathbf{u}$: Darcy velocity field (LT^{-1})
- p : blood pressure ($ML^{-1}T^{-2}$)
- c : concentration of leukocytes in blood (a number of leukocytes per unit of volume of blood)
- s : surface fraction occupied by the leucocytes having adhered (occupied surface divided by free total surface of fibers, *cf.* Fig. 1.2)

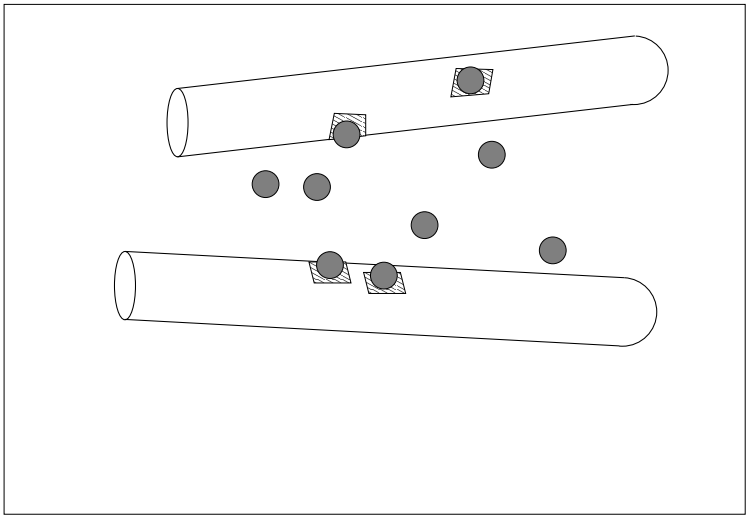

Figure 1.2: Leukocytes in solution and on the fibers. The variable s is the ratio between the shaded and the total area of the fibers.

- a : surface occupied on the fiber by a leukocyte adhered
- f : specific surface of the filter, *i.e.* surface fibers per unit of volume in the filter (L^{-1}). Note that this quantity is provided by the manufacturer of the filter.
- $\mathbf{K}$: hydraulic conductivity tensor (L^2)
- μ : dynamic viscosity ($ML^{-1}T^{-1}$)
- $\mathbf{D}$: dispersion tensor.
- ω : porosity (volume which can be occupied by the fluid divided by total volume)

where L, M, T indicate one unit of length, mass and time, respectively.

3.2.1 Fluid dynamics model

As regards the blood flow, we need to choose a model to represent the blood filtration in the filter. For this purpose, we consider two possibilities, Darcy model and Darcy-Brinkman model for flows in porous media. Both Darcy and Darcy-Brinkman equations can be derived by means of homogeneization techniques starting from the Stokes flow through an array of particles (for a detailed discusion we refer for example to [26]). Moreover, the Darcy-Brinkman model can be regarded as a correction of the Darcy one, featuring a viscous term inspired from the Stokes equations. Indeed, several authors recommended the use of the equations of Brinkman, to model the flow in a fibrous medium of large porosity (*cf.* [15], [12]). However, the Brinkman model corresponds to an asymptotic mode extremely specific in the analysis of the flows in porous environment by homogenisation (*cf.* [26], [20]). The equations of Brinkman thus cover an exceptionnel case which has little chance of corresponding to a physical reality.
We thus preserved the idea to use the equations of Darcy to calculate the flow in the filter.
The flow in the fibrous medium is thus governed by:

$$\mathbf{u} + \frac{\mathbf{K}}{\mu}\nabla p = 0, \tag{4}$$

$$\operatorname{div}\mathbf{u} = 0. \tag{5}$$

Various assumptions have been made in this commonly used model:

1. the fluid is Newtonian;
2. the flow is slow and so the same linear law applies at each instant;
3. the fluid is incompressible.

Remark 3.2 ([20]) *Starting from the steady Stokes equations in a periodic bounded porous medium $\Omega \subset \mathbb{R}^d$, with a no-slip (Dirichlet) boundary condition on the solid pores and according to the various scalings of the obstacle size a_ε in terms of the inter-obstacle distance ε, different limit problems arise. To sort these different regimes, we introduce a ratio r_ε defined by*

$$r_\varepsilon = \begin{cases} \left(\dfrac{\varepsilon^d}{a_\varepsilon^{d-2}}\right)^{1/2} & \text{for} \quad d \geq 3, \\ \varepsilon \left| \ln\left(\dfrac{a_\varepsilon}{\varepsilon}\right)\right|^{1/2} & \text{for} \quad d = 2. \end{cases} \tag{6}$$

so that at the limit the effective flow is described by the Darcy law if the obstacles are too big, i.e., $\boxed{\lim_{\varepsilon\to 0} r_\varepsilon = 0}$.
For smaller obstacles, different limit regimes occur (Brinkman or Stokes equations), there by, we obtain

1. *Brinkman law if the obstacles have a critical size, i.e.,* $\boxed{\lim_{\varepsilon\to 0} r_\varepsilon = r}$.

2. *the homogenized Stokes equations if the obstacles are too small, i.e.,* $\boxed{\lim_{\varepsilon\to 0} r_\varepsilon = +\infty}$.

In the blood filtration problem, typical values are $\varepsilon = 10^{-6}$, *and* $a_\varepsilon = 0.5$. *Putting* ε *and* a_ε *in the first relation of the expression (6), we obtain* $r_\varepsilon = O(10^{-9})$. *Consequently, it is reasonnable to assume that we are in the Darcy regime.*

3.2.2 Colloid dynamic model

We will briefly formulate the model. Let us consider a porous domain Ω in $\mathbb{R}^3$. Let $\mathbf{Q}$ denote the flux of the colloids and let R denote the reaction term. The colloid transport equation, can be derived from mass balance of colloids over a representative elementary volume (REV) of a porous medium.
If we apply mass balance to an arbitrary ball $\mathbf{B}$ in Ω, the integral conservation law takes the form

$$\frac{d}{dt}\int_B \omega\, c\, dx = -\int_{\partial B} \mathbf{Q}.\mathbf{n}\, ds + \int_B R\, dx, \tag{7}$$

where $\partial\mathbf{B}$ denotes the surface of the ball $\mathbf{B}$. Here, $\mathbf{n}$ is the outward unit normal vector.
Equation (7) states that the rate of change of colloid in the ball equals the net flux of colloid through the surface of the ball, plus the rate of production of the solute in the ball. The divergence theorem allows us to rewrite the surface integral and (7) becomes

$$\frac{d}{dt}\int_B \omega\, c\, dx = -\int_B \nabla.\mathbf{Q}\, dx + \int_B R\, dx. \tag{8}$$

Because the domain of integration $\mathbf{B}$ is arbitrary, the integrand must vanish and we obtain the mass balance law in the local, differential form

$$(\omega\, c)_t = -\nabla.\mathbf{Q} + R. \tag{9}$$

Here we are assuming that the functions are sufficiently smooth to allow application of the divergence theorem and permit pulling the time derivative inside the integral.
We could ask how the colloid gets from one place to another in a porous medium. There are three main mechanisms controlling colloid transport: advection, hydrodynamic dispersion, and adhesion.

1. Advection: which means that the particles are simply carried by the bulk motion of the fluid. This leads us to define the advective flux $\mathbf{Q}^{(a)}$

by

$$\mathbf{Q}^{(a)} = \mathbf{u}\, c.$$

2. Another way of transport is by hydrodynamic dispersion. It consists of molecular diffusion and kinematic dispersion. The molecular diffusion is the spreading caused by the random molecular motion and collisions of the particles themselves. This type of motion is driven by concentration gradients and the flux due to the diffusion is given by Fick's law. We call this the molecular diffusion flux $\mathbf{Q}^{(m)}$ and we take

$$\mathbf{Q}^{(m)} = -\omega \mathbf{D}^{(m)} \nabla c.$$

The kinematic dispersion is the spreading, or mixing phenomenon, caused by the variability of the complex, microscopic velocities through the pores in the medium. So, it is linked to the heterogeneities present in the medium and is present only if there is flow.
This heterogeneity is found within the porous media, whatever is the scale of observation. On the scale of the microscopic field speed, heterogeneity is mainly due to three factors (*cf.* [17]):

- in a pore, the profile of velocities is parabolic. There is a gradient of velocity from the surface of the solid to the axis of the pore;
- variable dimensions of the pores have as a consequence a variation of velocities from one pore to another;
- the steamlines vary compared to the principal direction of the flow.

The mathematical form of the dispersion flux $\mathbf{Q}^{(d)}$ is taken to be Fickian and given by

$$\mathbf{Q}^{(d)} = -\omega \mathbf{D}^{(d)}.\nabla c,$$

where $\mathbf{D}^{(d)}$ is the tensor of dispersion.
Now, consequently, the net flux is given by the sum of the advective, molecular, and dispersion fluxes:

$$\begin{aligned} \mathbf{Q} &= \mathbf{Q}^{(a)} + \mathbf{Q}^{(m)} + \mathbf{Q}^{(d)} \\ &= \mathbf{u}c - \omega\Big(\mathbf{D}^{(m)} + \mathbf{D}^{(d)}\Big).\nabla c. \end{aligned}$$

If we define the hydrodynamic dispersion tensor $\mathbf{D}$ by

$$\mathbf{D} = \mathbf{D}^{(m)} + \mathbf{D}^{(d)}$$

then the net flux is given simply as

$$\mathbf{Q} = \mathbf{u}c - \omega \mathbf{D}.\nabla c.$$

The Fickian term $-\omega \mathbf{D}.\nabla c$ is termed the hydrodynamic dispersion. It consists of molecular diffusion and kinematic dispersion.
In several studies the following expression of the dispersion tensor $\mathbf{D}(\mathbf{u})$ (in $2D$ *isotropic* medium) is used:

$$D(\mathbf{u}) = \begin{bmatrix} \alpha_L \frac{u_x^2}{|\mathbf{u}|} + \alpha_T \frac{u_y^2}{|\mathbf{u}|} + D^* & (\alpha_L - \alpha_T)\frac{u_x u_y}{|\mathbf{u}|} \\ (\alpha_L - \alpha_T)\frac{u_x u_y}{|\mathbf{u}|} & \alpha_T \frac{u_x^2}{|\mathbf{u}|} + \alpha_L \frac{u_y^2}{|\mathbf{u}|} + D^* \end{bmatrix},$$

where

- α_L: longitudinal dispersivity (L),
- α_T: transverse dispersivity(L),
- D^*: molecular diffusion (L^2T^{-1}).

This expression is used for molecular transport (*cf.* [40] p. 4). In studies treating the colloidal transport, the molecular D^* is replaced by D^*T, where D^* is called *particulate diffusion* of Stokes-Einstein and T is the tortuosity of the medium ([39], p. 210).

3. The third contribution to the mechanisms controlling colloid transport is called adhesion or adsorption: the function R, which we call a reaction term or source term, measure an adsorption rate. Adsorption is a process that causes the mobile tracer to adhere to the surface of solid surface, and thus become immobile.
In our case, the function R is given by

$$R = -k\frac{\partial s}{\partial t},$$

where $k = \dfrac{f}{a}$.
$\dfrac{\partial s}{\partial t}$ is given by the law:

$$\frac{\partial s}{\partial t} = ak(\mathbf{u})cB(s).$$

Here $k(\mathbf{u})$ is the coefficient of the reaction and $B(s)$ is called the dynamic blocking function.

Coefficient of reaction. The function $k(\mathbf{u})$ measures the reaction rate. In several work ([39], [29] p. 115), an expression of this type is used:

$$k(\mathbf{u}) = \alpha\eta|\mathbf{u}| \tag{10}$$

where the coefficient α (*sticking coefficient*) is the ratio between the particles having touched the collector (the fiber) and those actually adhered, and η (*single collector efficiency*) is the ratio between the particles having touched the collector and the particles which run around the collector. The parameter η takes into account the hydrodynamic forces of Van der Waals which are exerted on the colloides. Several works propose empirical semi calculations of η if the particles and the collectors are spherical for example ([27, 35, 36]).

The Dynamic Blocking Function. The dynamic blocking function $B(s)$ quantifies the probability of a particle contacting a portion of collector surface that is unoccupied by previously retained particles. Two types of dynamic blocking functions are generally recognized: the Langmuirian dynamic blocking function (so called from an analogy with the classical model of molecular adsorption (*cf.* [29] p. 39 et [37], p. 47):

$$B(s) = 1 - \beta s, \tag{11}$$

$$\beta = \frac{1}{s_{max}} \tag{12}$$

where s_{max} is the maximum attainable fractional surface coverage (In sandy aquifers, s_{max} is generally worth between 0.1 et 0.3 (*cf.* [2] p. 295) and β is the excluded area parameter and represents the normalized area blocked by a single cell (area blocked by cell/area of cell). The second type of the dynamic blocking function is the random sequential adsorption(RSA) dynamic blocking function. Recent experimental investigations have shown that the RSA model better describes the dynamics of particle deposition in porous media than the conventional Langmuirian model[37], p.46). The general form of the RSA dynamic blocking function is $B(s) = 1 - a_1\frac{s}{s_{max}} + a_2\left(\frac{s}{s_{max}}\right)^2 + a_3\left(\frac{s}{s_{max}}\right)^3$ where s_{max} is the maximum attainable surface coverage and a_1, a_2, and a_3 are virial coefficients that can be evaluated theoretically (for ideal particles and collector surfaces) or empirically.

Consequently, the above mechanisms can be described by the generalized advection-dispersion-adhesion equations:

$$\frac{\partial}{\partial t}(\omega c) + \operatorname{div}\left(\mathbf{u}c - \omega \mathbf{D}(\mathbf{u})\nabla c\right) = -\frac{f}{a}\frac{\partial s}{\partial t} \tag{13}$$

$$\frac{\partial s}{\partial t} = ak(\mathbf{u})cB(s) \tag{14}$$

Equations (4)-(14) together with appropriate boundary and initial conditions completely specify the problem at hand.

Remark 3.3 *This kind of system describes the evolution of a* tracer *(typically a chemical or a biological species) in a porous medium. This tracer is assumed to adhere to the surface of the solid skeleton. The places where this adhesion process occurs are named the* adsorption sites. *Denoting by C the mobile tracer, by S the adsorption sites on the immobile porous medium, and $\overline{CS}$ the product of the reaction between the tracer and the skeleton, this process can be represented as a formal chemical reaction:*

$$C + S \rightleftharpoons \overline{CS}.$$

This model is encountered in various applications. For example, it was proposed in cancer research to study the penetration of antibodies in tumourous tissue and their attachment to antigens (K. Fenmori et al. *[16]). It is also used to study the transport and attachment of colloids, bacteria or viruses, in sandy aquifers [39], [2].*

Dimensional analysis. Taking into account the orders of magnitude, we choose to work in CGS units. We introduce the variable without dimension $\tilde{c} = c/C_0$, where C_0 is the concentration of leukocytes before filtration.
The system (13)-(14), with (11) and (10) is written then:

$$\frac{\partial}{\partial t}(\omega \tilde{c}) + \operatorname{div}\left(\mathbf{u}\tilde{c} - \omega \mathbf{D}(\mathbf{u})\nabla \tilde{c}\right) = -k_1 \frac{\partial s}{\partial t}$$

$$\frac{\partial s}{\partial t} = k_2 |u| \tilde{c}\left(1 - \frac{s}{s_{max}}\right)$$

with

$$k_1 = \frac{f}{aC_0} \quad \text{[no dimension]}$$

and

$$k_2 = a\alpha\eta C_0 \quad [cm^{-1}]$$

With the values given in the following table, we find:

$$14 \leq k_1 \leq 375 \qquad \text{et} \qquad k_2 = 0.08\, cm^{-1}$$

The minimal value of k_1 corresponds to the prefilter, the highest value to the fine layers.

Parameters	Values	Units	Remarks
μ	0.5	poise ($gcm^{-1}s^{-1}$)	water: 0.01 poise
ω	de 0.85 à 0.91		source: INTS
C_0	8.10^6	leukocyte cm^{-3}	
f	de 110 à 3000	cm^{-1}	source: INTS
a	10^{-6}	cm^2 / leukocyte	
α	0.4		bacteria and sands [2]
η	0.025		idem
s_{max}	0.3		idem
α_L	5	cm	bacteria and sands [39]
α_T	0.2 α_L	cm	idem

Remark 3.4 *The system of Darcy with second member is written (cf [20] p. 46)*

$$\mathbf{u} + \frac{\mathbf{K}}{\mu}(\nabla\tilde{p} - \mathbf{f}) = 0,$$

where $\mathbf{f} = -\rho g \mathbf{e}_z$. *we thus has* $p = \tilde{p} + \rho g z$. *The quantity called* hydraulic conductivity *in the literature has the dimension of* $p/(\rho g)$.

3.3 Relation with other models of leukocyte filtration

In this section, we show that our model generalizes the mathematical model proposed by A. Bruil *et al.* [5], that is the most recent study which we know on the modeling of the filtration of the leucocytes. In [5], the domain is supposed to be $1D$, thus the Darcy velocity field is limited to $\mathbf{u} = (0, 0, u_z)$, and taking into account (5), u_z is necessarily constant in space. The differential system (4)-(5) is replaced by an algebraic relation:

$$u_z = Q A_F \tag{15}$$

where Q is the flow of blood and A_F the surface of the section of the filter $1D$. It is then supposed that the dispersion tensor $\mathbf{D}$ is zero and that the derivative in time c is negligible in (13). We note S the concentration of leukocytes adhered:

$$S = \frac{fs}{a}.$$

Equation (13) then reads:

$$u_z \frac{\partial c}{\partial z} = -\frac{\partial S}{\partial t} \tag{16}$$

It is exactly the equation (6) p. 158 of [5] (while noting z, u_z and S respectively h, w and σ)

The equation (14) is written:

$$\frac{\partial S}{\partial t} = fk(\mathbf{u})cB(S)$$

While noting λ_0 the specific surface $\alpha\eta f$ (in [5], λ_0 is proportional to f), by taking the expression (10) for the coefficient of reaction $k(\mathbf{u}) = \alpha\eta|u_z|$, and by taking a Langmuirian dynamic blocking function $B(S) = (1 - S/S_{max})$, we find (while supposing $u_z > 0$):

$$\frac{\partial c}{\partial z} = -\lambda_0(1 - S/S_{max})c. \tag{17}$$

It is exactly the equation (1) p. 157 of [5] joined to the formula (2) p. 157.

3.4 Filtration model in porous media with varying porosity

We present a reaction-dispersion-advection model with a varying porosity which depends on the adsorbed species concentration. The flow is driven by a pressure gradient satisfying Darcy's law with nonconstant Darcy velocity. We consider a chemical solute that interacts with the fixed porous matrix to produce an immobile chemical species attached to the matrix. The irreversible reaction is accompanied by a change in porosity. We assume the flow is pressure driven and is subject to Darcy's law

$$\mathbf{u} = -\mathbf{K}(\omega)\nabla p \tag{18}$$

where $\mathbf{u} = \mathbf{u}(x,t)$ is the Darcy velocity, $p = p(x,t)$ is the pressure, $\omega = \omega(x,t)$ is the porosity, and $\mathbf{K} = \mathbf{K}(\omega)$ is the hydraulic conductivity of the medium. We further assume the continuity equation

$$\omega_t + \operatorname{div}\mathbf{u} = 0 \tag{19}$$

Let $c = c(x,t)$ denotes the mass concentration of the mobile, chemical solute. Due to the balance law and by assuming that the volumetric flux of the concentration c of the transported colloid contains an advective term and a dispersion term, we obtain

$$(\omega c)_t = \operatorname{div}(\omega\mathbf{D}\nabla c - c\mathbf{u}) - r \tag{20}$$

where D is the tensor of dispersion and r is the reaction rate.
Next, we impose the kinetics law

$$r = s_t \quad = \quad \lambda\mathbf{u}cF(s),$$

where the positive constant λ is called the filter coefficient. The function F is a nonnegative, nonincreasing function of s. In this model decolmatage is

negligible.

Equations with variable porosity have been studied by several investigators. Here we only mention Herzig , Leclerc, and Le Goff [19], deMarsily [31], Logan [28], Cohn, Ledder, and Logan [10], and Ledder and Logan [25].

Remark 3.5 *In order to prove the kinematical flow relation (19), let us consider an arbitrary volume Ω in a three-dimentional porous domain where a fluid of density $\rho = \rho(x,t)$ is flowing with Darcy velocity $\mathbf{u} = \mathbf{u}(x,t)$,and suppose that the porosity is evolving in both space and time, i.e., $\omega = \omega(x,t)$, where $x \in \mathbb{R}^3$. We assume the flow is saturated, i.e., the pores are completely filled with fluid. If there are no fluid sources, we can balance the mass of fluid in Ω to conclude that*

$$\frac{d}{dt}\int_\Omega \rho\omega dx = -\int_{\partial\Omega} \rho\mathbf{u}.\mathbf{n}dA.$$

With an application of the divergence theorem over the arbitrary domain Ω, we obtain

$$(\rho\omega)_t + div\,(\rho\mathbf{u}) = 0,$$

which is the local fluid mass balance law.
Now, let us expand the derivatives to obtain

$$\rho\omega_t + \omega\rho_t + \rho\nabla.\mathbf{u} + \mathbf{u}.\nabla\rho = 0.$$

If we introduce the logarithmic density $\delta = \ln(\rho/\rho_0)$, where ρ_0 is a constant reference density, we can write the previous equation in the form

$$\nabla.\mathbf{u} = -\omega_t - (\omega\frac{\partial}{\partial t} + \mathbf{u}.\nabla)\delta.$$

With the usual calculus interpretation of the divergence, the right-hand side has two terms that can be regarded as source terms for the fluid velocity. If the density is constant , then the equation leads to the continuity equation

$$\omega_t + \nabla.\mathbf{u} = 0,$$

which relates porosity changes to velocity changes.

4 Appendix

4.1 Glossary of common terms

Adhesion: The property of remaining in close proximity, as that resulting from the physical attraction of molecules to a substance, or the molecular attraction existing between the surfaces of contacting bodies.

Adsorption: The attachment of one substance to the surface of another.
Antigen: Any substance which is capable, under appropriate conditions, of inducing a specific immune response and of reacting with the products of that response.
Leukocyte: White blood cell.
Leukoreduced: Products meeting the standard of $< 5x10^6$ WBCs/unit.

4.2 Characteristics of a standard filter

Layer of the filter	Thickness of the Layer (μm)	Porosity (%)	Diameter of the pores (μm)
Fine	490	85	7
Coarse	550	86	37
Pre-filter	2360	91	61

The formula giving the specific surface reads

$$\boxed{S = 4 \times \frac{1-\omega}{D_p}}$$

where ω is the porosity and D_p is the diameter of the pores.

5 Experimental Study

In order to test our filtration model, a series of tests were conducted at the Institut National de la Transfusion Sanguine (INTS). Blood bags of one and a half litres in size were filtered. The figure 1.1 gives us an idea about the principle of deleucocytation by filtration.
We shall describe the different steps taken during the process of filtration,as follows:

5.1 Protocol

1. Weigh the bag and the filter together.
2. Suspend the bag and *mix well* its contents, install a container on a balance to receive the blood.
3. Break the clips to allow the bag to empty itself in the filter.
4. Note the time which passes,from the arrival of the blood in the filter to its passage in the tube from which it exits.(i.e time required to traverse the filter)

5. The liquid containing the anticoagulant is ejected before the blood has reached. Collect this liquid in order to weigh it.

6. When the first drop of blood comes to the end of the tube,start the chronometer, collect the drops in the first tube.

7. Every 90 seconds, note the weight of the pot, then collect some drops in a tube.Weigh the tube.

8. Note the time at which the last drop of blood leaves the bag.

9. At the end of this manipulation, weigh together, the filter, the blood bag and the broken clips.

5.2 Results of the experiments

The blood was drawn at the Centre de Transfusion des Armées (CTA). The filtration of blood was done at the Institut National de la Transfusion Sanguine (INTS).

5.2.1 The flow rate measurement

The following figure represents the weight of the 'filtrat'(i.e. The total weight of the samples taken as well as the blood collected in the containers (in grams)) as a fonction of time(seconds).

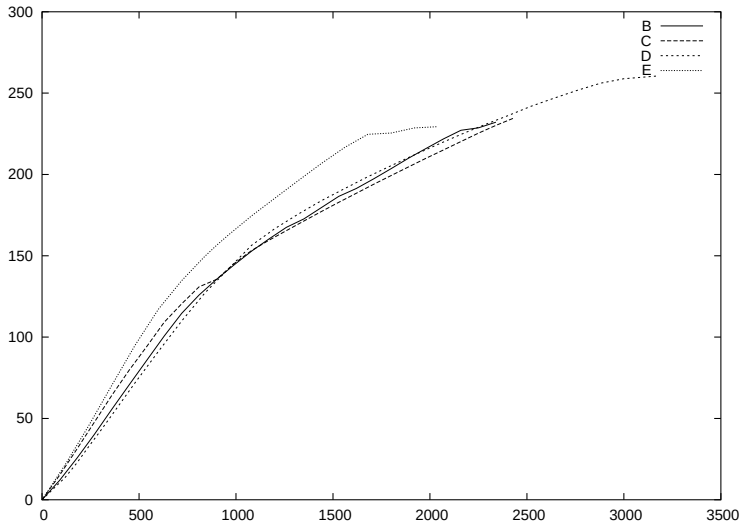

It can be noted that, in the case of the four bags B,C,D and E, the curves are close to each other.

5.2.2 Concentration mesure

It is necessary to explain here that all the measurements were taken in order to reply to certain questions that we had asked ourselves during the modelisation. We particularly wanted to know if the white blood cells in the "filtrat" were passed through the filter in the beginning or at the end of the filtration. We also wanted to know the relative importance of colmatage and adhesion in order to refine the model. The following figure represents the evolution of the concecntration of the leucocytes as a fonction of time (in seconds).

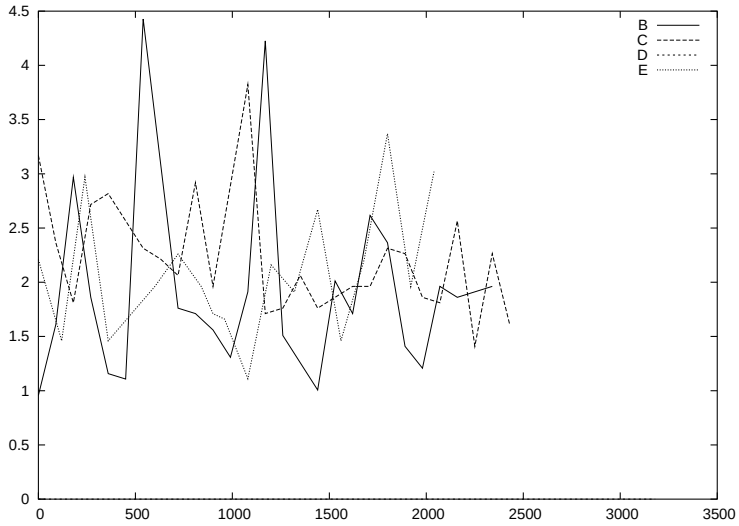

Figure 1.3: Concentration mesure in the filtrat (Institut National de la Transfusion Sanguine).

One could have looked forward to identifying certain qualitative behaviours (for example: Plateaus at the beginning or at the end of the filtration). Unfortunately the rersults that can be seen in the figure 1.3 are not of much help for validating or improving the model. Hence, no interesting conclusion was found for all the measurements.
The "chaotic" behaviour observed could be put down to the fact that different types of leucocytes react differently to the filtration. The proposed model could probably be more pertinent as it considers only one cellular lineage. The proposed model could probably be more pertinent as it considers only one cellular lineage *cf.* [1].

Bibliography for the model

[1] L. Barbe. *Mécanismes d'adhérence des leucocytes aux fibres synthétiques. Application à la filtration du sang.* Thèse, Université Paris VII, 2001.

[2] C. H. Bolster, A. L. Mills, G. M. Hornberger, and J. S. Herman. Effect of surface coatings, grain size, and ionic strength on the maximum attainable coverage of bacteria on sand surfaces. *Journal of Contaminant Hydrology*, 50:287–305, 2001.

[3] A. Bruil, W. G. van Aken, T Beugeling, et al. Asymmetric membrane filters for the removal of leukocytes from blood. J Biomed Mater Res 25: 1459-1480, 1991.

[4] A. Bruil, T. Beugeling, J. Feijen. A mathematical model for the leukocyte filtration process, in Bruil A (ed): Leukocyte Filters. *Thesis. University Twente. Enschede. The Netherlands*, pp. 159–172, 1993.

[5] A. Bruil, T. Beugeling, J. Feijen, and W. G. van Aken. The mechanisms of leukocyte removal by filtration. *Transfusion Medicine Reviews*, 9(2):145–166, 1995.

[6] A. Bruil, L. M. Brenneisen and J. G. A. Terlingen. In vitro leukocyte adhesion to modified polyurethane surface: II. Effect of wettability. *J. Colloid Interface Sci.*, 165:72–81, 1994.

[7] A. Bruil, J. I. Sheppard, J. Feijen, et al. In vitro leukocyte adhesion to modified polyurethane surface: III. Effect of flow, fluid medium, and platelets on PMN adhesion. *J. Biomater. Sci. Polym. Ed.*, 5(4):263–273, 1994.

[8] A. Bruil, J. G. Terlingen, T. Beugeling, et al. In vitro leukocyte adhesion to modified polyurethane surface: I. Effect of ionizable functional groups. *Biomaterials*, 13(13):915–923, 1992.

[9] G. Chavent and J. Jaffré. Mathematical models and finite elements for reservoir simulation: single phase, multiphase and multicomponent flows through porous media. North-Holland, 1986.

[10] S. Cohn, G. Ledder and J.-D. Logan. Analysis of a filtration model in porous media. *PanAmerican Math. J.*, 10(1):1–16, 2000.

[11] P. Diepenhorst. Removal of leukocyte from whole blood and erythrocyte suspensions by filtration through cotton wool-VII-Studies on possible mechanisms, in Diepenhorst P: Removal of Leukocytes From Blood by Filtration Through Cotton Wool. Meppel, Krips, thesis Deft University of Technology. The Netherlands, 1974, pp 86-90.

[12] L. Durlofsky and J. F. Brady. Analysis of the brinkman equation as a model for flow in porous media. *Phys. Fluid*, 30(11):3329–3341, 1987.

[13] S. Dzik. Leukodepletion blood filter: Filter design and mechanism of leukocyte removal. *Transfus. Med. Rev.*, 7(2):65–77, 1993.

[14] L. Eisenfield, H. Silver, J. McLaughlin, et al. Prevention of transfusion-assiciated cytomegalovirus infection in neonatal patients by the removal of white cells from blood. *Transfusion* 32:205–209, 1992.

[15] J. Feng and S. Weinbaum. A model for flow through a planar orifice in a fiber-filled medium with application to fenestral pores in biological tissue. submitted to *J. Fluid Mech.*, 1999.

[16] K. Fenmori, D. G. Covell, J. E. Fletcher, and J. N. Weinstein. Modeling analysis of the global and microscopic distribution of immunoglobulin G, $F(ab')_2$ and Fab in tumors. *Cancer Research*, 49:5656–5663, 1989.

[17] J. J. Fried and M. A. Combarnous. Dispersion in porous media. *Advances in hydroscience, Ed. V.T. Chow, Academic Press*, New-York, pp. 169–282, 1971.

[18] F. Grinnell. Cellular adhesiveness and extracellular substrata. *Int. Rev. Cytology*, 53:65–144, 1978.

[19] J.-P. Herzig, D.-M. Leclerc and P. LeGoff. Flow of suspension through porous media. Application to deep filtration. *Ind. Eng. Chem.*, 62(5):129–157, 1970.

[20] Ulrich Hornung, editor. Homogenization and porous media. Springer-Verlag, New York, 1997.

[21] K. J. Ives. Capture mechanisms in filtration, in Ives K.-J (ed): The Scientific Basis of Filtration. Leiden, the Netherlands, Noordhoff, pp 183–202, 1975.

[22] K. J. Ives. Mathematical models of deep bed filtration, in Ives K.-J (ed): The Scientific Basis of Filtration. Leiden, the Netherlands, Noordhoff, pp 203–224, 1975.

[23] T. Iwasaki. Some notes on sand filtration. *J. Am. Water Works Assoc.*, 29:1591–1602, 1937.

[24] T. S. Kickler, W. Bell, P. M. Ness, et al. Depletion white cells from platelet concentrates with a new adsorption filter. *Transfusion*, 29:411–414, 1989.

[25] G. Ledder and J.-D. Logan. Contamination and remediation waves in a filtration model. *Appl. Math. Lett.*, 13:75–84, 2000.

[26] T. Levy. Fluid flow through an array of fixed particles. *Int. J. Engng. Sci.*, 21(1):11–23, 1983.

[27] B. E. Logan, D. G. Jewett, R. G. Arnold, E. J. Bouwer, and C. R. O'Melia. Clarification of clean-bed filtration models. *J. Environ. Eng.*, 121:869–873, 1995.

[28] J.-D. Logan. Stability of wave fronts in a variable porosity model. *Appl. Math. Lett.*, 10(6):83–89, 1997.

[29] J. D. Logan. Transport modeling in hydrogeochemical systems. Springer-Verlag, 2001.

[30] R. I. Mackie. Rapid gravity filtration-Towards a deeper understanding. *Filtration Separation*, 26:32–35, 1989.

[31] G. de Marsily. Quantitative hydrogeology. *Academic Press, Inc., San Diego*, 1986.

[32] R. Mutharasan, D. Apelian, C. Romanowski. A laboratory investigation of aluminum filtration through deep-bed and ceramic open pore filters. *J. Metals*, 33:12–18, 1981.

[33] R. Pietersz, I. Steneker, H. Reesink. Comparison of five different filters for the removal of leukocytes from red cell concentrates. Vox Sang, 62:76–81, 1992.

[34] H. K. Prins, I. Steneker. Statistic simulation of leukocyte depletion by filtration with the aid of a computer model, in Steneker I: Leukocyte Depletion From Fresh Red Cell Concentrates by Fiber Filtration. Amsterdam, VU University Press, thesis Free University of Amsterdam. The Netherlands, pp 97–109, 1992.

[35] R. Rajagopalan and C. Tien. Trajectory analysis of deep-bed filtration with the sphere-in-cell porous media model. *AIChE J.*, 22(3):523–533, 1976.

[36] L. L. C. Rehmann, C. Welty, and R. W. Harvey. Stochastic analysis of virus transport in aquifers. *Water resources research*, 35(7):1987–2006, 1999.

[37] J. N. Ryan and M. Elimelech. Colloid mobilization and transport in groundwater. *Colloid and Surfaces, A: Physicochemical and Engineering aspecsts*, 107:1–56, 1996.

[38] I. Steneker, J. Biewenga. Histologic and immunohistochemical studies on the preparation of white cell-poor red cell concentrates: the filtration processes using three different polyester filters. *Transfusion*, 31(1):40–46, 1991.

[39] N. Sun, N. Z. Sun, M. Elimelech, and J. N. Ryan. Sensitivity analysis and parameter identifiability for colloid transport in geochemically heterogeneous porous media. *Water resources research*, 37(2):209–222, 2001.

[40] N. Z. Sun. Inverse problems in groundwater modeling. Kluwer, 1994.

[41] B. Wenz. Leukocyte-poor blood. *CRC Crit. Rev. Clin. Lab. Sci.* 24:1–20, 1986.

Part II

Mathematical studies

Chapter 2

A multiscale colloid transport model with anistropic degenerate diffusion

Le contenu de ce chapitre, réalisé en collaboration avec Jean-Frédéric Gerbeau et Benoît Perthame, a donné lieu à un rapport de recherche INRIA (numéro RR-4468). Il est paru dans Asymptotic Analysis *en Avril 2003.*

1 Introduction

This note deals with the following problem: find the solution c and s defined on $\mathbb{R}^d \times (0,T)$ (with $T > 0$ and $d \leq 3$), to the weakly coupled semilinear and degenerate parabolic-hyperbolic system

$$(P_k) \begin{cases} \partial_t c + \operatorname{div} \mathbf{A}(c) - \displaystyle\sum_{i,j=1}^{d} \frac{\partial^2 \phi_{ij}(c)}{\partial x_i \partial x_j} &= -k\, c\, s \quad \text{in } \mathcal{D}'((0,T)\times\mathbb{R}^d), \\ \partial_t s &= -k\, c\, s \quad \text{in } \mathcal{D}'((0,T)\times\mathbb{R}^d), \\ c(0,x) &= c_0(x) \geq 0 \quad \text{a.e. in } \mathbb{R}^d, \\ s(0,x) &= s_0(x) \geq 0 \quad \text{a.e. in } \mathbb{R}^d, \end{cases} \tag{1}$$

where k is a given positive constant. The assumptions on the data $\mathbf{A} : \mathbb{R} \to \mathbb{R}^d$, the $d \times d$ matrix $\phi(c) = (\phi_{ij}(c))$, c_0 and s_0 will be made precise later (Section 2), but let us just say that they cover the cases of completely degenerated diffusion (we only assume (ϕ'_{ij}) is a nonnegative matrix) and ill-prepared initial data (the product $c_0\, s_0$ does not vanish). Our purpose is to prove a global well-posedness theory for this system and to study the relaxation limit as $k \to \infty$, and especially to characterize this limit through

the generalized Stefan equation

$$(Q_\infty)\begin{cases} \partial_t w + \operatorname{div} \mathbf{A}(w_+) - \displaystyle\sum_{i,j=1}^{d} \frac{\partial^2 \phi_{ij}(w_+)}{\partial x_i \partial x_j} &= 0 \quad \text{in } \mathcal{D}'((0,T)\times\mathbb{R}^d), \\ w(0,x) &= c_0(x) - s_0(x) \quad \text{a.e. in } \mathbb{R}^d. \end{cases} \tag{2}$$

One of the difficulties is that the parabolic degeneracy leads to singular solutions (possibly shock waves in the purely hyperbolic case). In order to cover this generality, we therefore use methods based on S. Kruzhkov's style L^1 contraction property [72].
In chapter 4, we will give a numerical illustration of the asymptotic behaviour of the solution to system (P_k) as k becomes large (*cf.* the Figure 4.6).

This kind of system describes the evolution of a *tracer* (typically a chemical or a biological species) in a porous medium. This tracer is assumed to adhere to the surface of the solid skeleton. The places where this adhesion process occurs are named the *adsorption sites*. Denoting by C the mobile tracer, by S the adsorption sites on the immobile porous medium, and $\overline{CS}$ the product of the reaction between the tracer and the skeleton, this process can be represented as a formal chemical reaction:

$$C + S \rightleftharpoons \overline{CS}.$$

We let c and s denote the concentration of C and S respectively. The concentrations c and s are classically assumed to satisfy the following system:

$$\begin{cases} \partial_t c + \operatorname{div} \mathbf{A}(c) - \displaystyle\sum_{i,j=1}^{d} \frac{\partial^2 \phi_{ij}(c)}{\partial x_i \partial x_j} &= -R(c,s), \\ \partial_t s &= -R(c,s), \end{cases}$$

Where the function R is a reaction term. In this work, we assume that the above pseudo-chemical reaction is governed by the law of mass action and we neglect the backward reaction (namely the desorption). Thus, we have

$$R(c,s) = k\, c\, s, \tag{3}$$

where k is the forward rate constant.

This model is encountered in various applications. For example, it was proposed in cancer research to study the penetration of antibodies in tumurous tissue and their attachment to antigens (K. Fenmori *et al.* [47]). It is also used to study the transport and attachment of colloids, bacteria or viruses, in sandy aquifers. In these later cases the function $R(c,s)$ generally takes the form $cB(s)$, where B, the so-called *blocking function*, is typically polynomial (see for example N. Sun *et al.* [93], C.H. Bolster *et al.* [18]). These equations can also be viewed as a simple model of colloid filtration,

when the retained particules are small enough to consider that their adhesion on the filter do not modify the size of the pores (see M. Belhadj [15] for an application to blood filtration).

Concerning the mathematical theory, D. Hilhorst, R. van der Hout and L.A. Peletier proposed various mathematical studies on systems of this kind. In [55], they considered the large time behaviour and the limiting behaviour as $k \to \infty$ of a 1D version of this problem with $\mathbf{A} = 0$ and $\phi(c) = c$. In [56], they considered also the 1D case with $\mathbf{A} = 0$ and $\phi(c) = c$, but they took more general reaction terms. In [57], they kept $\mathbf{A} = 0$ but they extended their works to the multidimensional cases and nonlinear diffusions. More precisely they assume that $\phi(c) = \int_0^c D(\xi)\, d\xi$ with $D(\xi) > 0$ for $\xi > 0$. In [45], R. Eymard, D. Hilhorst, R. van der Hout and L.A. Peletier focused on reactions which are very fast in relation to the diffusion process. They continued and extended earlier studies in [55], [56], [57]. On the other hand, the purely hyperbolic case $\phi(c) = 0$ has been widely studied and we refer to the survey paper of R. Natalini [81] for further references and analysis. We would like also to point out that a possible approach is to use the nonlinear semigroup theory which provides easily a partial answer (uniqueness in a restricted sense) to the problem in the isotropic case at least.

In the present work, we restrict ourselves to the mass action kinetics (3), which is just one of the two kinds of reactions investigated in [57], but we consider a more general equation since we treat a completely degenerated and non-isotropic diffusions. Moreover, we also add the nonlinear convection term $\operatorname{div} \mathbf{A}(c)$, thus dealing with the complete hyperbolic-parabolic case. Finally, we do not assume that initial data are well-prepared i.e. $c_0 s_0 = 0$ and thus we implicitely treat the initial layer problem: a non-equilibrium initial data (an equilibrium is defined by a state (c, s) such that $c\, s = 0$) is immediately relaxed to an equilibrium in the limit $k \to \infty$. As mentioned earlier, we consider a purely L^1 well posedness theory. This requires to use a precise definition of entropy solutions, an issue solved in the purely hyperbolic case by S. Kruzhkov [72]. The parabolic case is much more involved and the entropy dissipation has to be controlled precisely in the relaxation process and in the construction of the solution. The main issue then is uniqueness of solutions satisfying these entropy inequalities, a result proved recently for isotropic matrices ($\phi_{ij} = 0 \quad \forall i \neq j$) by J. Carrillo [25] (see also R. Eymard *et al.* [46] for improved assumptions and K. H. Karlsen and N. H. Risebro [68] for numerical analysis of the problem). The recent improvment in this uniqueness proof by G. Q. Chen and B. Perthame [27] allows to treat non-isotropic degenerate diffusions to the expense of more precise entropy inequalities.

The paper is organized as follows. In Section 2, we prove an existence result for the above system based on the L^1 contraction property. We study

the behaviour of the solution as k tends to infinity in Section 3.

Remarks on notations We use the standard notations for the Sobolev spaces, but for simplicity, we will sometimes denote the spaces $L^1((0,T)\times\mathbb{R}^d)$ by $L^1_{t,x}$, $L^2(0,T;H^1(\mathbb{R}^d))$ by $L^2_t(H^1_x)$, and so on. Moreover, in the sequel C will denote various constants.

2 Existence result

We make the following assumptions on the data:

$$(\phi_{ij}) \in \mathcal{C}^2(\mathbb{R}) \text{ is symmetric, } (\phi'_{ij}) \text{is a nonnegative matrix,} \tag{4}$$

$$\mathbf{A} = (A_1, \ldots, A_d) \in (\mathcal{C}^1(\mathbb{R}))^d, \mathbf{A}(0) = 0, \tag{5}$$

$$c_0 \in L^1(\mathbb{R}^d) \cap L^\infty(\mathbb{R}^d), c_0 \geq 0 \text{ a.e. in } \mathbb{R}^d, \text{ and } \int_{\mathbb{R}^d} |x|^2 c_0 \, dx < \infty, \tag{6}$$

$$s_0 \in L^1(\mathbb{R}^d) \cap L^\infty(\mathbb{R}^d), \text{ and } s_0 \geq 0 \text{ a.e. in } \mathbb{R}^d. \tag{7}$$

We denote by $(\phi')^{1/2}$ a symmetric square root of ϕ' and ψ its antiderivative,

$$\sum_{k=1}^{d} (\phi'^{1/2})_{ik} (\phi'^{1/2})_{jk} = \phi'_{ij}, \quad \psi'_{ik}(c) = (\phi'^{1/2}(c))_{ik}. \tag{8}$$

The main result of this Section is the following existence result which states the main properties that will be used for the relaxation limit.

Theorem 1
Under assumptions (4)-(7), problem (P_k) admits a unique solution $(c,s) \in \mathcal{C}(\mathbb{R}^+; L^1(\mathbb{R}^d))^2$. Moreover the following properties hold:

(i) Maximum principle:

$$0 \leq c(t,x) \leq \|c_0\|_{L^\infty(\mathbb{R}^d)}, \quad \text{a.e. in } \mathbb{R}^+ \times \mathbb{R}^d, \tag{9}$$

$$0 \leq s(t,x) \leq \|s_0\|_{L^\infty(\mathbb{R}^d)}, \quad \text{a.e. in } \mathbb{R}^+ \times \mathbb{R}^d. \tag{10}$$

(ii) Contraction property: let (c,s) and $(\overline{c},\overline{s})$ be two solutions corresponding respectively to the initial data (c_0,s_0) and $(\overline{c}_0,\overline{s}_0)$. Then for any $t \geq 0$,

$$\|c(t)-\overline{c}(t)\|_{L^1(\mathbb{R}^d)} + \|s(t)-\overline{s}(t)\|_{L^1(\mathbb{R}^d)} \leq \|c_0-\overline{c}_0\|_{L^1(\mathbb{R}^d)} + \|s_0-\overline{s}_0\|_{L^1(\mathbb{R}^d)}. \tag{11}$$

(iii) Comparison property: let (c,s) and $(\overline{c},\overline{s})$ be two solutions corresponding respectively to the initial data (c_0,s_0) and $(\overline{c}_0,\overline{s}_0)$. If $c_0 \leq \overline{c}_0$ and $s_0 \leq \overline{s}_0$ then for any $t \geq 0$,

$$c(t) \leq \overline{c}(t) \quad \text{and} \quad s(t) \leq \overline{s}(t) \quad \text{a.e. in } \mathbb{R}^d. \tag{12}$$

(iv) Entropy inequality: for any two smooth increasing functions S and Σ , with S convex, and with the notations $(\mathbf{A^S})' = \mathbf{A}'S'$, $(\phi_{ij}^S)' = \phi_{ij}' S'$, $(\psi_{ik}^S)' = (S'')^{1/2}\,(\phi'^{1/2})_{ik}$, we have $\forall\, k = 1, \dots d$,

$$\sum_{i=1}^{d} \frac{\partial (\phi'^{1/2}(c))_{ik}}{\partial x_i} \in L^2(\mathbb{R}^+ \times \mathbb{R}^d),$$

$$S''(c) \sum_{i=1}^{d} \frac{\partial (\phi'^{1/2}(c))_{ik}}{\partial x_i} = \sum_{i=1}^{d} \frac{\partial \psi_{ik}^S(c)}{\partial x_i} := (\nabla \cdot \psi^S(c))_k,$$

$$\partial_t [S(c) + \Sigma(s)] + div\, \mathbf{A^S}(c) - \sum_{i,j=1}^{d} \frac{\partial^2 \phi_{ij}^S(c)}{\partial x_i \partial x_j} + \sum_{k=1}^{d} |\nabla \cdot \psi^S(c)|^2 \leq 0. \qquad (13)$$

Before recalling the proof of this Theorem, let us point out that, even though we did not see a complete statement and proof for a coupled system, the principles behind are not new (see for instance [25], [27], [46] or the earlier work by P. Marcati [78]). Also some assumptions can be slightly improved; the space quadratic moment in (6) is not needed, and a purely L^1 assumption on c is enough (see [84], [27]).

Lemma 1
We assume there is an $\alpha > 0$ such that

$$(\phi') \geq \alpha . Id \qquad (14)$$

Then any solution $(c, s) \in \mathcal{C}^\infty(\mathbb{R}^+; \mathcal{S}(\mathbb{R}^d))$ to equations (1) i.e. with data in $\mathcal{S}(\mathbb{R}^d)$, satisfies properties (9)–(13). In addition we have for any $t \geq 0$,

$$\begin{aligned} \|\partial_t c(t)\|_{L^1(\mathbb{R}^d)} + \|\partial_t s(t)\|_{L^1(\mathbb{R}^d)} \quad &\leq \quad \beta \|\nabla c_0\|_{L^1(\mathbb{R}^d)} + \| \sum_{i,j=1}^{d} \frac{\partial^2 \phi_{ij}(c_0)}{\partial x_i \partial x_j} \|_{L^1(\mathbb{R}^d)} \\ &\quad + 2k \|c_0 s_0\|_{L^1(\mathbb{R}^d)} \end{aligned} \qquad (15)$$

where $\beta = \sup_{|\xi| \leq \|c_0\|_{L^\infty(\mathbb{R}^d)}} |\mathbf{A}'(\xi)|$.

Proof of Lemma 1. We first notice that

$$s(t,x) = s_0(x) \exp\left(-k \int_0^t c(\xi, x)\, d\xi \right), \qquad (16)$$

thus, in view of (7), $s \geq 0$ almost everywhere. Multiplying the first equation of (1) by $c_- = \max(0, -c)$ and integrating, we obtain:

$$\frac{1}{2} \frac{d}{dt} \int_{\mathbb{R}^d} c_-^2 + \int_{\mathbb{R}^d} |\phi'^{1/2}(c) \cdot \nabla c_-|^2 = - \int_{\mathbb{R}^d} k s (c_-)^2 - \int_{\mathbb{R}^d} \mathbf{A}'(c) \cdot \nabla c_- c_-.$$

For the time being, we assume there exists $\beta > 0$ such that

$$\|A_i'\|_{L^\infty(\mathbb{R})} \leq \beta, \tag{17}$$

for $i = 1, \ldots, d$. Thus,

$$\frac{d}{dt}\int_{\mathbb{R}^d} c_-^2 + \alpha \int_{\mathbb{R}^d} |\nabla c_-|^2 \leq \frac{\beta^2}{\alpha}\int_{\mathbb{R}^d} c_-^2.$$

Gronwall's lemma thus gives $c_- = 0$ since c_0 is supposed to be nonnegative. Next, introducing the function $v = c - \|c_0\|_{L^\infty(\mathbb{R}^d)}$ and using analogous argument with the function $v_+ = \max(0, v)$, we finally obtain (9). Notice that relation (10) is obvious in view of (16).

Next, we relax assumption (17) by a standard argument that we just sketch: we introduce a cut-off function $\zeta \in \mathcal{C}^\infty(\mathbb{R})$ satisfying $\zeta(\xi) = 1$ if $\xi \leq \|c_0\|_{L^\infty(\mathbb{R}^d)}$ and $\zeta(\xi) = 0$ if $\xi \geq \|c_0\|_{L^\infty(\mathbb{R}^d)} + 1$, and we let $\tilde{\mathbf{A}} = \zeta \mathbf{A}$. The function $\tilde{\mathbf{A}}$ clearly satisfies a relation like (17), thus we can use the above arguments. In particular we can prove (9), which implies $\tilde{\mathbf{A}}(c) = \mathbf{A}(c)$.

We now turn to the proof of properties (11) and (12). Let S_δ be a $\mathcal{C}^2(\mathbb{R})$ convex real function, and let (c, s) and $(\overline{c}, \overline{s})$ be two regular solutions to (1) corresponding to the initial regular data (c_0, s_0) and $(\overline{c}_0, \overline{s}_0)$. A substraction and a multiplication by $S_\delta'(c - \overline{c})$ yields:

$$\begin{aligned}\frac{\partial}{\partial t} S_\delta(c-\bar{c}) + \operatorname{div}\left(S_\delta'(c-\bar{c})(\mathbf{A}(c) - \mathbf{A}(\bar{c}))\right) - S_\delta''(c-\overline{c})\nabla(c-\bar{c})\cdot(\mathbf{A}(c) - \mathbf{A}(\bar{c})) \\ - S_\delta'(c-\bar{c})\sum_{i,j=1}^{d} \frac{\partial^2(\phi_{ij}(c) - \phi_{ij}(\bar{c}))}{\partial x_i \partial x_j} = S_\delta'(c-\bar{c})(-k(c-\bar{c})s + k\bar{c}(s-\bar{s})).\end{aligned} \tag{18}$$

The integral over $\mathbb{R}^d$ of the second term of (18) vanishes. We estimate the third one as follows:

$$-\int_{\mathbb{R}^d} |S_\delta''(c-\overline{c})\nabla(c-\bar{c})\cdot(\mathbf{A}(c)-\mathbf{A}(\bar{c}))| = \int_{\mathbb{R}^d} |(c-\overline{c})S_\delta''(c-\overline{c})\nabla(c-\bar{c})\cdot\frac{\mathbf{A}(c)-\mathbf{A}(\overline{c})}{c-\overline{c}}|.$$

Thus, we can choose S_δ such that $S_\delta(c) \to |c|$ in $L^\infty(\mathbb{R})$ as $\delta \to 0$, and $(c-\overline{c})S_\delta''(c-\overline{c})$ bounded and vanishing as $\delta \to 0$ uniformly away from 0. Therefore the third term of (18) also vanishes in $L^1(\mathbb{R}^d)$ for all times because

c, $\overline{c}$ are smooth and decaying here. For the fourth term, we notice that:

$$
\begin{aligned}
-\sum_{i,j=1}^{d}\int_{\mathbb{R}^d} S'_\delta(c-\overline{c})\,\frac{\partial^2\Big(\phi_{ij}(c)-\phi_{ij}(\overline{c})\Big)}{\partial x_i\partial x_j}
&= \sum_{i,j=1}^{d}\int_{\mathbb{R}^d} S''_\delta(c-\overline{c})\partial_{x_i}(c-\overline{c})\Big(\phi'_{ij}(c)\partial_{x_j}c-\phi'_{ij}(\overline{c})\partial_{x_j}\overline{c}\Big)\\
&= \sum_{i,j=1}^{d}\int_{\mathbb{R}^d} S''_\delta(c-\overline{c})\partial_{x_i}(c-\overline{c})\phi'_{ij}(c)\partial_{x_j}(c-\overline{c})\\
&\quad+\sum_{i,j=1}^{d}\int_{\mathbb{R}^d} S''_\delta(c-\overline{c})\partial_{x_i}(c-\overline{c})\Big(\phi'_{ij}(c)-\phi'_{ij}(\overline{c})\Big)\partial_{x_j}\overline{c}\\
&= \sum_{i,j=1}^{d}\int_{\mathbb{R}^d} S''_\delta(c-\overline{c})\partial_{x_i}(c-\overline{c})\phi'_{ij}(c)\partial_{x_j}(c-\overline{c})\\
&\quad+\sum_{i,j=1}^{d}\int_{\mathbb{R}^d}(c-\overline{c})S''_\delta(c-\overline{c})\partial_{x_i}(c-\overline{c})\frac{\phi'_{ij}(c)-\phi'_{ij}(\overline{c})}{c-\overline{c}}\partial_{x_j}\overline{c}.
\end{aligned}
$$

The first term is nonnegative. Passing to the limit as $\delta\to 0$ in the second, it vanishes as in the third term.
Finally, we deduce from (18)

$$\frac{d}{dt}\int_{\mathbb{R}^d}|c-\overline{c}|\le -k\int_{\mathbb{R}^d}|c-\overline{c}|s+k\int_{\mathbb{R}^d}\overline{c}|s-\overline{s}|.$$

Similarly, we easily obtain:

$$\frac{d}{dt}\int_{\mathbb{R}^d}|s-\bar{s}|\le k\int_{\mathbb{R}^d}|c-\bar{c}|s-k\int_{\mathbb{R}^d}\bar{c}|s-\bar{s}|.$$

By summing these last two inequalities, we deduce

$$\frac{d}{dt}\int_{\mathbb{R}^d}(|c-\bar{c}|+|s-\bar{s}|)\le 0,$$

which gives the contraction property (11). Choosing S_δ such that $S_\delta(c)\to c_+$ as $\delta\to 0$ gives, by the same arguments, the comparison property (12).

Finally, let us prove (15). We denote $\partial_t c$ (resp. $\partial_t s$) by u (resp. v), we differentiate the first two equations of (1) with respect to t and we multiply them respectively by $\mathrm{sgn}(u)$ and $\mathrm{sgn}(v)$:

$$
\left\{\begin{array}{l}
\dfrac{\partial|u|}{\partial t}+\displaystyle\sum_{i=1}^{d}\frac{\partial}{\partial x_i}\Big(A'_i(c)|u|\Big)-\mathrm{sgn}(u)\sum_{i,j=1}^{d}\frac{\partial^2\Big(\phi'_{ij}(c)u\Big)}{\partial x_i\partial x_j}=-k|u|s-\mathrm{sgn}(u)kcv,\\
\qquad\qquad\qquad\qquad\qquad\qquad\qquad\qquad\qquad\qquad\qquad\qquad\partial_t|v|=-\mathrm{sgn}(v)kus-kc|v|.
\end{array}\right.
\tag{19}
$$

Thanks to the decay assumption, $(c,s) \in \mathcal{S}(\mathbb{R}^d)$, the integral of $\partial_{x_i}\Big(A_i'(c)|u|\Big)$ over $\mathbb{R}^d$ vanishes. Let us check that the integral of $-\mathrm{sgn}(u)\displaystyle\sum_{i,j=1}^{d}\frac{\partial^2\Big(\phi_{ij}'(c)u\Big)}{\partial x_i\partial x_j}$ is nonnegative. We denote by H_δ a monotone C^∞ function such that $H_\delta(u)\to \mathrm{sgn}(u)$ in $L^1(\mathbb{R})$ as $\delta\to 0$, we have:

$$\begin{aligned}-\int_{\mathbb{R}^d} H_\delta(u)\frac{\partial^2\Big(\phi_{ij}'(c)u\Big)}{\partial x_i\partial x_j} &= \int_{\mathbb{R}^d} H_\delta'(u)\partial_{x_i}u\Big(\phi_{ij}'(c)\partial_{x_j}u+\partial_{x_j}\phi_{ij}'(c)u\Big)\\ &\geq \int_{\mathbb{R}^d}\frac{\partial}{\partial x_i}H_\delta(u)u\partial_{x_j}\phi_{ij}'(c)\\ &= -\int_{\mathbb{R}^d}\mathcal{K}_\delta(u)\frac{\partial^2\phi_{ij}'(c)}{\partial x_i\partial x_j}.\end{aligned}$$

With $\mathcal{K}_\delta'(u)=H_\delta'(u)u$ and $\mathcal{K}_\delta(u)\to 0$ as $\delta\to 0$. Therefore letting $\delta\to 0$, this inequality becomes

$$-\int_{\mathbb{R}^d}\mathrm{sgn}(u)\frac{\partial^2\Big(\phi_{ij}'(c)u\Big)}{\partial x_i\partial x_j}\geq 0.$$

Thus, we deduce from (19),

$$\frac{d}{dt}\int_{\mathbb{R}^d}|u|+\frac{d}{dt}\int_{\mathbb{R}^d}|v|\leq -k\int_{\mathbb{R}^d}|u|s+k\int_{\mathbb{R}^d}c|v|+k\int_{\mathbb{R}^d}|u|s-k\int_{\mathbb{R}^d}c|v|\leq 0,$$

and therefore

$$\begin{aligned}\int_{\mathbb{R}^d}|\partial_t c|+|\partial_t s| &\leq \int_{\mathbb{R}^d}|(\partial_t c)_{t=0}|+|(\partial_t s)_{t=0}|\\ &\leq \int_{\mathbb{R}^d}|\mathrm{div}\,\mathbf{A}(c_0)|+\int_{\mathbb{R}^d}\Big|\sum_{i,j=1}^{d}\frac{\partial^2\phi_{ij}(c_0)}{\partial x_i\partial x_j}\Big|+2\int_{\mathbb{R}^d}kc_0s_0.\end{aligned}$$

It remains to show (13), which simply follows from the chain rule and space-time integration (we may always assume that $S(0)=\Sigma(0)=0$ and therefore S and Σ are nonnegative on the range of interest for (c,s)), thus we skip the calculations. This achieves the proof of Lemma 1. $\diamondsuit$

Lemma 2
We assume $c_0\in L^2(\mathbb{R}^d)\cap L^\infty(\mathbb{R}^d)$, and we assume that the diffusion does not degenerate, i.e. *(14) is satisfied. Then, for all $T>0$, problem (1) has a solution $(c,s)\in L^2(0,T;H^1(\mathbb{R}^d))\cap\mathcal{C}([0,T];L^2(\mathbb{R}^d))$. If we assume moreover that $c_0,s_0\in\mathcal{S}(\mathbb{R}^d)$ and $\mathbf{A},\phi\in\mathcal{C}^\infty(\mathbb{R})$, then $c,s\in\mathcal{C}^\infty((0,T);\mathcal{S}(\mathbb{R}^d))$.*

Proof of Lemma 2.

Step 1. We first assume there exists $\beta>0$ such that

$$\|\phi'\|_{L^\infty(\mathbb{R})}\leq\beta \quad\text{and}\quad \|A_i'\|_{L^\infty(\mathbb{R})}\leq\beta, \tag{20}$$

for $i = 1, \ldots, d$. We restrict problem (1) to $\Omega_R = \{x \in \mathbb{R}^d, |x| \leq R\}$, R being a given nonnegative real, and we complement it with Dirichlet homogenous boundary conditions on $\partial\Omega_R$ for c. We thus consider the system

$$\begin{aligned} \partial_t c + \operatorname{div} \mathbf{A}(c) - \operatorname{div}(\phi'(c)\nabla c) &= -k\, c\, s, && (21)\\ \partial_t s &= -k\, c\, s, && (22)\\ c(t,x) &= 0 \text{ on } [0,T] \times \partial\Omega_R, && (23)\\ c(0,\cdot) &= c_0 \chi_R \quad \text{on } \Omega_R, && (24)\\ s(0,\cdot) &= s_0 \chi_R \quad \text{on } \Omega_R, && (25) \end{aligned}$$

where χ_R denotes the characteristic function of Ω_R. We introduce the following convex set of the Banach space $L^2(0,T;L^2(\Omega_R))$:

$$\mathcal{C} = \{v \in L^2(0,T;L^2(\Omega_R)), \|v\|^2_{L^2(0,T;L^2(\Omega_R))} \leq m, \text{ and } v \geq 0 \text{ a.e. in } (0,T)\times\Omega_R\},$$

m being a nonnegative constant that will be fixed later. For $\overline{c} \in \mathcal{C}$, we define $\overline{s}$ by

$$\overline{s}(x,t) = s_0(x) \exp\left(-k \int_0^t \overline{c}(x,\xi)\, d\xi\right), \qquad (26)$$

which is the solution to $\partial_t \overline{s} = -k\overline{c}\,\overline{s}$ satisfying $\overline{s}|_{t=0} = s_0$. Notice that in particular, for all $t \in [0,T]$, $\|\overline{s}(t)\|_{L^\infty(\Omega_R)} \leq \|s_0\|_{L^\infty(\Omega_R)}$. Then, we define c as the solution in $L^2(0,T;H^1_0(\Omega_R)) \cap L^\infty(0,T;L^2(\Omega_R))$ to:

$$\partial_t c + \operatorname{div}\left(\frac{\mathbf{A}(\overline{c})}{\overline{c}} c\right) - \operatorname{div}(\phi'(\overline{c})\nabla c) = -k\, c\, \overline{s}.$$

Notice that the existence of c comes from standard theory on non-degenerate linear parabolic problems. We denote by $\mathcal{T}$ the application $\overline{c} \to \mathcal{T}\overline{c} = c$. Our purpose is to prove that, for $\overline{c} \in \mathcal{C}$, $\mathcal{T}\overline{c} \in \mathcal{C}$ (for a suitable m), and to prove that $\mathcal{T}\overline{c}$ lies in a compact set of $L^2(0,T;L^2(\Omega_R))$ in order to apply Schauder fixed point theorem.

It is well-known that $\partial_t c \in L^2(0,T;H^{-1}(\Omega_R))$, which yields in particular $c \in \mathcal{C}([0,T];L^2(\Omega_R))$ and which makes rigorous all the manipulations we are going to do now. Multiplying by c and integrating we obtain:

$$\frac{1}{2}\frac{d}{dt}\int_{\Omega_R} c^2 + \sum_{i,j=1}^d \int_{\Omega_R} \phi'_{ij}(\overline{c})\nabla_i c \cdot \nabla_j c = -k\int_{\Omega_R} c^2 \overline{s} + \int_{\Omega_R} \frac{\mathbf{A}(\overline{c})}{\overline{c}} c \cdot \nabla c,$$

which gives, using (14), (20) and the fact that $\overline{s} \geq 0$,

$$\frac{d}{dt}\int_{\Omega_R} c^2 + \alpha \int_{\Omega_R} |\nabla c|^2 + \leq \frac{\beta^2}{\alpha}\int_{\Omega_R} c^2.$$

In particular,

$$\sup_{t\in[0,T]} \|c(t)\|^2_{L^2(\Omega_R)} \leq \|c_0\|_{L^2(\Omega_R)} e^{\beta^2 T/\alpha}.$$

Thus, choosing $m = T\|c_0\|_{L^2(\mathbb{R}^d)}e^{\beta^2 T/\alpha}$, we have $\|c\|_{L^2(0,T;L^2(\Omega_R))} \leq m$. Next, multiplying (21) by $c_- = \max(0,-c)$ and integrating, we obtain:

$$\frac{1}{2}\frac{d}{dt}\int_{\Omega_R} c_-^2 + \int_{\Omega_R} \frac{\mathbf{A}'(\overline{c})}{\overline{c}} \cdot \nabla c_- c_- + \sum_{i,j=1}^{d} \int_{\Omega_R} \phi'_{ij}(\overline{c}) \nabla_i c \cdot \nabla_j c = -\int_{\Omega_R} ksc_-,$$

which gives:

$$\frac{1}{2}\frac{d}{dt}\int_{\Omega_R} c_-^2 + \alpha \int_{\Omega_R} |\nabla c_-|^2 \leq \beta \int_{\Omega_R} |\nabla c_-| c_-.$$

Young inequality and Gronwall's lemma thus give $c_- = 0$, since c_0 is supposed to be nonnegative. Thus $c \in \mathcal{C}$.
We now check that $\partial_t c$ is bounded in $L^2(0,T;H^{-1}(\Omega_R))$. Let $v \in L^2(0,T;H_0^1(\Omega_R))$:

$$\begin{aligned}
\int_0^T < \partial_t c, v > &= \int_0^T \int_{\Omega_R} \left(-\phi'_{ij}(\overline{c}) \nabla_i c \cdot \nabla_j v + \frac{\mathbf{A}(\overline{c})}{\overline{c}} c \cdot \nabla v - k\overline{s}cv \right) \\
&\leq (\beta \|c\|_{L_t^2(H_x^1)} + \beta \|\overline{c}\|_{L_{x,t}^2}) \|v\|_{L_t^2(H_x^1)} + k\|s_0\|_{L_x^\infty} \|c\|_{L_{t,x}^2} \|v\|_{L_{t,x}^2} \\
&\leq C\|v\|_{L_t^2(H_x^1)}.
\end{aligned}$$

Thus, $\partial_t c$ is bounded in $L^2(0,T;H^{-1}(\Omega_R))$, and since c is also bounded in $L^2(0,T;H^1(\Omega_R))$, this proves that c is compact in $L^2(0,T;L^2(\Omega_R))$, and therefore the application $\mathcal{T}$ has a fixed point which is a solution to (21)-(25). Notice that we can finally relax assumption (20) as in the proof of Lemma 1.

Step 2. We denote by (c_R, s_R) the solution on Ω_R built above. For $R_1 > R_2$, we have obviously $c_0\chi_{R_1} \geq c_0\chi_{R_2}$ and $s_0\chi_{R_1} \geq s_0\chi_{R_2}$. Thus, for all $t > 0$, $(c_R(t), s_R(t))_R$ is an increasing sequence, bounded in $(L^2(\mathbb{R}^d))^2$ (in step 1, the definition of the bound m was independent of Ω_R). Letting $R \to \infty$ and applying the monotone convergence theorem, this proves the existence of the solution on $\mathbb{R}^d$. The regularity result is a consequence of classical theory of non-degenerate parabolic problems (see [74] and [95] for example). $\diamondsuit$

Proof of Theorem 1. We proceed in two steps.

Step 1. In this step, we assume that $c_0 \in \mathcal{S}(\mathbb{R}^d)$ and $s_0 \in \mathcal{S}(\mathbb{R}^d)$. We denote by ϕ_ε (resp. $\mathbf{A}_\varepsilon$) a suitable regularization of ϕ (resp. $\mathbf{A}$), in particular, we assume that $\phi'_\varepsilon \geq \varepsilon Id$. We consider the system

$$\left\{ \begin{array}{rcl} \partial_t c_\varepsilon + \operatorname{div} \mathbf{A}_\varepsilon(c_\varepsilon) - \operatorname{div}\left(\phi'_\varepsilon(c_\varepsilon)\nabla c_\varepsilon\right) &=& -k\, c_\varepsilon\, s_\varepsilon, \\ \partial_t s_\varepsilon &=& -k\, c_\varepsilon\, s_\varepsilon. \end{array} \right. \tag{27}$$

We now aim at showing that the set $\{(c_\varepsilon, s_\varepsilon)\}_{\varepsilon>0}$ is compact in $\mathcal{C}(0,T;L^1(\mathbb{R}^d))$.

Let $h = (h_1, \ldots, h_d) \in \mathbb{R}^d$, with $h_i > 0$ for $i = 1, \ldots, d$. We define $\tau_h c_\varepsilon(t,x) = c_\varepsilon(t, x+h)$ and $\tau_h s_\varepsilon(t,x) = s_\varepsilon(t,x+h)$. Clearly, $\tau_h c_\varepsilon$ and $\tau_h s_\varepsilon$

satisfies (27) with initial data defined by $\tau_h c_0(x) = c_0(x+h)$ and $\tau_h s_0(x) = s_0(x+h)$. Thus, the contraction property (11) gives for all $t \in [0,T]$:

$$\begin{aligned} \|\tau_h c_\varepsilon(t) - c_\varepsilon(t)\|_{L^1(\mathbb{R}^d)} + &\|\tau_h s_\varepsilon(t) - s_\varepsilon(t)\|_{L^1(\mathbb{R}^d)} \\ &\leq \|\tau_h c_0 - c_0\|_{L^1(\mathbb{R}^d)} + \|\tau_h s_0 - s_0\|_{L^1(\mathbb{R}^d)}. \end{aligned} \tag{28}$$

The right-hand side of this inequality tends to zero as $h \to 0$, thus, the Riez-Fréchet-Kolmogorov theorem (see [19] for example) implies the local relative compactness of $(c_\varepsilon(t,\cdot), s_\varepsilon(t,\cdot))$ in $(L^1(\mathbb{R}^d))^2$ for all $t \in [0,T]$. To show the global relative compactness, we multiply

$$\partial_t c_\varepsilon + \operatorname{div} \mathbf{A}_\varepsilon(c_\varepsilon) - \operatorname{div}\left(\phi_\varepsilon'(c_\varepsilon)\nabla c\right) = -k c_\varepsilon s_\varepsilon$$

by $|x|^2/2$ and we integrate by parts. We obtain, using $c_\varepsilon \geq 0$ and $s_\varepsilon \geq 0$,

$$\frac{d}{dt}\int_{\mathbb{R}^d} \frac{|x|^2}{2} c_\epsilon \, dx - \int_{\mathbb{R}^d} x \cdot \mathbf{A}_\varepsilon(c_\epsilon) \, dx - d\int_{\mathbb{R}^d} Tr\phi_\varepsilon(c_\epsilon) \, dx \leq 0.$$

Now, denoting $\int_{\mathbb{R}^d} \frac{|x|^2}{2} c_\epsilon \, dx$ by $\mathcal{R}(t)$, and using (9),

$$\frac{d}{dt}\mathcal{R}(t) \leq C\left(\int_{\mathbb{R}^d} |x| c_\epsilon \, dx + \int_{\mathbb{R}^d} c_\epsilon \, dx\right),$$

where, here and in the sequel, C denotes various constants independent of ε. Thus

$$\frac{d}{dt}\mathcal{R}(t) \leq C(\mathcal{R}(t) + M(t)),$$

with $M(t) = \int_{\mathbb{R}^d} c_\epsilon \, dx$. Since $M(t) \leq M(0)$, Gronwall lemma implies that $\mathcal{R}(t)$ is bounded by a value independent of ε as soon as $\mathcal{R}(0)$ is finite, which was assumed in (6). This yields the equiintegrability of $\{c_\varepsilon\}_\varepsilon$. Therefore, using analogous arguments for $\{s_\varepsilon\}_\varepsilon$, we deduce the relative compactness of $\{(c_\varepsilon, s_\varepsilon)\}$ in $(L^1(\mathbb{R}^d))^2$ for all $t \in [0,T]$.

Finally, we obtain from (15), for $0 < t_1 < t_2 < T - \eta$,

$$\begin{aligned} &\sup_{t\in[t_1,t_2]} \|c_\varepsilon(t+\eta) - c_\varepsilon(t)\|_{L^1(\mathbb{R}^d)} + \sup_{t\in[t_1,t_2]} \|s_\varepsilon(t+\eta) - s_\varepsilon(t)\|_{L^1(\mathbb{R}^d)} \\ &\leq \sup_{t\in[t_1,t_2]} \left\| \int_0^\eta \partial_t c_\varepsilon(t+\xi) \, d\xi \right\|_{L^1(\mathbb{R}^d)} + \sup_{t\in[t_1,t_2]} \left\| \int_0^\eta \partial_t s_\varepsilon(t+\xi) \, d\xi \right\|_{L^1(\mathbb{R}^d)} \\ &\leq \beta\eta \|\nabla c_0\|_{L^1(\mathbb{R}^d)} + \eta \|\operatorname{div}\left(\phi_\varepsilon'(c_0)\nabla c_0\right)\|_{L^1(\mathbb{R}^d)} + 2k\eta \|c_0 \, s_0\|_{L^1(\mathbb{R}^d)}. \end{aligned}$$

Thus, by Ascoli theorem, $\{(c_\varepsilon, s_\varepsilon)\}_\varepsilon$ is relatively compact in $\mathcal{C}(0,T;L^1(\mathbb{R}^d))^2$. Therefore, up to an extraction, $(c_\varepsilon, s_\varepsilon)$ converges in $\mathcal{C}(0,T;L^1(\mathbb{R}^d))^2$ and a.e. to (c,s). Passing to the limit in (27), we deduce that (c,s) is a solution to (1). Moreover passing to the limit in the relations established in Lemma 1,

this solution satisfies (9)– (13).

Step 2. We now relax the regularity assumptions on (c_0, s_0). Let c_0^n and s_0^n be two sequences of $\mathcal{S}(\mathbb{R}^d)$ converging to c_0 and s_0 in $L^1(\mathbb{R}^d)$. According to step 1, there exists a solution (c_n, s_n) to system (1) corresponding to the initial data (c_0^n, s_0^n) which satisfies the contraction property (11). This last point implies in particular that (c_n, s_n) is a Cauchy sequence in the Banach space $\mathcal{C}(0,T;L^1(\mathbb{R}^d))$. Thus, (c_n, s_n) converges in $\mathcal{C}(0,T;L^1(\mathbb{R}^d))$ to (c,s) which is solution to (1) and which satisfies properties (9)–(12). As for (13), we have a uniform $L^2(\mathbb{R}^+ \times \mathbb{R}^d)$ bound on $\nabla \cdot \phi'^{1/2}(c^n)$. Therefore, following [27] the strong limit $\psi^S(c)$ of $\psi^S(c^n)$ satisfies the chain rule by strong-weak convergence, and $|\nabla \cdot \psi^S(c)| \leq lim_{n\to\infty} |\nabla \cdot \psi^S(c^n)|$ as a weak L^2 limit. Hence we deduce the inequality (13) for (c,s). $\diamondsuit$

3 Asymptotic behaviour

Theorem 2
We make the assumptions (4)-(7). As k tends to infinity, the solution (c_k, s_k) to (P_k), has a limit in $L^1((0,T)\times\mathbb{R}^d)^2$ denoted by $(c,s) \in L^\infty(\mathbb{R}^+; L^1(\mathbb{R}^d))^2$ that satisfies

$$(P_\infty) \begin{cases} \partial_t(c-s) + div\,\mathbf{A}(c) - \displaystyle\sum_{i,j=1}^{d} \frac{\partial^2 \phi_{ij}(c)}{\partial x_i \partial x_j} &= 0, \quad \text{in } \mathcal{D}'((0,T)\times\mathbb{R}^d), \\ c \geq 0,\ s \geq 0,\ c\,s &= 0, \quad \text{a.e. in } (0,T)\times\mathbb{R}^d, \\ c(0,x) - s(0,x) &= c_0(x) - s_0(x) \quad \text{a.e. in } \mathbb{R}^d. \end{cases}$$

Moreover, (c,s) is the unique entropy solution to (P_∞) i.e. for any two smooth increasing functions S and Σ, with S convex, and with the notations $(\mathbf{A^S})' = \mathbf{A}'S'$, $(\phi^S)' = \phi' S'$, $(\psi^S)' = (S'')^{1/2}\phi'^{1/2}$, it satisfies

$$\nabla \cdot \phi'^{1/2}(c) \in (L^2(\mathbb{R}^+ \times \mathbb{R}^d))^d, \quad \nabla \cdot \psi^S(c) = (S'')^{1/2}\phi'^{1/2}(c),$$

$$\partial_t[S(c) + \Sigma(s)] + div\,\mathbf{A^S}(c) - \sum_{i,j=1}^{d} \frac{\partial^2 \phi_{ij}^S(c)}{\partial x_i \partial x_j} + \sum_{k=1}^{d} |\nabla \cdot \psi^S(c)|^2 \leq 0. \qquad (29)$$

Finally, $w = c - s \in \mathcal{C}(\mathbb{R}^+; L^1(\mathbb{R}^d))$ is the unique entropy solution to the generalized Stefan equation (2).

Proof.

Relation with the generalized Stefan equation, uniqueness Before proving the hard core of this theorem, let us explain the relation between its limit (P_∞) and (Q_∞) in (2). From the sign condition on (c,s), and $c\,s = 0$, we can invert $(c,s) \to w = c - s$ as follows:

$$w \geq 0 \leftrightarrow c = w,\ s = 0, \quad \text{and} \quad w \leq 0 \leftrightarrow s = -w,\ c = 0.$$

This defines a lipschitz continuous inverse for c: $c = w_+$ and the two problems are thus equivalent. Also the entropy inequalities can be translated in terms of w. We firstly restrict our choice to $S(0) = \Sigma(0) = 0$ and extend S to negative values by $S(w) = S(w_+) + \Sigma(w_-)$; thus we reach all smooth functions $S(w)$ such that S is convex for $w \geq 0$ and $\mathrm{sgn} S'(w) = \mathrm{sgn} w$, and we have $\nabla \cdot \psi^S(w) \in L^2(\mathbb{R}^+ \times \mathbb{R}^d)$ and

$$\partial_t S(w) + \mathrm{div}\, \mathbf{A^S}(w) - \sum_{i,j=1}^{d} \frac{\partial^2 \phi_{ij}^S(w)}{\partial x_i \partial x_j} + |\nabla \cdot \psi^S(w)|^2 \leq 0, \tag{30}$$

with A^S, ϕ^S, ψ_{ij}^S extended by 0 to negative values of their argument. Endowed with its initial value, this hyperbolic-parabolic admits a unique entropy solution in $\mathcal{C}(\mathbb{R}^+; L^1(\mathbb{R}^d))$ (see the references in the introduction). Therefore we have obtained the relation between the two problems and the uniqueness of the limit.

Existence of a limit For $h \in \mathbb{R}^d$, we denote by $\tau_h c_k$ (resp. $\tau_h s_k$) the function $(t,x) \to \tau_h c_k(t,x) = c_k(t, x+h)$ (resp. $(t,x) \to \tau_h s_k(t,x) = s_k(t,x+h)$). For $\eta \in \mathbb{R}$, we denote by $\mathcal{T}_\eta c_k$ the function $(t,x) \to \mathcal{T}_\eta c_k(t,x) = c_k(t+\eta, x)$). We denote by $\omega(\cdot)$ the initial L^1 modulus of continuity

$$\omega(h) = \sup_{|\bar{h}| \leq h} \|c^0(\cdot + \bar{h}) - c^0(\cdot)\|_{L^1(\mathbb{R}^d)} + \|s^0(\cdot + \bar{h}) - s^0(\cdot)\|_{L^1(\mathbb{R}^d)}.$$

We begin by proving the compactness of s_k. Integrating $\partial_t s_k = -k c_k s_k$ and using $s_k \geq 0$, we obtain for all $T > 0$,

$$k \int_0^T \!\!\int_{\mathbb{R}^d} c_k s_k \, dx \, dt = -\int_{\mathbb{R}^d} \Big(s_k(T,x) - s_k(0,x) \Big) \, dx \leq \int_{\mathbb{R}^d} s_0 \, dx \stackrel{\text{def}}{=} m_0. \tag{31}$$

Thus we have

$$k \|c_k \, s_k\|_{L^1(\mathbb{R}^+ \times \mathbb{R}^d)} \leq m_0, \qquad c_k s_k \to 0 \text{ in } L^1(\mathbb{R}^+ \times \mathbb{R}^d) \text{ as } k \to \infty. \tag{32}$$

Notice that this also shows that $\|\partial_t s_k\|_{L^1_{t,x}} \leq m_0$, and since

$$\begin{aligned} \|\tau_h s_k - s_k\|_{L^1(\mathbb{R}^+ \times \mathbb{R}^d)} &\leq T \|\tau_h c_0 - c_0\|_{L^1(\mathbb{R}^d)} + T \|\tau_h s_0 - s_0\|_{L^1(\mathbb{R}^d)} \\ &\leq T\, \omega(|h|), \end{aligned}$$

we deduce the local compactness of $(s_k)_k$ in $L^1((0,T) \times \mathbb{R}^d)$.

Let us now prove the compactness of $(c_k)_k$ relying on an improvment by A. E. Tzavaras [98] of a classical regularization argument. First of all, we have space compactness because using (11),

$$\begin{aligned} \|\tau_h c_k - c_k\|_{L^1((0,T) \times \mathbb{R}^d)} &\leq T \|\tau_h c_0 - c_0\|_{L^1(\mathbb{R}^d)} + T \|\tau_h s_0 - s_0\|_{L^1(\mathbb{R}^d)} \\ &\leq T\, \omega(|h|). \end{aligned} \tag{33}$$

Let ε be a positive constant that will be fixed later, and let $\rho_\varepsilon \in \mathcal{C}^\infty(\mathbb{R}^d)$ be a mollifier kernel vanishing outside the ball of radius ε centered in 0. Let t_1 and t_2 be such that $0 < t_1 < t_2 < T - \eta$, we have

$$\begin{aligned}\int_{t_1}^{t_2}\int_{\mathbb{R}^d} |\mathcal{T}_\eta c_k - c_k| \;\leq\; & \int_{t_1}^{t_2}\int_{\mathbb{R}^d} |\mathcal{T}_\eta c_k - \mathcal{T}_\eta(c_k * \rho_\varepsilon)| + \int_{t_1}^{t_2}\int_{\mathbb{R}^d} |c_k * \rho_\varepsilon - c_k| \\ & + \int_{t_1}^{t_2}\int_{\mathbb{R}^d} |\mathcal{T}_\eta(c_k * \rho_\varepsilon) - c_k * \rho_\varepsilon|.\end{aligned}$$

The first and the second terms of the right hand side are treated by the same way:

$$\int_{t_1}^{t_2}\int_{\mathbb{R}^d} |c_k * \rho_\varepsilon - c_k| \leq \int_{t_1}^{t_2}\int_{|y|<\varepsilon}\int_{\mathbb{R}^d} |c_k(t, x-y) - c_k(t,x)| \leq T\,\omega(\varepsilon).$$

For the third term of the right hand side, we first notice that

$$\partial_t(c_k * \rho_\varepsilon) = -\sum_{i=1}^d A_i(c_k) * \frac{\partial \rho_\varepsilon}{\partial x_i} + \sum_{i,j=1}^d \phi_{ij}(c_k) * \frac{\partial^2 \rho_\varepsilon}{\partial x_i \partial x_j} - k(c_k s_k) * \rho_\varepsilon,$$

thus, using (31),

$$\begin{aligned}\int_{t_1}^{t_2}\int_{\mathbb{R}^d} |\mathcal{T}_\eta(c_k * \rho_\varepsilon) - c_k * \rho_\varepsilon| \;&\leq\; \int_{t_1}^{t_2}\int_{\mathbb{R}^d}\int_{\xi=0}^{\eta} |\partial_t(c_k * \rho_\varepsilon)(t+\xi, x)| \\ &\leq\; \frac{\eta}{\varepsilon}\|\mathbf{A}(c_k)\|_{L^1_{t,x}} + \frac{\eta}{\varepsilon^2}\|\phi(c_k)\|_{L^1_{t,x}} + \eta\|k c_k s_k\|_{L^1_{t,x}} \\ &\leq\; C\left(\eta + \frac{\eta}{\varepsilon} + \frac{\eta}{\varepsilon^2}\right),\end{aligned}$$

where C is a constant independent of ε, η and k. Thus, choosing $\varepsilon = \eta^{1/3}$, there exists a constant $C > 0$, independent of k, such that

$$\|\mathcal{T}_\eta c_k - c_k\|_{L^1((t_1,t_2)\times\mathbb{R}^d)} \leq C\left(\eta^{1/3} + \omega(\eta^{1/3})\right). \tag{34}$$

We deduce from (33) and (34) the local compactness of $(c_k)_k$ in $L^1((0,T)\times\mathbb{R}^d)$. We can check the equiintegrability of $(c_k)_k$ and $(s_k)_k$ as in the proof of Theorem 1. We deduce that the set $(c_k, s_k)_k$ is compact in $L^1((0,T)\times\mathbb{R}^d)$, and thus, up to an extraction, $(c_k, s_k) \to (c, s)$ in $L^1((0,T)\times\mathbb{R}^d)$ as $k \to \infty$. Passing to the limit in (1) and using (32), we finally obtain (P_∞).

Time continuity of w=c-s The above proof uses compactnes in $L^1((0,T)\times\mathbb{R}^d)$ in order to be compatible with the generic initial layer (and possibly shock layer) which leads to the fact that $\partial_t c$ and $\partial_t s$ are only bounded measures in time. Nevertheless an additional cancellation arises on $c - s$ which

allows to prove time continuity. We argue as in previous subsection.

$$\begin{aligned}\int_{\mathbb{R}^d} |\mathcal{T}_\eta(c_k - s_k) * \rho_\varepsilon - (c_k - s_k) * \rho_\varepsilon| &\leq \int_{\xi=0}^{\eta} \int_{\mathbb{R}^d} |\partial_t (c_k - s_k)(\xi, \cdot) * \rho_\varepsilon| \\ &\leq \frac{\eta}{\varepsilon} \|\mathbf{A}(c_k)\|_{L^\infty_t L^1_x} + \frac{\eta}{\varepsilon^2} \|\phi(c_k)\|_{L^\infty_t L^1_x} \\ &\leq C\left(\frac{\eta}{\varepsilon} + \frac{\eta}{\varepsilon^2}\right).\end{aligned}$$

Also, we have

$$\int_{\mathbb{R}^d} |(c_k - s_k) * \rho_\varepsilon - (c_k - s_k)| \leq \omega(\varepsilon).$$

Therefore, we obtain choosing again $\varepsilon = \eta^{1/3}$, that, for some constant C independent of k and η, we have

$$\int_{\mathbb{R}^d} |\mathcal{T}_\eta(c_k - s_k) - (c_k - s_k)| \leq C\left(\eta^{1/3} + \omega(\eta^{1/3})\right).$$

which proves time continuity uniformly in k and achieves the proof of the asymptotic Theorem. $\diamondsuit$

Acknowledgements: The authors wish to thank François Bouchut for fruitful discussions.

Chapter 3

Homogenization approach to filtration through a fibrous medium

Le travail présenté dans ce chapitre a été effectué en collaboration avec Eric Cancès, Jean-Frédéric Gerbeau et Andro Mikelić. Il a donné lieu à un rapport de recherche INRIA (numéro RR-5277). Il a été soumis pour publication.

1 Introduction

Filtration through fibrous porous media is of considerable interest in various engineering systems. Common examples of fibrous media include industrial filters, biological tissues, certain polymer membranes and many materials produced in the paper industry.
In most applications, flow in porous media is modelled by using a generalized form of Darcy's law:

$$\mathbf{u} = -\frac{\boldsymbol{K}}{\nu}\nabla p, \tag{1}$$

where $\mathbf{u}$ is the filtration velocity, p denotes the fluid pressure, ν is the fluid viscosity and $\boldsymbol{K}$ stands for the permeability tensor of the porous material.
Darcy equations can be derived by means of homogenization techniques starting from the Stokes flow through an array of particles.
Ene and Sanchez-Palencia seem to be first to give a derivation of it, from the Stokes system, using a formal multiscale expansion (see [42]). This derivation was made rigorous in the case of a $2D$ periodic porous medium by L. Tartar in [94]. This result was generalized in number of other papers. We mention the generalization to $3D$ by G. Allaire [3] and to a random statistically homogeneous porous medium by Beliaev and Kozlov [16]. Another approach,

very much present in the engineering literature is the spatial volume averaging. For computing effective parameters averaging is equivalent to the usual stochastic homogenization. For the introduction to the method we refer to [69]. The derivation of Darcy's law by volume averaging is in [100]. For our setting, getting the " closure equation " isn't clear and it is more natural to use homogenization.

The knowledge of the permeability which expresses the flow resistance of a fibrous porous medium is an important matter in the design of industrial filters and artificial porous media. Hence many works have been conducted to study the permeability of different fibre distributions in the medium. These works can be divided into pure experimental ones, pure theoretical ones, and works based on an analytical approach with elements of computational methods for the determination of permeability. A comprehensive review of the literature on permeability of fibrous media has been elaborated by Jackson and James [64]. These authors discuss a variety of theoretical models and present a large collection of experimental data for both natural and synthetic fibrous media. Predominantly, these models use two-dimensional representations of fibrous media, and consider both parallel and transverse flow through spatially periodic arrays of cylinders (for a detailed discussion we refer for example to [40, 53, 75, 76, 87, 90]).

For two-dimensional sparse media, Howells [60] developed a theory for dilute random arrays of parallel cylinders using an averaged-equation approach. Sangani and Yao [88, 89] conducted numerical simulations of random arrays of parallel cylinders, finding good agreement with the predictions of Howells at low concentrations.

While there is a large literature on two-dimensional models, relatively few papers have been written that address three-dimensional, fibrous porous media.

For three-dimensional media, there are two studies cited by Jackson and James (see [63, 91]). In [54], Higdon and Ford use a rigorous numerical technique, the spectral boundary element formulation, to calculate the hydraulic permeability of ordered, three dimensional fibrous media. In [70], the tensor of permeability of the fibrous porous media is determined based upon a generalized cell model proposed by Neale et al. [82]. For three dimensional disordered fibrous media we cite for example [29, 61].

In this work, we are concerned with studying the flow through a realistic class of fibrous media using homogenization techniques. In section 2, we give a description of the locally quasi-periodic fibrous medium, consisting of layers of parallel fibers. This particular fibre geometry corresponds to a description of a biological tissue and was first studied by M. Briane. We note that our approach applies to other geometries studied in the papers of Briane from 1993-94. Next, we present our model problem (Stokes problem) and we homogenize it, using a two-scale expansion. We derive the effective Darcy equation and the permeability. The formal result, which differs signif-

icantly from the standard derivation of the Darcy law for a filtration through a periodic rigid porous medium, is rigorously justified in the Appendix.
For computing the effective permeability tensor, we identify and solve a variational problem called the *cell problem*. For a practical calculation of the permeability tensor, we introduce and solve two generic cell problems described by a $2D$ Stokes problem and a $2D$ Poisson problem respectively. Consequently, we obtain a new formula of the permeability tensor which is function of the geometry of the above-mentioned generic cells. For the sake of illustration, we present an example of numerical results that show the influence of the orientation of the fibers in two cases: parallel fibers and variable orientations.
Our goal in section 3 is to present a rigorous theoretical analysis consisting in determining formulae of the permeability in the low solid fraction limit. We show that the leading terms of our formulae are consistent with empirical formulae given in the literature. Also, we compare the predictions of asymptotic formulae with the results of numerical simulations.
As already said, we address in the Appendix the technical question of the error made, when the physical velocity and the physical pressure are approximated by the homogenized quantities introduced in section 2.

Our conclusion is that the homogenization approach allows to calculate the permeability of fibrous media in a very efficient way. It also allows to confirm the validity, at the leading order of the low fraction limit, of the empirical formulas used in engineering. Let us note that the generalization to the determination of the dynamic permeability (see [1] and references therein for the definition) of fibrous media is straightforward. Our computations generalize those performed for the parallel fibers, with periodic or random distribution of the centers (see e.g. [49]).

2 Permeability of a fibrous medium

2.1 Notations and geometry definition

One of the rare mathematical references on fibrous porous media is the work by M. Briane. He considered homogenization of an elliptic 2nd order operator with oscillatory coefficients in such setting. More precisely, he studied the behavior of fibrous materials with respect to heat conduction. The conductivity matrix took different values in the fibres and in the intersticial medium.

The assumptions on the fiber geometry were motivated by biomechanical applications and Briane studied three cases. They all deal with tiny fibers, perpendicular to the x_1-axis and making locally an angle $\gamma(x_1)$ with the x_2-axis.

His first model was a stratified periodic structure and its drawback was that fibers were not cylindrical. The drawback was rectified by the sophis-

ticated third model, which is no more locally periodic. For more details we refer to Briane's papers [21, 22, 23]. The second model was, according to Briane (see his Ph. D. thesis [21] , page 202) the closest to the biomechanical models used in applications. In this case, the fibrous material was locally periodic and its particularity was that the variations of the orientation function γ did not appear in the effective equation.

Motivated by its importance in the applications, we will deal with it.

To define the geometry of the porous medium, we follow the second case considered by M. Briane in [22] (see also [21, 23]). Let Ω be a domain in $\mathbb{R}^3$ which consists of N_ε layers, denoted by $\Omega^{\varepsilon,n}$, $n = 1, \ldots, N_\varepsilon$, perpendicular to the Ox_1 axis. The thickness along Ox_1 of each layer is ε^r, with $0 < r < 1$. Let $x^{\varepsilon,n}$ be a given point in $\Omega^{\varepsilon,n}$, for $n = 1, \ldots, N_\varepsilon$, and γ a $\mathcal{C}^1(\mathbb{R})$ function. In the layer $\Omega^{\varepsilon,n}$, there are $1/\varepsilon^{1-r}$ rows of fibers of radius εR which constitute a periodic network of cylinders whose axes are parallel, perpendicular to Ox_1, and make an angle $\gamma_{\varepsilon,n} = \gamma(x_1^{\varepsilon,n})$ with Ox_2. This angle is constant inside a layer, but changes from one layer to another. It is shown on Figure 3.1 a geometry with a function γ which varies linearly with the coordinate x_1 of the layers. Figure 3.2 shows a magnified view of this configuration.

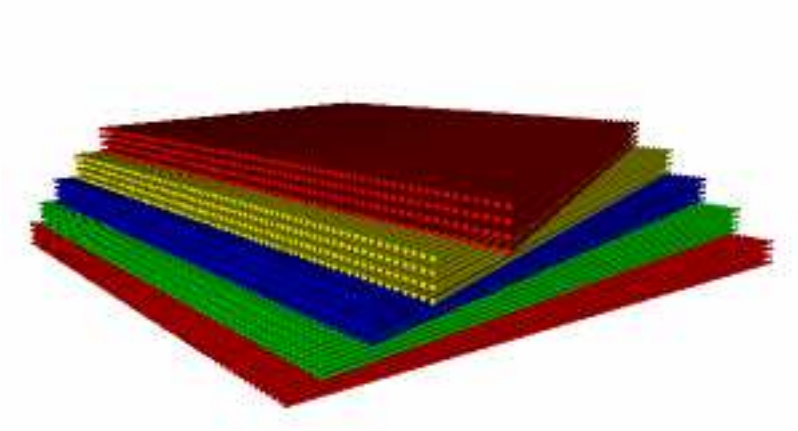

Figure 3.1: Microscopic geometry of the fibers (the vertical is Ox_1).

To be more precise, let $R \in (0,1)$, $\mathcal{Y} = [-1,1] \times [-1,1]$ and let χ be the $\mathcal{Y}-$ periodic function defined on $\mathcal{Y}$ by:

$$\chi(y) = 1 \quad \text{if } |y| \leq R, \qquad \text{and } \chi(y) = 0 \quad \text{if } |y| > R.$$

We denote by $\mathcal{Y}_F$ the set $\{y \in \mathcal{Y}, \chi(y) = 0\}$ and by ρ the function defined on $\mathbb{R} \times \mathbb{R}^3$ with values in $\mathbb{R}^2$:

$$\rho(\zeta, x) = (x_1, x_3 \cos\gamma(\zeta) - x_2 \sin\gamma(\zeta))$$

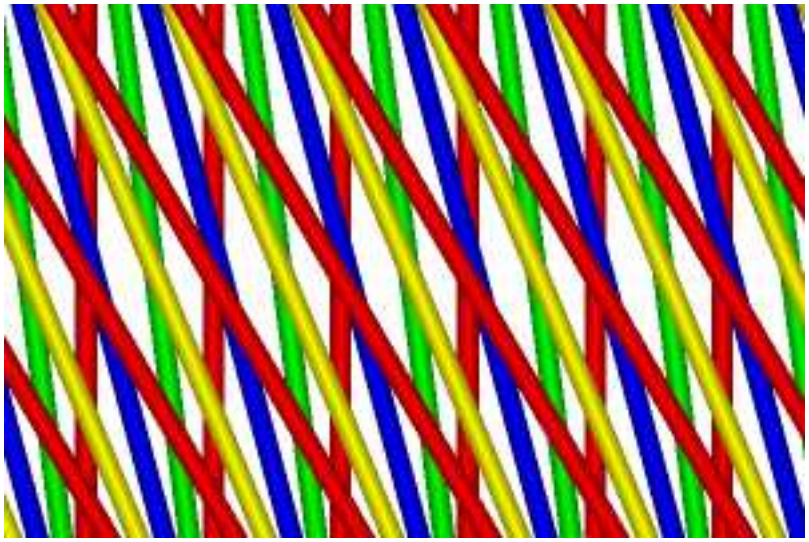

Figure 3.2: Microscopic geometry of the fibers (view along Ox_1).

with $x = (x_1, x_2, x_3)$. In the layer n, the fibrous domain is defined by

$$\Omega_s^{\varepsilon,n} = \left\{ x \in \Omega, \chi\left(\frac{\rho(x_1^{\varepsilon,n}, x)}{\varepsilon}\right) = 1 \right\},$$

and the fluid domain $\Omega^{\varepsilon,n}$ by:

$$\Omega^{\varepsilon,n} = \Omega \backslash \Omega_s^{\varepsilon,n}.$$

We then defined Ω^ε (resp. Ω_s^ε) as the union of all the layers $\Omega^{\varepsilon,n}$ (resp. $\Omega_s^{\varepsilon,n}$).

2.2 Homogenization

The flow in Ω^ε is assumed to be governed by the Stokes equations:

$$\begin{aligned} -\nu \triangle \mathbf{u}^\varepsilon + \nabla p^\varepsilon &= \mathbf{f} && \text{in } \Omega^\varepsilon, && (2)\\ \operatorname{div} \mathbf{u}^\varepsilon &= 0 && \text{in } \Omega^\varepsilon, && (3)\\ \mathbf{u}^\varepsilon &= 0 && \text{on } \partial\Omega^\varepsilon. && (4) \end{aligned}$$

Each layer is homogenized independently, which is justified by the difference of scales of the fibers (ε) and the layer (ε^r). In order to homogenize the Stokes system (2)-(4) in $\Omega^{\varepsilon,n}$, the functions $\mathbf{u}$ and p are supposed to have the following expansions (see [17]):

$$\mathbf{u}^\varepsilon(x) = \varepsilon^2 \mathbf{u}^0\left(x, \frac{\rho(x_1^{\varepsilon,n}, x)}{\varepsilon}\right) + \dots \qquad (5)$$

$$p^\varepsilon(x) = p^0\left(x, \frac{\rho(x_1^{\varepsilon,n}, x)}{\varepsilon}\right) + \varepsilon p^1\left(x, \frac{\rho(x_1^{\varepsilon,n}, x)}{\varepsilon}\right) + \dots \tag{6}$$

To perform the formal two-scale analysis, it is convenient to introduce a mapping $\varphi_{\varepsilon,n}$ from a reference configuration $\hat{\Omega}^{\varepsilon,n}$ onto $\Omega^{\varepsilon,n}$. We define $\hat{u}$ in the reference configuration by $\hat{u}(\hat{x}_1, \hat{x}_2, \hat{x}_3) = u(x_1, x_2, x_3)$, with $(x_1, x_2, x_3) = \varphi_{\varepsilon,n}(\hat{x}_1, \hat{x}_2, \hat{x}_3)$. The functions $\hat{p}$ and $\hat{\mathbf{f}}$ are defined accordingly. The deformation gradient is given by

$$\boldsymbol{F} = \left[\frac{\partial x_i}{\partial \hat{x}_j}\right]_{i,j=1,2,3}.$$

The determinant of $\boldsymbol{F}$ is denoted by J and $\boldsymbol{F}^{-1}$ is denoted by $\boldsymbol{G}$. Using the following identities: $\nabla p = \boldsymbol{G}^T \nabla_{\hat{x}} \hat{p}$, $\nabla \mathbf{u} = \nabla_{\hat{x}} \hat{\mathbf{u}} \boldsymbol{G}$, $\operatorname{div}_{\hat{x}}(J \nabla_{\hat{x}} \hat{\mathbf{u}} \boldsymbol{G} \boldsymbol{G}^T) = J \operatorname{div}(\nabla \mathbf{u})$ and $\operatorname{div}_{\hat{x}}(J \boldsymbol{G}^T) = 0$, we obtain:

$$\begin{aligned} -\nu \operatorname{div}_{\hat{x}}(J \nabla_{\hat{x}} \hat{\mathbf{u}}^\varepsilon \boldsymbol{G} \boldsymbol{G}^T) + \operatorname{div}_{\hat{x}}(J \hat{p}^\varepsilon \boldsymbol{G}^T) &= J \hat{\mathbf{f}} \quad \text{in } \hat{\Omega}^{\varepsilon,n}, & (7)\\ \operatorname{div}_{\hat{x}}(J \boldsymbol{G} \hat{\mathbf{u}}^\varepsilon) &= 0 \quad \text{in } \hat{\Omega}^{\varepsilon,n}, & (8)\\ \hat{\mathbf{u}}^\varepsilon &= 0 \quad \text{on } \partial\hat{\Omega}^{\varepsilon,n}. & (9) \end{aligned}$$

We note that for a matrix valued function A, $(\operatorname{div} A)_i = \sum_j \dfrac{\partial A_{ij}}{\partial x_j}$. Thus, denoting by g_{ij} the components of $\boldsymbol{G}$ and by h_{ij} the components of $\boldsymbol{G}\boldsymbol{G}^T$, we have for $i = 1, 2, 3$:

$$\begin{aligned} -\nu \sum_{j=1}^{3} \frac{\partial}{\partial \hat{x}_j}\left[J \sum_{k=1}^{3} \frac{\partial \hat{u}_i}{\partial \hat{x}_k} h_{kj}\right] + \sum_{j=1}^{3} \frac{\partial (J g_{ji} \hat{p}^\varepsilon)}{\partial \hat{x}_j} &= J \hat{f}_i \quad \text{in } \hat{\Omega}^{\varepsilon,n}, & (10)\\ \sum_{i,j=1}^{3} \frac{\partial (J g_{ji} \hat{u}_i)}{\partial \hat{x}_j} &= 0 \quad \text{in } \hat{\Omega}^{\varepsilon,n}, & (11)\\ u_i^\varepsilon &= 0 \quad \text{on } \partial\hat{\Omega}^{\varepsilon,n}. & (12) \end{aligned}$$

In the reference configuration $\hat{\Omega}^{\varepsilon,n}$, the functions $\hat{\mathbf{u}}$ and $\hat{p}$ have the following expansions

$$\hat{\mathbf{u}}^\varepsilon(\hat{x}) = \varepsilon^2 \hat{\mathbf{u}}^0\left(\hat{x}, \frac{\hat{x}_1}{\varepsilon}, \frac{\hat{x}_2}{\varepsilon}\right) + \dots \tag{13}$$

$$\hat{p}^\varepsilon(\hat{x}) = \hat{p}^0(\hat{x}, \frac{\hat{x}_1}{\varepsilon}, \frac{\hat{x}_2}{\varepsilon}) + \varepsilon \hat{p}^1\left(\hat{x}, \frac{\hat{x}_1}{\varepsilon}, \frac{\hat{x}_2}{\varepsilon}\right) + \dots \tag{14}$$

with $\hat{x} = (\hat{x}_1, \hat{x}_2, \hat{x}_3)$. We denote by $\hat{z} = (\hat{z}_1, \hat{z}_2) = (\hat{x}_1/\varepsilon, \hat{x}_2/\varepsilon)$ the fine scale. First, putting these expressions into (10), we obtain with the $O(1/\varepsilon)$ terms:

$$\frac{\partial}{\partial \hat{z}_1}(g_{1i} \hat{p}^0) + \frac{\partial}{\partial \hat{z}_2}(g_{2i} \hat{p}^0) = 0, \qquad i = 1, 2, 3.$$

The matrix $\boldsymbol{G}$ being regular, these relations yield $\partial_{\hat{z}_1}\hat{p}^0 = \partial_{\hat{z}_2}\hat{p}^0 = 0$, and thus

$$\hat{p}^0 = \hat{p}^0(\hat{x}). \tag{15}$$

Next, the $O(1)$ terms in (10) and (11) give

$$\begin{aligned} &-\nu\frac{\partial}{\partial\hat{z}_1}[Jh_{11}\frac{\partial\hat{u}_i^0}{\partial\hat{z}_1} + Jh_{12}\frac{\partial\hat{u}_i^0}{\partial\hat{z}_2}] - \nu\frac{\partial}{\partial\hat{z}_2}[Jh_{21}\frac{\partial\hat{u}_i^0}{\partial\hat{z}_1} + Jh_{22}\frac{\partial\hat{u}_i^0}{\partial\hat{z}_2}] \\ &+\sum_{r=1}^{2}\frac{\partial}{\partial\hat{z}_r}(Jg_{ri}\hat{p}^1) = J\hat{f}_i - \sum_{r=1}^{3}\frac{\partial}{\partial\hat{x}_r}(Jg_{ri}\hat{p}^0) \end{aligned} \tag{16}$$

in $\hat{\Omega}^{\varepsilon,n}\times\mathcal{Y}_F$, for $i = 1, 2, 3$, and

$$\frac{\partial}{\partial\hat{z}_1}\left[\sum_{i=1}^{3}Jg_{1i}\hat{u}_i^0\right] + \frac{\partial}{\partial\hat{z}_2}\left[\sum_{i=1}^{3}Jg_{2i}\hat{u}_i^0\right] = 0 \tag{17}$$

in $\hat{\Omega}^{\varepsilon,n}\times\mathcal{Y}_F$. We have moreover

$$\hat{\mathbf{u}}^0(\hat{x},\hat{z}_1,\hat{z}_2) = 0 \quad \text{on } \hat{\Omega}^{\varepsilon}\times\partial\mathcal{Y}_F\backslash\partial\mathcal{Y}, \tag{18}$$

$$(\hat{\mathbf{u}}^0,\hat{p}^1) \text{ is } \mathcal{Y}\text{-periodic in}(\hat{z}_1,\hat{z}_2), \tag{19}$$

$$\sum_{i,j=1}^{3} g_{ji}\int_{\mathcal{Y}_F}\frac{\partial\hat{u}_i^0}{\partial\hat{x}_j}(\hat{x},\hat{z}_1,\hat{z}_2)\,d\hat{z}_1 d\hat{z}_2 = 0 \qquad \text{in } \hat{\Omega}^{\varepsilon,n}, \tag{20}$$

$$\int_{\partial\mathcal{Y}_F}\hat{\mathbf{u}}^0(\hat{x},\hat{z}_1,\hat{z}_2)\cdot\mathbf{n}\,d\hat{z}_1\,d\hat{z}_2 = 0 \qquad \text{on } \partial\hat{\Omega}^{\varepsilon,n}. \tag{21}$$

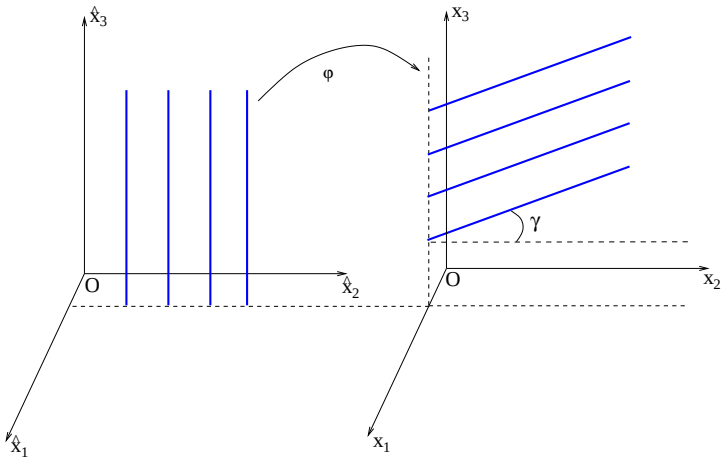

Figure 3.3: The mapping $\varphi_{\varepsilon,n}$

For the mapping $\varphi_{\varepsilon,n}$, we choose a rotation that transforms fibers parallel to the $O\hat{x}_3$ axis on the fibers of the layer $\Omega^{\varepsilon,n}$ (see Fig. 3.3). More precisely:

$$(\hat{x}_1,\hat{x}_2,\hat{x}_3)=\varphi^{-1}_{\varepsilon,n}(x_1,x_2,x_3)=\left|\begin{array}{l} x_1 \\ -x_2\sin\gamma_{\varepsilon,n}+x_3\cos\gamma_{\varepsilon,n} \\ -x_2\cos\gamma_{\varepsilon,n}-x_3\sin\gamma_{\varepsilon,n}\end{array}\right. \tag{22}$$

For this choice, we have

$$\boldsymbol{G}=\begin{bmatrix} 1 & 0 & 0 \\ 0 & -\sin\gamma_{\varepsilon,n} & \cos\gamma_{\varepsilon,n} \\ 0 & -\cos\gamma_{\varepsilon,n} & -\sin\gamma_{\varepsilon,n}\end{bmatrix}, \qquad J=1, \qquad \boldsymbol{G}\boldsymbol{G}^T=Id$$

and equations (16) and (17) simply read:

$$\left\{\begin{array}{rcl} -\nu\triangle_{\hat{z}_1,\hat{z}_2}\hat{u}^0_1+\dfrac{\partial\hat{p}^1}{\partial\hat{z}_1} &=& \hat{f}_1-\dfrac{\partial\hat{p}^0}{\partial\hat{x}_1} \\ -\nu\triangle_{\hat{z}_1,\hat{z}_2}\hat{u}^0_2-\sin\gamma_{\varepsilon,n}\dfrac{\partial\hat{p}^1}{\partial\hat{z}_2} &=& \hat{f}_2-\sin\gamma_{\varepsilon,n}\dfrac{\partial\hat{p}^0}{\partial\hat{x}_2}-\cos\gamma_{\varepsilon,n}\dfrac{\partial\hat{p}^0}{\partial\hat{x}_3} \\ -\nu\triangle_{z1,z2}\hat{u}^0_3+\cos\gamma_{\varepsilon,n}\dfrac{\partial\hat{p}^1}{\partial\hat{z}_2} &=& \hat{f}_3+\cos\gamma_{\varepsilon,n}\dfrac{\partial\hat{p}^0}{\partial\hat{x}_2}-\sin\gamma_{\varepsilon,n}\dfrac{\partial\hat{p}^0}{\partial\hat{x}_3} \\ \dfrac{\partial\hat{u}^0_1}{\partial\hat{z}_1}+\dfrac{\partial}{\partial\hat{z}_2}\Big(-\hat{u}^0_2\sin\gamma_{\varepsilon,n}+\hat{u}^0_3\cos\gamma_{\varepsilon,n}\Big) &=& 0.\end{array}\right. \tag{23}$$

The scales cannot be separated in this system. Nevertheless, taking advantage of the fact that the right-hand side does not depend on $\hat{z}$, we can obtain the solution by solving the following "cell" problem: Let $\{\omega^j,\pi^j\}$, $j=1,2,3$ the functions defined as the solutions to:

$$\left\{\begin{array}{rcll} -\triangle_{\hat{z}_1,\hat{z}_2}\omega^j_1(x_1,\hat{z}_1,\hat{z}_2)+\partial_{\hat{z}_1}\pi^j &=& \delta_{1j} & \text{in } \mathcal{Y}_F, \\ -\triangle_{\hat{z}_1,\hat{z}_2}\omega^j_2(x_1,\hat{z}_1,\hat{z}_2)-\sin\gamma(x_1)\partial_{\hat{z}_2}\pi^j &=& \delta_{2j} & \text{in } \mathcal{Y}_F, \\ -\triangle_{\hat{z}_1,\hat{z}_2}\omega^j_3(x_1,\hat{z}_1,\hat{z}_2)+\cos\gamma(x_1)\partial_{\hat{z}_2}\pi^j &=& \delta_{3j} & \text{in } \mathcal{Y}_F, \\ \partial_{\hat{z}_1}\omega^j_1+\partial_{\hat{z}_2}(-\sin\gamma(x_1)\omega^j_2+\cos\gamma(x_1)\omega^j_3) &=& 0 & \text{in } \mathcal{Y}_F, \\ \omega^j(x_1,\hat{z}_1,\hat{z}_2) &=& 0 & \text{on } \partial\mathcal{Y}_F\backslash\partial\mathcal{Y}, \\ \{\omega^j,\pi^j\} \text{ is } \mathcal{Y}\text{-periodic in } (\hat{z}_1,\hat{z}_2). & & & \end{array}\right. \tag{24}$$

Proposition 2

1. Problem (24) admits a unique solution $(\boldsymbol{\omega}^j,\pi^j)\in H^1(\mathcal{Y}_F)^3\times L^2(\mathcal{Y}_F)$.
2. The function $\mathbf{u}^0$ in (5) is given by

$$\mathbf{u}^0(x,z_1,z_2)=\frac{1}{\nu}\sum_{j=1}^{3}\left(f_j(x)-\frac{\partial p^0}{\partial x_j}(x)\right)\boldsymbol{\omega}^j(x_1,z_1,z_2) \tag{25}$$

3. The effective pressure p^0 in (6) only depends on x and is solution to the Darcy problem:

$$\left\{ \begin{array}{rcll} \mathbf{u}^D(x) & = & \dfrac{\boldsymbol{K}(x_1)}{\nu}\left(\mathbf{f} - \nabla p^0(x)\right) & \text{in } \Omega, \\ \operatorname{div} \mathbf{u}^D & = & 0, & \text{in } \Omega, \\ \mathbf{u}^D \cdot \mathbf{n} & = & 0, & \text{on } \partial\Omega. \end{array} \right. \tag{26}$$

where the permeability matrix $\boldsymbol{K} = [K_{i,j}]_{i,j=1,2,3}$ is given by

$$K_{ij}(x_1) = \frac{1}{|\mathcal{Y}|} \int_{\mathcal{Y}_F} \omega_i^j(x_1, z_1, z_2) dz_1 dz_2. \tag{27}$$

Note that formula (27) is not convenient from the numerical viewpoint since it depends on the macroscopic variable x_1. A more practical formula involving cell problems independent of x_1 will be given in section 2.3.

Proof.

1. The analysis of (24) is rather straightforward. We postpone it until section 2.3 where a constructive proof is given (see Remark 2.1).

2. The fact that p^0 does not depend on the fine scale has been established above (see (15)). Next, we multiply equations (24) by $\dfrac{1}{\nu}\left(\hat{f}_j(\hat{x}) - (\boldsymbol{G}^T \nabla_{\hat{x}} \hat{p}^0)_j\right)$, for $j = 1, 2, 3$. Then, summing these equations, we obtain that $(\hat{u}_1^0, \hat{u}_2^0, \hat{u}_3^0, \hat{p}^1)$ defined by

$$\hat{u}_i^0 = \sum_{j=1}^{3} \frac{1}{\nu}\left(\hat{f}^j - (\boldsymbol{G}^T \nabla_{\hat{x}} \hat{p}^0)_j\right) \omega_i^j$$

and

$$\hat{p}^1 = \sum_{j=1}^{3} \left(\hat{f}^j - (\boldsymbol{G}^T \nabla_{\hat{x}} \hat{p}^0)_j\right) \pi^j$$

is solution to (23). Thus using the relation $\nabla p^0 = \boldsymbol{G}^T \nabla_{\hat{x}} \hat{p}^0$, we obtain (25).

3. Defining the Darcy velocity by:

$$\mathbf{u}^D(x) = \frac{1}{|\mathcal{Y}|} \int_{\mathcal{Y}_F} \mathbf{u}^0(x, z_1, z_2)\, dz_1\, dz_2$$

we straightforwardly obtain (26) with the definition (27) of the permeability tensor. $\diamondsuit$

The rigorous justification of the approximation is quite technical, but follows the general ideas used in the homogenization of the Stokes system in a porous medium and in the study of the interface conditions between two different porous media. We address it in some details in the Appendix. In fact we will not only prove that our filtration velocity and the effective pressure are the limits of the rescaled physical velocities and pressures, but we will also give an error estimate in terms of ε.

2.3 Cell problems

In order to address the effective computation of the permeability, we introduce the following generic cell problems: let $U_1^j(z_1,z_2)$, $U_2^j(z_1,z_2)$, $P^j(z_1,z_2)$, $j=1,2$ be the functions defined as the solutions to the 2D Stokes problems:

$$\left\{\begin{array}{rcll} -\triangle_{z_1,z_2} U_1^j + \partial_{z_1} P^j &=& \delta_{1j} & \text{in } \mathcal{Y}_F, \\ -\triangle_{z_1,z_2} U_2^j + \partial_{z_2} P^j &=& \delta_{2j} & \text{in } \mathcal{Y}_F, \\ \partial_{z_1} U_1^j + \partial_{z_2} U_2^j &=& 0 & \text{in } \mathcal{Y}_F, \\ U_1^j = U_2^j &=& 0 & \text{on } \partial\mathcal{Y}_F \backslash \partial\mathcal{Y}, \\ \{U_1^j, U_2^j, P^j\} \text{ is } \mathcal{Y}\text{-periodic in } z_1, z_2, & & & \end{array}\right. \tag{28}$$

and let $V(z_1,z_2)$ be the solution to the 2D Poisson problem:

$$\left\{\begin{array}{rcll} -\triangle V &=& 1 & \text{in } \mathcal{Y}_F, \\ V &=& 0 & \text{on } \partial\mathcal{Y}_F \backslash \partial\mathcal{Y}, \\ V \text{ is } \mathcal{Y}\text{-periodic in } z_1, z_2. & & & \end{array}\right. \tag{29}$$

We introduce $\tilde{\Omega}(x_1,z_1,z_2) = [\tilde{\omega}_i^j]_{i,j=1,2,3}$ defined by

$$\tilde{\Omega}(x_1,z_1,z_2) = \boldsymbol{R}^{-1}(x_1)\Omega(x_1,z_1,z_2),$$

with $\Omega(x_1,z_1,z_2) = [\omega_i^j]_{i,j=1,2,3}$ and

$$\boldsymbol{R}(x_1) = \begin{bmatrix} 1 & 0 & 0 \\ 0 & \cos\gamma(x_1) & -\sin\gamma(x_1) \\ 0 & \sin\gamma(x_1) & \cos\gamma(x_1) \end{bmatrix}.$$

Combining the equations of system (28) and (29) we obtain:

$$\tilde{\Omega}(x_1,z_1,z_2) = \begin{bmatrix} U_1^1(z_1,z_2) & 0 & U_1^2(z_1,z_2) \\ 0 & V(z_1,z_2) & 0 \\ U_2^1(z_1,z_2) & 0 & U_2^2(z_1,z_2) \end{bmatrix} \boldsymbol{R}^{-1}(x_1).$$

From which we finally deduce

$$\boldsymbol{K}(x_1) = \boldsymbol{R}(x_1)\boldsymbol{K}_0\boldsymbol{R}^{-1}(x_1) \tag{30}$$

with

$$\boldsymbol{K}_0 = \frac{1}{|\mathcal{Y}|} \begin{bmatrix} \displaystyle\int_{\mathcal{Y}_F} U_1^1 & 0 & \displaystyle\int_{\mathcal{Y}_F} U_1^2 \\ 0 & \displaystyle\int_{\mathcal{Y}_F} V & 0 \\ \displaystyle\int_{\mathcal{Y}_F} U_2^1 & 0 & \displaystyle\int_{\mathcal{Y}_F} U_2^2 \end{bmatrix}. \tag{31}$$

The developed expression for the permeability is given by

$$\boxed{\boldsymbol{K}(x_1) = \begin{pmatrix} \overline{K}_{11} & -\overline{K}_{12}s & \overline{K}_{12}c \\ -\overline{K}_{21}s & \overline{K}_{22}s^2 + \overline{V}c^2 & (\overline{V} - \overline{K}_{22})cs \\ \overline{K}_{21}c & (\overline{V} - \overline{K}_{22})cs & \overline{V}s^2 + \overline{K}_{22}c^2 \end{pmatrix}} \tag{32}$$

where the following notations have been used: $c = \cos\gamma(x_1)$, $s = \sin\gamma(x_1)$,

$$\overline{V} = \frac{1}{|\mathcal{Y}|}\int_{\mathcal{Y}_F} V \qquad \text{and} \qquad \overline{K}_{ij} = \frac{1}{|\mathcal{Y}|}\int_{\mathcal{Y}_F} U_j^i. \tag{33}$$

Consequently, once solved the three generic cell problems (28) with j=1,2 and (29), the permeability is obtained at any macroscopic coordinate x_1 by computing two simple matrix-matrix products (30).

For example, Figure 3.4 shows the velocity and pressure fields for the generic cell problem (28) with $j = 1$.

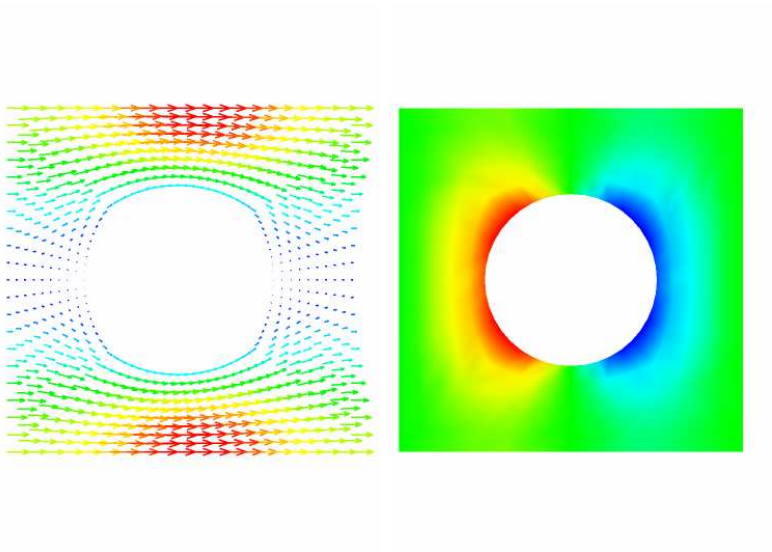

Figure 3.4: Velocity and pressure field for a cell problem

Remark 2.1 *Note that, the existence and uniqueness of* $(\boldsymbol{U}^j, P^j)$ *and* V *being obvious, the relations*

$$[\omega_i^j(x_1, z_1, z_2)] = R(x_1)\begin{bmatrix} U_1^1(z_1,z_2) & 0 & U_1^2(z_1,z_2) \\ 0 & V(z_1,z_2) & 0 \\ U_2^1(z_1,z_2) & 0 & U_2^2(z_1,z_2) \end{bmatrix} R^{-1}(x_1)$$

and

$$\pi^1 = P^1, \qquad \pi^2 = -\sin\gamma\ P^2, \qquad \pi^3 = \cos\gamma\ P^2$$

give a constructive proof of the existence and uniqueness of the solution to (24).

Remark 2.2 *Multiplying the first two equations of (28) by* U_1^i *and* U_2^i *respectively and integrating by parts, we obtain:*

$$\int_{\mathcal{Y}_F} \nabla \boldsymbol{U}^i \cdot \nabla \boldsymbol{U}^j = \int_{\mathcal{Y}_F} \boldsymbol{U^i} \cdot \boldsymbol{e}_j.$$

Vectors $\boldsymbol{U}^1$ *and* $\boldsymbol{U}^2$ *being independent, the matrix* $[\int_{\mathcal{Y}_F} \nabla \boldsymbol{U}^i \cdot \nabla \boldsymbol{U}^j]_{i,j=1,2}$ *is invertible. In view of the definition of* $\boldsymbol{K}_0$ *and relation (30), this implies that* $\boldsymbol{K}(x_1)$ *is regular.*

2.4 Numerical simulations

Due to the variable orientation of the fibers, the cell problems (24)depends on the macroscopic variable. At a first glance, it seems necessary to solve a huge number of cell problems just like in nonlinear models (see for example [49] where a parallel strategy is considered). Nevertheless, the trick that we have described in the previous section allows us to solve only two "generic" cell problems. The generic solutions can then be combined to generate the solutions of (24) for arbitrary macroscopic points. Compared to an approach where the "real" cell problems (24) are actually solved, this procedure allows a substantial reduction of the computational effort and makes unnecessary the use of parallel algorithms.

From a practical viewpoint, the procedure is therefore the following:

1. **Microscopic resolution** (independent of the fibers orientation).
   1.1. Solve once and for all the generic cell problems (28) and (29) (see below for the description of the discretization method).
   1.2. Compute the generic permeability $\boldsymbol{K}_0$ with formula (31).
2. **Macroscopic resolution** (which depends on the function γ defining the fibers orientation)

   Solve the macroscopic problem (26) (see below for the description of the discretization method). Whenever the value of the permeability $\boldsymbol{K}(x_1)$ is needed – typically at each integration points of the finite element – we use formula (30) and the pre-computed values of the generic permeability $\boldsymbol{K}_0$.

The discretization methods that we used to solve the various problems are reliable and standard, so we just sketch their description. The generic cell problems (28) are solved using Q2 finite element for the velocity and discontinuous P1 for the pressure. This pair of elements is known to satisfy the inf-sup condition ([50]), and is elementwise mass preserving. The Darcy equations (26) are also solved by mixed finite elements: the velocity is approximated in the lowest order 3D Raviart-Thomas finite element space (see for example [85]), and the pressure is constant by element. This choice ensures the continuity of the normal component of the velocity and an exact elementwise mass balance. Moreover, we adopt a mixed-hybrid formulation: a symmetric definite positive system is first solved by a preconditioned conjugate gradient method to compute the trace of the pressure on the faces on the elements; next the pressure and the velocity are recovered by a local procedure.

2.4.1 Parallel fibers: influence of the orientation

In this experiment, we impose a pressure drop between two opposite faces of a unit cube. The fibers are parallel and we investigate the influence of the angle between the fibers and the flow (which is mainly directed along Ox_2). We report on Figure 3.5 the curves of the flux through a face of the cube *versus* the angle for three different sizes of the fibers. As expected, the flux is maximal (resp. minimal) for a flow parallel (resp. orthogonal) to the fibers, and is greater for smaller fibers.

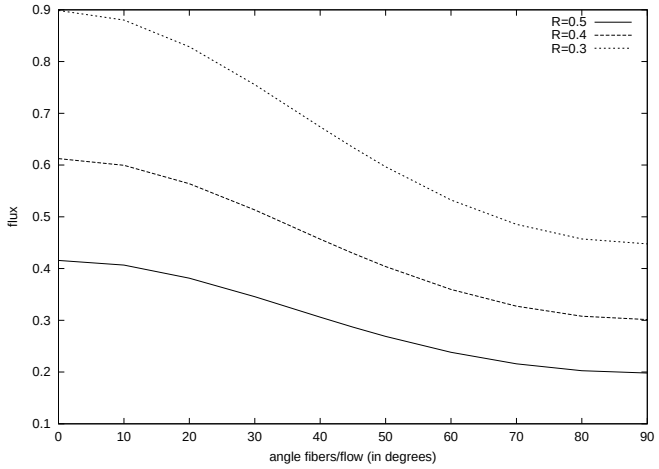

Figure 3.5: Influence of the angle between the fibers and the flow, and of the radius of the fibers.

2.4.2 An example with non-parallel fibers

In this experiment, we still impose a pressure drop between two opposite faces of a unit cube, but now the angle between the fibers and Ox_2 is variable: $\gamma(x_1) = 2\pi x_1$. Figure 3.6 shows the influence of the orientation of the fibers on the velocity vectors.

3 Low solid fraction limit

In the applied literature (see *e.g.* [64] or [70] and references therein), the permeability in the low solid fraction limit is often assumed to be scalar and is searched of the form $k = a^2 f(\phi)$, where a is the diameter of the fibers and ϕ the volume fraction of the solid material. More sophisticated models

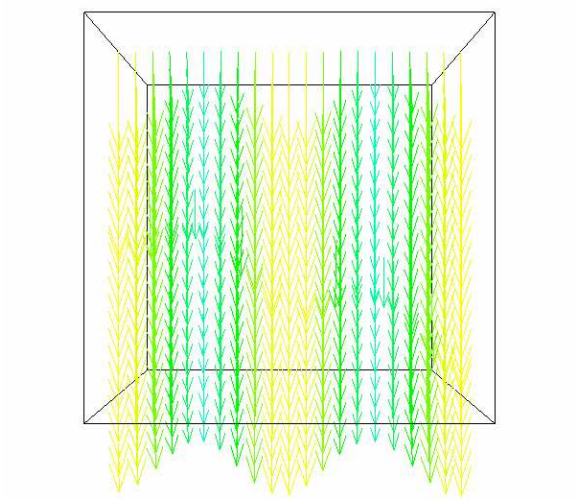

Figure 3.6: Velocity obtained with fibers making an angle $\gamma(x_1) = 2\pi x_1$ with Ox_2 (on this picture Ox_1 is horizontal and Ox_2 vertical).

provide a homogeneous permeability tensor of the form

$$\mathbf{K} = \begin{pmatrix} K_\perp & 0 & 0 \\ 0 & K_{||} & 0 \\ 0 & 0 & K_\perp \end{pmatrix} \tag{34}$$

where $K_{||}$ (resp. $K_\perp$) corresponds to the permeability in the direction parallel (resp. orthogonal) to the fibers. The following expressions are derived in [52] in the case of fibers with circular section:

$$K_{||} = \frac{a^2}{4\varphi}\left(\log(1/\varphi) - 1.5 + 2\varphi - \frac{\varphi^2}{2}\right), \tag{35}$$

$$K_\perp = \frac{a^2}{8\varphi}\left(\log(1/\varphi) + \frac{\varphi^2 - 1}{\varphi^2 + 1}\right). \tag{36}$$

Many other expressions have been proposed in the literature and compared to experiments. Although they present slight differences, most of them share the same leading order terms. We refer to [64] and the references therein for a review of the most commonly used formulae and to [70] for some recent developments. In [73], these formulas were obtained by solving analytically approximated cell problems where periodicity were replaced by convenient boundary conditions.

Our expression for the permeability (32) with $\gamma(x_1) = 0$ is:

$$\boldsymbol{K} = \begin{pmatrix} \overline{K}_{11} & 0 & \overline{K}_{12} \\ 0 & \overline{V} & 0 \\ \overline{K}_{21} & 0 & \overline{K}_{22} \end{pmatrix} \tag{37}$$

where $\overline{K}_{ij}$ and $\overline{V}$ are defined in (33). The purpose of this section is to compare this formula with (34). More precisely we shall compare $K_{||}$ with $\overline{V}$ and

$$\begin{pmatrix} \overline{K}_{11} & \overline{K}_{12} \\ \overline{K}_{21} & \overline{K}_{22} \end{pmatrix} \quad \text{with} \quad \begin{pmatrix} K_\perp & 0 \\ 0 & K_\perp \end{pmatrix}.$$

In section 3.1, it is shown that the leading terms of our formulae are consistant with (35) and (36). In section 3.2, we compare the predictions of the asymptotic formulae with the results of numerical simulations of the model proposed in section 2.

3.1 Rigorous determination of the leading order terms

It has been seen in section 2, that the computation of the permeability tensor requires the solution of the auxiliary 2D Stokes problems

$$-\Delta_z \mathbf{U}^j + \nabla_z P^j = e_j \quad \text{in } \mathcal{Y}_F \tag{38}$$

$$\mathrm{div}_z \mathbf{U}^j = 0 \quad \text{in } \mathcal{Y}_F \tag{39}$$

$$\mathbf{U}^j = 0 \quad \text{on } \partial\mathcal{Y}_F \setminus \partial\mathcal{Y} \tag{40}$$

$$\{\mathbf{U}^j, P^j\} \quad \text{is } \mathcal{Y}-\text{periodic} \tag{41}$$

and the auxiliary 2D Poisson problem

$$-\Delta_z V = 1 \quad \text{in } \mathcal{Y}_F \tag{42}$$

$$V = 0 \quad \text{on } \partial\mathcal{Y}_F \setminus \partial\mathcal{Y} \tag{43}$$

$$V \quad \text{is } \mathcal{Y}-\text{periodic} \tag{44}$$

Let us now suppose that the size of $B = \mathcal{Y} \setminus \mathcal{Y}_F$ is of order η, *i.e.* that $B = \eta B_0$ where the radius of B_0 is of order 1. We would like to know what happens with the averages of $\mathbf{U}^j$ and V when $\eta \to 0+$. This is the low solid fraction limit. We assume that η and ε go to zero in such a way that

$$\eta \gg \frac{1}{\varepsilon} e^{-1/\varepsilon^2}, \tag{45}$$

so that at the limit the effective flow is described by the Darcy law. For smaller obstacles, different limit regimes occur (Brinkman or Stokes equations).

Following [6], where this problem was studied rigorously, we set

$$-\Delta_z w^k + \nabla_z q^k = 0 \quad \text{in } \mathbb{R}^2 \setminus B_0 \tag{46}$$

$$\mathrm{div}_z w^k = 0 \quad \text{in } \mathbb{R}^2 \setminus B_0 \tag{47}$$

$$w^k = 0 \quad \text{on } \partial B_0 \tag{48}$$

$$w^k = (\log r) e_k \quad \text{in infinity}, \quad r = |z|. \tag{49}$$

Then (46) -(49) has a unique solution being the sum of the special solution for the case of the unit circle and of the solution for a "difference" problem, where the velocity has a logarithmic asymptotic behavior at infinity. For details we refer to [7], [4], [5] and [6]. The asymptotic behavior is given by the following result:

Proposition 3 ([6])
We have

$$\{P^j(\eta y), \mathbf{U}^j(\eta y)\} \rightharpoonup \frac{1}{\pi}\{q^j(y), w^j(y)\} \tag{50}$$

weakly in $L^2_{loc}(\mathbb{R}^2 \setminus B_0)/\mathbb{R} \times H^1_{loc}(\mathbb{R}^2 \setminus B_0)^2$. Furthermore

$$\lim_{\eta \to 0} \frac{1}{|\log \eta||\mathcal{Y}|} \int_{\mathcal{Y}_F} U^j_k \, dy = \frac{\delta_{jk}}{\pi}. \tag{51}$$

This result shows that the 2×2 matrix $(\overline{K}_{ij})$ is asymptotically a scalar matrix, confirming the observations from [52, 64, 70]. It also shows that

$$\overline{K}_{11} = \overline{K}_{22} \approx \frac{1}{\pi}|\log \eta|.$$

Formula (36) is therefore consistant with our result at the leading order with $a = \eta$ and $\phi = \pi\eta^2/4$ ($\pi\eta^2$ is the solid surface in the cell and 4 is the cell surface $[-1,1]^2$) .

We now discuss the low solid fraction limit for V. A detailed mathematical article on the computation of dispersive media is [71]. It concentrates mainly on the Neumann boundary conditions. In such a case, simple asymptotic formulas of Rayleigh type have a high accuracy. In the case of Dirichlet boundary conditions, this kind of asymptotic formulas is unfortunately much less accurate. The case of low solid fraction for the Dirichlet problem in a perforated domain has been addressed in [67] but only in 3D. In 2D we establish the following result.

Proposition 4
We have

$$V(\eta y) \rightharpoonup \frac{2v}{\pi} \quad \text{weakly in} \quad H^1_{loc}(\mathbb{R}^2 \setminus B_0) \tag{52}$$

where v is the unique solution for the problem

$$-\Delta v = 0 \quad \text{in } \mathbb{R}^2 \setminus B_0 \tag{53}$$

$$v = 0 \quad \text{on } \partial B_0 \tag{54}$$

$$v = \log r \quad \text{at infinity}, \quad r = |y|. \tag{55}$$

Furthermore

$$\lim_{\eta \to 0} \frac{1}{|\log \eta||\mathcal{Y}|} \int_{\mathcal{Y}_F} V(y) \, dy = \frac{2}{\pi}. \tag{56}$$

Proof. It is a simplified version of the corresponding result for the Stokes system in [6] and we give only an outline.

First we introduce the sequence $V^{0,\eta}$ defined by

$$\begin{cases} V^{0,\eta} = 0 \quad \text{in } B_1 \\ V^{0,\eta} = \dfrac{2}{\pi}\log r \quad \text{in } B_{1/\eta} \setminus B_1 \\ V^{0,\eta} = -\dfrac{2}{\pi}\log \eta \quad \text{in } \mathbb{R}^2 \setminus B_{1/\eta} \end{cases} \tag{57}$$

where $B_{1/\eta}$ is the ball of radius $1/\eta$ and $V^{1,\eta}(x) = V(\eta x) - V^{0,\eta}(x)$. Then it is easy to see that $\nabla V^{1,\eta}$ is uniformly bounded in $L^2(\eta^{-1}\mathcal{Y} \setminus B_0)$ and pass to the limit $\eta \to 0$. As in [6] , we establish the a priori estimate in L^2 with the weight $(r+1)\log(r+2)$ for $V^{1,\eta}$. It leads to the conclusion that (52) holds true.

Next we have

$$\frac{1}{|\mathcal{Y}|}\int_{\mathcal{Y}_F} V(y)\, dy = \frac{2}{\pi}\log\frac{1}{\eta} + O(|\log\frac{1}{\eta}|^{1/2}) \tag{58}$$

where $V^\eta(x) = V(\eta x)$ and the proposition is proved.$\diamondsuit$

The above result shows that the leading term in $\overline{V}$ is $\frac{2}{\pi}|\log\eta|$ which shows that our result is asymptotically consistent with formula (35) (taking as before $a = \eta$ and $\phi = \eta^2\pi/4$).

3.2 Numerical results

In order to assess the previous results, the cell problems (38)-(41) and (42)-(44) have been numerically solved for fibers with circular sections, with a solid fraction ranging from 0.2 to 0.002. To this purpose, for each solid fraction, a specific mesh has been generated to achieve the resolution of the cell problems. The procedure described in section 2.4 has then been applied to obtain the permeability tensor. Equations (35) and (36) have been plotted with $a = \eta$ (the radius of the inclusion) and $\phi = \pi\eta^2/4$. The agreement of $\overline{K}_{ii}$ with formula (36) is reasonable and both curves have the same asymptotic behavior (Fig. 3.7, left). The agreement of $\overline{V}$ with formula (35) is excellent on the whole range of solid fraction (Fig. 3.7, right).

All the previous computations have been done with *circular* section fibers. An interesting property given by Propositions 3 and 4 is that the leading term of the asymptotic behavior is independent of the shape of the solid inclusion. To illustrate this fact, we present on Fig. 3.8 the results given by (56) and (51) compared to numerical simulations with *square* section fibers. The good agreement is striking.

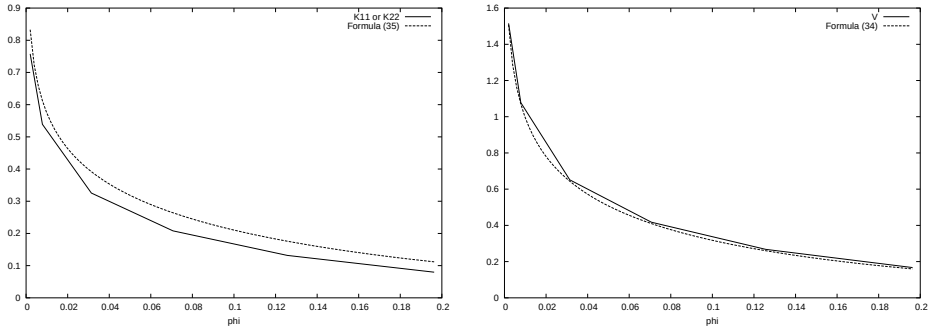

Figure 3.7: Fibers with a circular section. Left: comparison between $\overline{K}_{ii}$ and Formula (36). Right: comparison between $\overline{V}$ and Formula (35).

ϕ	$\overline{V}$	$\overline{K}_{ii}$
0.196299	0.167123	0.079633
0.125631	0.267833	0.131824
0.070667	0.417707	0.208051
0.031407	0.651478	0.325558
0.007851	1.077900	0.538937
0.001962	1.515430	0.757714

Table 3.1: Numerical values corresponding to Figure 3.7.

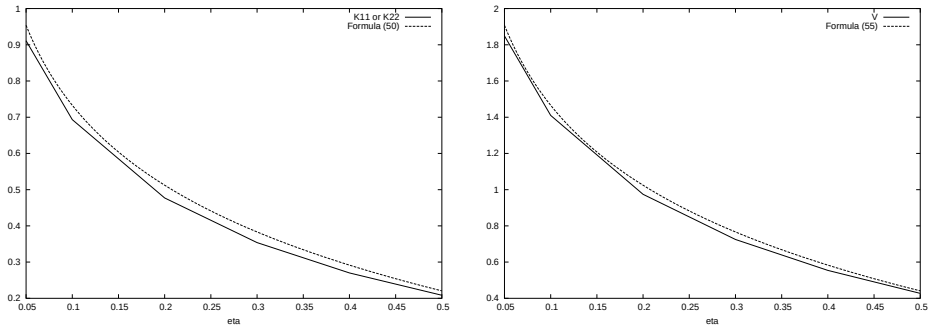

Figure 3.8: Fibers with a square section. Left: comparison between $\overline{K}_{ii}$ and Formula (51). Right: comparison between $\overline{V}$ and Formula (56).

η	$\overline{V}$	$\overline{K}_{ii}$
0.5	0.427491	0.208525
0.4	0.554049	0.270007
0.3	0.724945	0.353740
0.2	0.974281	0.477150
0.1	1.409805	0.693221
0.05	1.848851	0.911036

Table 3.2: Numerical values corresponding to Figure 3.8.

Appendix

In this appendix we discuss the error made, when the physical velocity and the physical pressure are approximated by the homogenized quantities, introduced in section 2.

In the case of a periodic porous medium, the Darcy law was justified by L. Tartar in the late seventies. The proof that the Darcy velocity is the weak limit of $\mathbf{u}^\varepsilon/\varepsilon^2$ is in [94] . For more details and generalizations to 3D geometries, one can consult the review chapter by G. Allaire in [8] . In fact, in the absence of external boundaries, it is possible to prove that $\mathbf{u}^\varepsilon/\varepsilon^2 - \mathbf{u}^0$ and $p^\varepsilon - p^0$ have L^2-norms of order ε. This confirms the formal asymptotic expansions. Nevertheless, the rigorous mathematical proof, which can be found in [80] , requires also to correct the compressibility effects, coming from $\mathbf{u}^\varepsilon$. In fact, it is optimal to work in the Hilbert space, having finite L^2-norms of both the velocity field and its divergence.

Presence of outer boundaries complicates seriously the estimates. It was established in [79] that in the presence of an outer boundary, where physical velocity is zero, $\mathbf{u}^0(x, x/\varepsilon)$ is a L^2-approximation of order $\varepsilon^{1/(3m)}$, where $m = 2$ in the 2D case and $m = 3$ in 3D. For Laplace operator, such an approximation is known to be of order $\sqrt{\varepsilon}$.

In our particular situation, we have also the interfaces. Namely, $\mathbf{u}^0$ is constructed using (25) and it reads

$$\mathbf{u}^0(x, \frac{\rho(x_1^{\varepsilon,n}, x)}{\varepsilon}) = \frac{1}{\nu}\sum_{j=1}^{3}\left(f_j(x) - \frac{\partial p^0}{\partial x_j}(x)\right)\boldsymbol{\omega}^j(x_1, z_1, z_2),$$
$$z_1 = \frac{x_1}{\varepsilon},\ z_2 = \frac{x_3}{\varepsilon}\cos\gamma(x^{\varepsilon,n}) - \frac{x_2}{\varepsilon}\sin\gamma(x^{\varepsilon,n}) \tag{59}$$

$$p^1(x, \frac{\rho(x_1^{\varepsilon,n}, x)}{\varepsilon}) = \sum_{j=1}^{3}\left(f_j(x) - \frac{\partial p^0}{\partial x_j}(x)\right)\boldsymbol{\pi}^j(x_1, z_1, z_2) \tag{60}$$

where $\{\omega^j, \pi^j\}$ are defined by (24). Clearly, it depends on the parameter $x^{\varepsilon,n}$, saying in which layer we are.

Thus, inside every layer the differences

$$w_i^\varepsilon = \mathbf{u}_i^\varepsilon/\varepsilon^2 - \mathbf{u}_i^0(x, \frac{\rho(x_1^{\varepsilon,n}, x)}{\varepsilon}); \quad q^\varepsilon = p^\varepsilon - p^0(x) - \varepsilon p^1(x, \frac{\rho(x_1^{\varepsilon,n}, x)}{\varepsilon}) \quad (61)$$

satisfy the system

$$-\nu\varepsilon^2\Delta w_i^\varepsilon + \frac{\partial}{\partial x_i}q^\varepsilon = -\Psi_i^\varepsilon \quad \text{in} \quad \Omega^{\varepsilon,n}, i = 1,2,3, \quad (62)$$

$$\text{div } w^\varepsilon = -\text{div}_x \mathbf{u}^0(x, \frac{\rho(x_1^{\varepsilon,n}, x)}{\varepsilon}) \quad \text{in} \quad \Omega^{\varepsilon,n} \quad (63)$$

with

$$\Psi_i^\varepsilon = \varepsilon^2 J^{-1}\sum_{j=1}^{3}\frac{\partial}{\partial\hat{x}_j}\left[J\sum_{k=1}^{3}\frac{\partial\hat{u}_i^0}{\partial\hat{x}_k}h_{kj}\right] + \varepsilon J^{-1}\Bigg\{\sum_{j=1}^{3}\frac{\partial}{\partial\hat{x}_j}\left[J\sum_{k=1}^{2}\frac{\partial\hat{u}_i^0}{\partial\hat{z}_k}h_{kj}\right] + \sum_{j=1}^{2}\frac{\partial}{\partial\hat{z}_j}\left[J\sum_{k=1}^{3}\frac{\partial\hat{u}_i^0}{\partial\hat{x}_k}h_{kj}\right]\Bigg\} - \varepsilon J^{-1}\sum_{j=1}^{3}\frac{\partial}{\partial\hat{x}_j}\left[Jg_{ji}p^1\right]. \quad (64)$$

After [80], we have

$$|\int_{\Omega^{\varepsilon,n}}\Psi^\varepsilon\varphi\ dx| \le C\varepsilon^2\|\nabla\varphi\|_{L^2(\Omega^{\varepsilon,n})} \quad (65)$$

for every $\varphi \in H^1(\Omega^{\varepsilon,n})$, being zero at the fibres boundaries.

Then one corrects the compressibility effects, by introducing the auxiliary problem

$$\mathcal{L}_{div}Q \equiv \frac{\partial Q_1}{\partial z_1} + \frac{\partial}{\partial z_2}\Big(-\sin\gamma(x_1)Q_2 + \cos\gamma(x_1)Q_3\Big) = \text{div}_{\hat{x}}\ (JG\hat{\mathbf{u}}^0) \quad \text{in} \quad \mathcal{Y}_F \quad (66)$$

$$Q \ \text{ is } \ \mathcal{Y}-\text{periodic in } \ (z_1, z_2). \quad (67)$$

Using the decomposition from section 2, we see that

$$\text{div}_x\int_{\mathcal{Y}_F}\mathbf{u}^0(x, z_1, z_2)dz_1dz_2 = \text{div}_x\mathbf{u}^D = 0$$

is the necessary and sufficient condition for existence of at least one solution for (66)-(67). Clearly, there is no uniqueness and we can choose a smooth solution Q for (66)-(67).

Now, as in [80], we have

$$-\nu\varepsilon^2\Delta(w_i^\varepsilon + \frac{\varepsilon}{\nu}Q(x, \frac{\rho(x_1^{\varepsilon,n}, x)}{\varepsilon})) + \frac{\partial}{\partial x_i}q^\varepsilon = -\Psi_i^\varepsilon - \frac{\varepsilon^3}{\nu}\Delta Q(x, \frac{\rho(x_1^{\varepsilon,n}, x)}{\varepsilon}) \quad \text{in} \quad \Omega^{\varepsilon,n},\ i = 1,2,3, \quad (68)$$

$$\text{div}\ (w^\varepsilon + \frac{\varepsilon}{\nu}Q(x, \frac{\rho(x_1^{\varepsilon,n}, x)}{\varepsilon})) = \frac{\varepsilon}{\nu}\text{div}_x\ Q(x, \frac{\rho(x_1^{\varepsilon,n}, x)}{\varepsilon}) \quad \text{in} \quad \Omega^{\varepsilon,n}. \quad (69)$$

This means that $\{w^\varepsilon + \frac{\varepsilon}{\nu} Q(x, \frac{\rho(x_1^{\varepsilon,n},x)}{\varepsilon}), q^\varepsilon\}$ satisfies the Stokes system (68)-(69) with the force and the source terms of order ε^2 in appropriate norms.

In the situation without external boundary one could proceed as in [80] and conclude that the L^2-norms of $\{w^\varepsilon + \frac{\varepsilon}{\nu} Q(x, \frac{\rho(x_1^{\varepsilon,n},x)}{\varepsilon})\}$ and q^ε are of order ε.

We are in presence of many layers $\Omega^{\varepsilon,n}$ and the geometry differs from one layer to another. Consequently, the coefficients in problem (24) change with n and they depend on $x^{\varepsilon,n}$. Thus, there is a jump of $\mathbf{u}^0$ at the interface between different layers. Furthermore, the layers are of size ε^r and this fact could also influence the estimates. By " gluing together " the layers, this difficulty will be avoided.

Homogenization of problems containing several different subdomains, is closely linked with the determination of the effective flow conditions at the interface between two different porous media. At mathematically rigorous level, these problems were considered by W. Jäger and A. Mikelić in a number of papers. The general theory of the corresponding boundary layers is in [65]. Our particular situation, with layers of fibres which should be glued together, has a lot of similarities with the determination of the transmission conditions at the interface between two porous media with different pore structures. The transmission conditions, involving continuity of the pressure and of the normal velocities, were rigorously established in the article [66]. We will follow the approach from [66].

Let us suppose that the interface between the layers $\Omega^{\varepsilon,n}$ and $\Omega^{\varepsilon,n+1}$ is at $x_1 = c$. Because of (22), the interface is stable under the mapping $\varphi_{\varepsilon,n}$ and, following [66], we introduce the boundary layer problem which corrects the jump of $\mathbf{u}^0$. We denote by $\mathcal{L}_S$ the Stokes operator corresponding to system (24). We denote the operator $\mathcal{L}_S^+$ when the parameter in the coefficients is $x^{\varepsilon,n+1}$, and by $\mathcal{L}_S^-$ otherwise (i.e. when the parameter is $x^{\varepsilon,n}$). Analogously, $\{\omega^{j,+}, \pi^{j,+}\}$ (resp. $\{\omega^{j,-}, \pi^{j,-}\}$) is the solution for (24) for $x = x^{\varepsilon,n+1}$ (resp. for $x = x^{\varepsilon,n}$). Then the boundary layer problem reads

$$\mathcal{L}_S^+(\{\omega^{j,bl}, \pi^{j,bl}\}) = 0 \quad \text{in} \quad Z^+ = \cup_{k\in I\!N\cup\{0\}} \left(\mathcal{Y}_F + k\vec{e}_1\right) \tag{70}$$

$$\mathcal{L}_S^-(\{\omega^{j,bl}, \pi^{j,bl}\}) = 0 \quad \text{in} \quad Z^+ = \cup_{k\in I\!N} \left(\mathcal{Y}_F - k\vec{e}_1\right) \tag{71}$$

$$\left[\omega^{j,bl}\right] = \omega^{j,+} - K_{1j}(x^{\varepsilon,n+1})\vec{e}_1 - (\omega^{j,-} - K_{1j}(x^{\varepsilon,n})\vec{e}_1) \quad \text{at } z_1 = 0 \tag{72}$$

$$\left[\frac{\partial \omega_i^{j,bl}}{\partial z_1} - \pi^{j,bl}\delta_{1i}\right] = \frac{\partial \omega_i^{j,+}}{\partial z_1} - \pi^{j,+}\delta_{1i} - (\frac{\partial \omega_i^{j,-}}{\partial z_1} - \pi^{j,-}\delta_{1i}) \quad \text{at } z_1 = 0 \tag{73}$$

$$\{\omega^{j,bl}, \pi^{j,bl}\} \quad \text{is periodic in} \quad z_2. \tag{74}$$

We note that the normal component of the jump $\left[\omega^{j,bl}\right]$ at the interface $x_1 = c$ has a zero mean.

Then by slightly generalizing the theory from [66], we get the solvability of problem (70)-(74) and the Saint-Venant principle saying that

$$|\nabla\omega^{j,bl}| + |\omega^{j,bl}| \leq c_0 e^{-c_1|y_1|}, \quad \text{for some positive constants } c_0 \text{ and } c_1 \tag{75}$$

$$|\nabla\pi^{j,bl}| + |\pi^{j,bl} - H(z_1)C_1^j - H(-z_1)C_2^j| \leq c_0 e^{-c_1|y_1|}. \tag{76}$$

Consequently, in the neighborhoods of the separating planes $x_1 = c$ between two adjacent layers, our asymptotic expansion reads

$$\frac{\mathbf{u}^\varepsilon}{\varepsilon^2} = \mathbf{u}^0(x, \frac{\rho(x_1^{\varepsilon,n}, x)}{\varepsilon})H(c - x_1) + \mathbf{u}^0(x, \frac{\rho(x_1^{\varepsilon,n+1}, x)}{\varepsilon})H(x_1 - c) +$$
$$\sum_{j=1}^{3} \frac{\varepsilon}{\nu}(f_j - \frac{\partial p^0}{\partial x_j})(x)\omega^{j,bl} + (\text{ compressibility corrections } + \text{ higher order terms}) \tag{77}$$

$$p^\varepsilon = p^0(x) + \varepsilon p^1(x, \frac{\rho(x_1^{\varepsilon,n}, x)}{\varepsilon})H(c - x_1) + \varepsilon p^1(x, \frac{\rho(x_1^{\varepsilon,n+1}, x)}{\varepsilon})H(x_1 - c) +$$
$$\sum_{j=1}^{3} \frac{\varepsilon^2}{\nu}(f_j - \frac{\partial p^0}{\partial x_j})(x)\pi^{j,bl} + (\text{ higher order terms}) \tag{78}$$

Let us check that the jump of $\frac{\mathbf{u}^\varepsilon}{\varepsilon^2}$ at $x_1 = c$ is zero.

First, in the tangential direction we have continuity of traces, by construction.

Next, in the normal direction we have

$$\frac{\mathbf{u}_1^\varepsilon}{\varepsilon^2} = \sum_{j=1}^{3}(K_{1j}(x^{\varepsilon,n+1}) - K_{1j}(x^{\varepsilon,n}))f_j - \frac{\partial p^0}{\partial x_j})|_{x_1=c} = 0, \tag{79}$$

since we imposed at the interfaces the continuity of $K(f - \nabla p^0)\vec{e}_1$, as the transmission condition. We note that it follows from those considerations that the continuity of the normal components of the filtration velocity is one of the necessary and sufficient conditions for having the correct order of approximation.

For this new approximation, we write an analogue of the system (68)-(69). Then, it is used for obtaining the estimate for the L^2-norm of the difference between $\{\frac{\mathbf{u}^\varepsilon}{\varepsilon^2}, p^\varepsilon\}$ and the correction. Calculations are analogous to the ones from [66] and we have the following conclusions:

- a) The pressure is continuous at the layer interfaces. We note that the absolute value of the pressure jump is one of the leading terms in the error estimate and it should be set to zero in order to get an approximation. It is the second (and last) necessary and sufficient condition for obtaining the correct order of approximation. For detailed calculations we refer to [66] .

- b) $\omega^{j,bl}$ is of order $c_0 \exp\{-c_1 \varepsilon^{r-1}\}$ at the other interfaces and we can simply ignore it there.
- c) Using that $\rho \in C^1$, we get that the boundary layer terms are of order $\varepsilon^{r+3/2}$. Since we have ε^{-r} boundary layers, this means a contribution of order $\varepsilon^{3/2}$.
- d) Keeping $K(x^{\varepsilon,n})$ and $K(x^{\varepsilon,n+1})$ deteriorates significantly the regularity of p^0 . For this reason, $K(x_1)$ should be used. This introduces an approximation error of order ε^r. For small r, a possible solution is to take several intermediate values of $x^{\varepsilon,n}$. Attempts to work with less regular K lead to weaker error estimates and give raise to a global error of order $\varepsilon^{1/8}$ (see [66]).

To conclude, in analogy with the results from [66] , we have

Theorem 3
Let B_n be the n^{th} layer, containing fibres. Then we have

$$\|\frac{\mathbf{u}^\varepsilon}{\varepsilon^2} - \sum_{over\ layers} \chi_{B_n}(x) \frac{1}{\nu} \sum_{j=1}^{3} \left(f_j(x) - \frac{\partial p^0}{\partial x_j}(x) \right) \boldsymbol{\omega}^j(x_1, \frac{x_1}{\varepsilon}, \frac{x_3}{\varepsilon} \cos\gamma(x^{\varepsilon,n}) - \frac{x_2}{\varepsilon} \sin\gamma(x^{\varepsilon,n}))\|_{L^2(\Omega)} \leq C\varepsilon^{\min\{1/6,r\}}, \tag{80}$$

$$\|p^\varepsilon - p^0\|_{L^2_0(\Omega)} \leq C\varepsilon^{\min\{1/6,r\}}. \tag{81}$$

With an appropriate choice of layers, the estimates (80)-(81) imply an interior estimate of order $\sqrt{\varepsilon}$.

Acknowledgements: The research of A.M. was supported by the GDR MOMAS (Modélisation Mathématique et Simulations numériques liées aux problèmes de gestion des déchets nucléaires: 2439 - ANDRA, BRGM, CEA, EDF, CNRS) as a part of the project "*Modélisation micro-macro des phénomènes couplés de transport-chimie-déformation en milieux argileux* "

Part III

Numerical studies

Chapter 4

Numerical approximation

Les méthodes numériques présentées dans ce chapitre ont été implémentées dans la bibliothèque LIFE-V développée conjointement à l'INRIA, à l'EPFL et au Politecnico de Milan (www.lifev.org).

1 Introduction

The present chapter is devoted to the numerical approximation of the mathematical models which have been introduced in chapter 1 and analyzed in the course of chapter 2 and 3. Section 2 is devoted to the numerical approximation of the fluid dynamics problem. We introduce the basic tools for the numerical approximation of the Darcy problem and we discuss the mixed hybrid finite element formulation for the space discretization. Section 3 is devoted to the discretization of the transport equation. We use a splitting technique for the space discretization and the Euler method for the time discretization.
The goal of the section 4 is to present a modified method of upwinding that reduces the numerical diffusion introduced by the upwind scheme.

2 Numerical approximation of the flow problem

The mixed finite element method provides a direct and accurate approximation of the flux. However, mixed finite element discretizations give rise to large systems of algebraic equations, which are difficult to solve, because they are derive from a saddle point formulation. The introduction of inter-element multipliers, commonly called *hybridization*, is frequently used to transform this saddle point problem into a problem whose matrix is symmetric and positive definite (*see* [20]).
The main favorable property of these methods is that both the primary unknown and its gradient are approximated simutaneously with the same order of convergence. Besides, they preserve the physics of the problem, i.e. they

locally conserve mass and preserve the continuity of fluxes (*see* [20, 31, 85]). Some comparison studies show that the mixed hybrid finite element is superior to the standard finite element in terms of accuracy. It is also more efficient to the conforming method in terms of computational effort [2, 62]. In this section, we describe how the above mentioned techniques can be applied to the following second order elliptic equations

$$\left\{\begin{array}{rcll} \mathbf{u}+\mathbf{K}\nabla p &=& 0 & \text{in } \Omega, \\ \operatorname{div}\mathbf{u} &=& f & \text{in } \Omega, \\ p &=& p_b & \text{on } \Gamma_D, \\ \mathbf{u}.\mathbf{n} &=& u_b & \text{on } \Gamma_N, \end{array}\right. \tag{1}$$

where Ω is a bounded domain in $\mathbb{R}^3$ with polygonal boundary $\partial\Omega = \Gamma_D \cup \Gamma_N$; $\mathbf{K}$ is the so-called hydraulic conductivity, that is assumed to be symmetric and positive definite; $\mathbf{n}$ indicates the outward unit normal vector along $\partial\Omega$; $f \in L^2(\Omega)$ represents the sink/source function; p_b and u_b are respectively the Dirichlet and Neumann boundary conditions.
Under the above assumptions, it is immediate to chek that the problem (1) admits a unique solution.
The basic idea of the mixed methods is to approximate simultaneously the pressure p and its gradient , or more generally a gradient related velocity field $\mathbf{u}$ and compute the Darcy velocity $\mathbf{u}$ as an unknown independent function. Introducing the Hilbert spaces

$$V := H(\operatorname{div};\Omega) = \{\mathbf{v} \in (L^2(\Omega))^3 \mid \nabla.\mathbf{v} \in L^2(\Omega)\}, \tag{2}$$

$$H_{g,N}(\operatorname{div};\Omega) \;=\; \{\mathbf{v} \in H(\operatorname{div};\Omega) \mid \mathbf{v}.\mathbf{n} = g \text{ on } \Gamma_N\}, \tag{3}$$

the mixed formulation of (1) can be stated as: Find $(\mathbf{u},p) \in H_{g,N}(\operatorname{div};\Omega) \times L^2(\Omega)$ such that

$$\left\{\begin{array}{rcll} a(\mathbf{u},\mathbf{v}) - b(\mathbf{v},p) &=& g(\mathbf{v}) & \forall\, \mathbf{v} \in H_{0,N}(\operatorname{div};\Omega), \\ b(\mathbf{u},q) &=& f(q) & \forall\, q \in L^2(\Omega). \end{array}\right. \tag{4}$$

The bilinear form b on $V \times L^2(\Omega)$ is defined by $b(\mathbf{v},q) = \displaystyle\int_\Omega \operatorname{div}\ \mathbf{v}\ q\ dx$, a is continuous linear form on $V \times V$ defined by $a(\mathbf{u},\mathbf{v}) = \displaystyle\int_\Omega \mathbf{u}.\mathbf{v}\ dx$, g and f are continuous linear forms on V and $L^2(\Omega)$, resp., defined by

$$g(\mathbf{v}) = \int_{\Gamma_D} p_b\ (\mathbf{v}.\mathbf{n})\ ds \quad \text{and} \quad f(q) = \int_\Omega f\ q\ dx.$$

2.1 Discretization with the mixed-hybrid finite element

In the present section we consider the discretization of the space variables. First of all, let us introduce a triangulation $\mathcal{T}_h$ of the domain Ω, i.e. a finite decomposition of $\overline{\Omega}$ into polyhedrons, such that

1. each K is a polyhedron with non-empty internal part K;
2. $K_1 \cap K_2 = \emptyset$ for each distinct $K_1, K_2 \in \mathcal{T}_h$;
3. if $F = K_1 \cap K_2 \neq \varnothing$ and $K_1 \neq K_2$, then F is a common face, side or vertex of K_1 and K_2;
4. $\mathrm{diam}(K) \leq h$ for each $K \in \mathcal{T}_h$.

In our case, we consider hexahedra elements in $3D$. We denote by ε_h the set of edges of $\mathcal{T}_h$. Respecting the partition of $\partial\Omega$ into Dirichlet boundary Γ_D (where $p = p_b$ is given) and Neumann boundary Γ_N (where $\mathbf{u}.\mathbf{n} = u_b$ is given), ε_h can be subdivided into three disjoint subsets $\varepsilon_h = \varepsilon_h^I \cup \varepsilon_h^D \cup \varepsilon_h^N$. Here $\varepsilon_h^I := \{e \in \varepsilon_h | e \nsubseteq \partial\Omega\}$ is the set of inner edges, $\varepsilon_h^D := \{e \in \varepsilon_h | e \subset \Gamma_D\}$ is the set of edges lying on the Dirichlet boundary and $\varepsilon_h^N := \{e \in \varepsilon_h | e \subset \Gamma_N\}$ is the set of edges lying on the Neumann boundary. For every $K \in \mathcal{T}_h$ we denote by $P_k(K)$, $k \geq 0$, the set of polynomials of degree $\leq k$ on K. Analogously, we define $P_k(e)$ for $k \geq 0$ and $e \in \varepsilon_h$.
For the approximation of the Darcy velocity $\mathbf{u}$, we use the mixed finite element method on Raviart-Thomas elements of lowest order (*see* [20]) for the spatial discretization of the first two equations of (1). Thus $\mathbf{u}$ is approximated by $\mathbf{u}_h \in V_h$, where

$$V_h := RT_0(\Omega; \mathcal{T}_h) := \{v_h \in H(\mathrm{div}\,; \Omega) \mid v_h|_K \in RT_0(K) \quad \text{for all} \quad K \in \mathcal{T}_h\}$$

and $RT_0(K)$ is defined by

$$RT_0(K) := \{\chi_K / \chi_K = (ax + b, cy + d, ez + f), a, b, c, d, e, f \in \mathbb{R}\}.$$

The pressure p is approximated by a piecewise constant function $p_h \in Q_h$, where Q_h is defined by

$$Q_h := \{q_h \in L^2(\Omega) \mid q_h|_K \in P_0(K) \quad \text{for all} \quad K \in \mathcal{T}_h\}.$$

Here $P_0(K)$ is the space of constants on K.
Note that any $\mathbf{v}_h|_K \in RT_0(K)$ is uniquely defined by the flux across the edges of K

$$v_e := \int_e \mathbf{v}_h|_K . \mathbf{n}_e ds, \quad e \subset \partial K,$$

where $\mathbf{n}_e$ is an arbitrarily oriented unit normal vector to $e \in \varepsilon_h$.
The property $\mathbf{v}_h \in H(div;\Omega)$ requires the continuity of these flux values:

Lemma 3
The following definition for V is equivalent to (2):

$$V = \Big\{ \mathbf{v} \in \Big(L^2(\Omega)\Big)^3;\ (div\,\mathbf{v})|_K \in L^2(K) \quad \forall\, K \in \mathcal{T}_h;$$
$$\sum_{K\in\mathcal{T}_h} \int_{\partial K} \mathbf{v}.\mathbf{n}_K \varphi d\sigma = 0 \quad \forall\, \varphi \in \mathcal{D}(\Omega) \Big\}.$$

Here n_K denotes the exterior unit normal of K and $\mathcal{D}(\Omega) = C_0^\infty(\Omega)$ is the space of test functions.

Proof. Obviously, $''\subseteq''$ holds, since $V \subset \Big(L^2(\Omega)\Big)^3$ and $(\operatorname{div}\mathbf{v})|_K \in L^2(K)$ for all $K \in \mathcal{T}_h$. Furthermore, for all $\mathbf{v} \in V$ and $\phi \in \mathcal{D}(\Omega)$ Green's formula implies

$$\begin{aligned}
\sum_{K\in\mathcal{T}_h} \int_{\partial K} \mathbf{v}.\mathbf{n}_K \varphi d\sigma &= \sum_{K\in\mathcal{T}_h} \Big(\int_K \mathbf{v}.\nabla\varphi dx + \int_K \operatorname{div}\mathbf{v}\varphi dx \Big) \\
&= \int_\Omega \mathbf{v}.\nabla\varphi dx + \int_\Omega \operatorname{div}\mathbf{v}\varphi dx \\
&= \int_{\partial\Omega} \mathbf{v}.\mathbf{n}_K \varphi d\sigma = 0.
\end{aligned}$$

To prove that $''\supseteq''$ holds, too, we must show that each $\mathbf{v} \in \Big(L^2(\Omega)\Big)^3$, which fulfills the above requirements, has a generalized divergence in $L^2(\Omega)$. To this end, we define $\omega \in L^2(\Omega)$ by $\omega|_K = \operatorname{div}\mathbf{v}$ for all $K \in \mathcal{T}_h$. Then for all $\varphi \in \mathcal{D}(\Omega)$ it holds

$$\begin{aligned}
\int_\Omega \omega\varphi dx &= \sum_{K\in\mathcal{T}_h} \int_K \operatorname{div}\mathbf{v}\varphi dx = \sum_{K\in\mathcal{T}_h} \Big(\int_{\partial K} (\mathbf{v}.\mathbf{n}_K)\varphi d\sigma - \int_K \mathbf{v}.\nabla\varphi dx \Big) \\
&= \sum_{K\in\mathcal{T}_h} \int_K \mathbf{v}.\nabla\varphi dx = -\int_\Omega \mathbf{v}.\nabla\varphi dx.
\end{aligned}$$

Hence, ω is the (generalized) divergence of $\mathbf{v}$, as desired. This concludes the proof of the lemma. $\diamond$

To take into account the flux boundary conditions on Γ_N, we consider the subspace $V_h^{\mathbf{u}_b,\Gamma_N}$ of V_h, which is defined by

$$V_h^{\mathbf{u}_b,\Gamma_N} := \Big\{ \mathbf{v}_h \in V_h \;\Big|\; \int_e \mathbf{v}_h.\mathbf{n} ds = \int_e u_b ds \quad \text{for all} \quad e \in \varepsilon_h^N \Big\}.$$

If $u_b \equiv 0$ on Γ_N, we obtain the space V_h^{0,Γ_N}.
Then the discrete mixed formulation reads as follows: Find $(\mathbf{u}_h, p_h) \in V_h^{\mathbf{u}_b,\Gamma_N} \times Q_h$ such that for every $(\mathbf{v}_h, q_h) \in V_h^{0,\Gamma_N} \times Q_h$

$$\left\{ \begin{array}{rcl} a(\mathbf{u}_h, \mathbf{v}_h) - b(\mathbf{v}_h, p_h) & = & g(\mathbf{v}_h), \\ b(\mathbf{u}_h, q_h) & = & f(q_h). \end{array} \right. \tag{5}$$

Unfortunately, the systems of algebraic equations resulting from the mixed finite element discretization are semidefinite. In order to obtain symmetric definite positive systems, we apply the following classical technique, called hybridization:

Hybridization: We eliminate the continuity constraints in the definition of V_h and enforce the required continuity instead through additional equations involving Lagrange multipliers defined on the edges $e \in \varepsilon_h$. Thus we replace V_h by

$$W_h := RT_{-1}(\Omega; \mathcal{T}_h) := \left\{ \mathbf{v}_h \in \left(L^2(\Omega)\right)^2 \;\middle|\; \mathbf{v}_h|_K \in RT_0(K) \quad \text{for all} \quad K \in \mathcal{T}_h \right\},$$

and $V_h^{u_b,\Gamma_N}$ by the corresponding $W_h^{u_b,\Gamma_N}$ of W_h.
W_h is the discontinuous first order Raviart-Thomas finite element space. Notice that $V_h \subset W_h$, and that an element $\mathbf{v}_h$ of W_h belongs to V_h if and only if $\mathbf{v}_h \in H(div; \Omega)$.
In addition, we define the space of Lagrange multipliers by

$$\Lambda_h^{p_b,\Gamma_D} := \left\{ \lambda_h \in L^2(E_h) \;\middle|\; \lambda_h|_e \in P_0(e) \; \forall \, e \in \varepsilon_h, \; \int_e (\lambda_h - p_b) ds = 0 \; \forall \, e \in \varepsilon_h^D \right\},$$

where $E_h = \cup_{e \in \varepsilon_h} e$. Then the *hybridized* mixed formulation reads as: Find $(\mathbf{u}_h, p_h, \mu_h) \in W_h^{u_b,\Gamma_N} \times Q_h \times \Lambda_h^{p_b,\Gamma_D}$, such that for every $(\mathbf{v}_h, q_h, \lambda_h) \in W_h^{0,\Gamma_N} \times Q_h \times \Lambda_h^{0,\partial\Omega}$

$$\left\{ \begin{array}{rcl} a(\mathbf{u}_h, \mathbf{v}_h) - \displaystyle\sum_{K \in \mathcal{T}_h} b_K(\mathbf{v}_h, p_h) + \sum_{K \in \mathcal{T}_h} d_K(\mu_h, \mathbf{v}_h) & = & 0, \\ \displaystyle\sum_{K \in \mathcal{T}_h} b_K(\mathbf{u}_h, q_h) & = & f(q_h), \\ \displaystyle\sum_{K \in \mathcal{T}_h} d_K(\lambda_h, \mathbf{u}_h) & = & 0. \end{array} \right. \tag{6}$$

where $b_K(\mathbf{v}_h, q_h) = \displaystyle\int_K \text{div } \mathbf{v}_h \; q_h \; dx$ and $d_K(\lambda_h, \mathbf{v}_h) = \displaystyle\int_{\partial K} \lambda_h \; (\mathbf{v}_h . \mathbf{n}_K) \; ds$ for $K \in \mathcal{T}_h$.

The solutions $\mathbf{u}_h$ and p_h of (6) coincide with the solutions $\mathbf{u}_h$ and p_h of (5). Therefore we are allowed to use the same notation for them.

Theorem 4

1. *Let $(\mathbf{u}_h, p_h) \in V_h \times Q_h$ be a solution of (5). Then there exists a unique $\mu_h \in \Lambda_h^g$ such that $(\mathbf{u}_h, p_h, \mu_h)$ is a solution of (6).*

2. *Let $(\mathbf{u}_h, p_h, \mu_h) \in W_h \times Q_h \times \Lambda_h^g$ be a solution of (6). Then $(\mathbf{u}_h, p_h)$ is a solution of (5).*

Proof. (cf. the proof of Thm. V.1.1 in [20]). $\diamond$

Remark 2.1 *The Lagrangian multiplier μ_h represents an approximation of the trace of the solution p on ε_h. This value can be used together with p_h to obtain a better approximation of p* (see[*11*]).

Some remarks on the algorithmic aspects: In order to reformulate the problem (6) in algebraic form, we introduce the following basis vectors:

1. $(\chi_K)_{K \in \mathcal{T}_h}$ is the basis associated to the space Q_h, χ_K denotes the characteristic function of an element K.

2. $(\chi_e)_{e \in \varepsilon_h}$ is the basis associated to the space Λ_h, χ_e denotes the characteristic function of an edge e.

3. The corresponding basis vectors to W_h are denoted by $\mathbf{w}_{K,e}$.
   The vector $\mathbf{w}_{K,e}$ has the following properties:

   - $\mathbf{w}_{K,e}$ is null on $\Omega \backslash \overline{K}$,
   - $\nabla.\mathbf{w}_{K,e}$ is constant on K and $\displaystyle\int_K \nabla.\mathbf{w}_{K,e}(x)dx = 1$,
   - $\mathbf{w}_{K,e}(x).\mathbf{n}_f$ is constant along each edge f and $\displaystyle\int_f \mathbf{w}_{K,e}(x).\mathbf{n}_{K,f}dx = \delta_{ef}$.

By virtue of these definitions, the unknown functions $\mathbf{u}_h, p_h$ and μ_h can be represented by

$$\mathbf{u}_h = \sum_{K \in \mathcal{T}_h} \sum_{e \in \partial K} \mathbf{u}_{K,e} \mathbf{w}_{K,e},$$

$$p_h = \sum_{K \in \mathcal{T}_h} p_K \chi_K,$$

$$\mu_h = \sum_{e \in \varepsilon_h} \mu_e \chi_e,$$

where p_K is the mean value of the pressure over K and μ_e is the mean value of the pressure over the edge e.
Figure 4.1 shows the approximated unknowns and the basis functions on the $2D$ reference element.

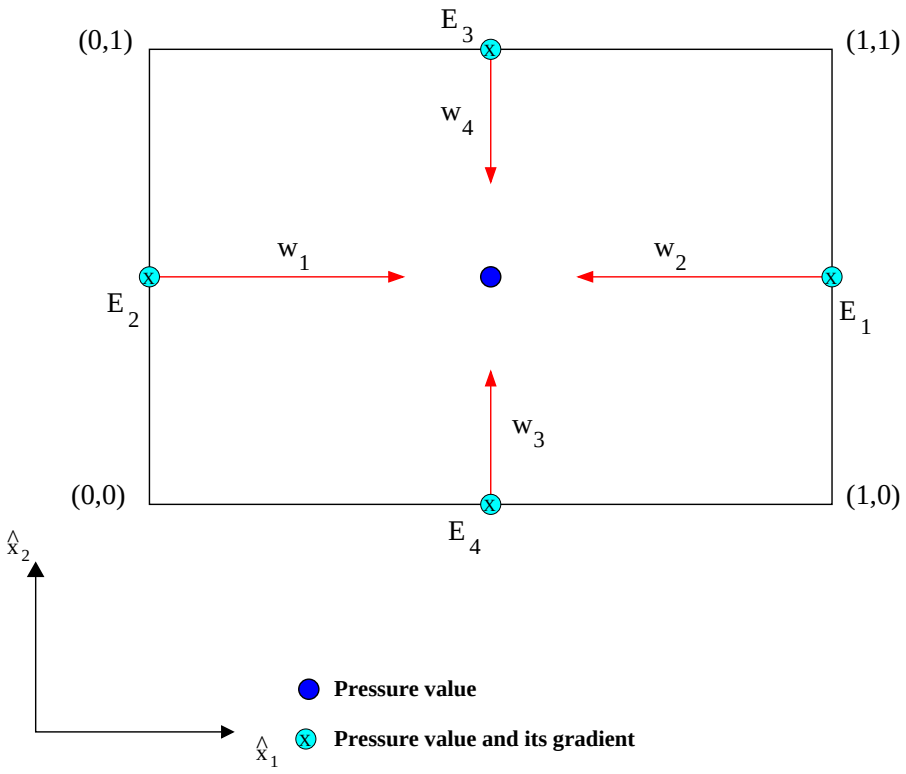

Figure 4.1: The approximated unknowns and the basis functions on the reference element: the 2D case

Employing the basis functions $\mathbf{w}_{K,\overline{e}}$ for $\overline{e} \notin \varepsilon_h^N$ and $K \in \mathcal{T}_h$ with $\overline{e} \subset \partial K$, χ_K for $K \in \mathcal{T}_h$, and $\chi_{\overline{e}}$ for $\overline{e} \in \varepsilon_h^I$ as test functions, we obtain from (6) the following system of algebraic equations:

$$\left\{ \begin{array}{lcll} a(\mathbf{u}_K, \mathbf{w}_{K,\overline{e}}) - p_K + \mu_{\overline{e}} & = & 0, & K \in \mathcal{T}_h,\ \overline{e} \subset \partial K, \\ \displaystyle\sum_{e \in \partial K} u_{K,e} - \int_K f dx & = & 0, & K \in \mathcal{T}_h, \\ u_{K,\overline{e}} + u_{K',\overline{e}} & = & 0, & \overline{e} \in \varepsilon_h^I,\ \overline{e} = \partial K \cap \partial K'. \end{array} \right. \tag{7}$$

Here $\mathbf{u}_K \in RT_0(K)$ is defined by $\mathbf{u}_K = \displaystyle\sum_{e \in \partial K} u_{K,e} \mathbf{w}_{K,e}$.
For the derivation of (7) we employed the fact that the basis functions $\mathbf{w}_{K,e}$ of W_h satisfy

$$\int_\Omega \text{div } \mathbf{w}_{K,e} dx = \int_K \text{div } \mathbf{w}_{K,e} dx = \int_{\partial K} \mathbf{w}_{K,e}.\mathbf{n}_K d\sigma = \int_e \mathbf{w}_{K,e}.\mathbf{n}_K d\sigma = 1,$$

where $\mathbf{n}_K$ denotes the unit outer normal of K.
After an assembling procedure, we obtain the following algebraic restatement:

$$\left\{ \begin{array}{lcr} A\mathbf{u} + B^T p + D^T \mu & = & 0 \\ B\mathbf{u} & = & -\mathbf{F} \\ D\mathbf{u} & = & 0, \end{array} \right. \tag{8}$$

where $\mathbf{F}$ is a vector defined by: $\mathbf{F} = \left(\text{approximation of } \displaystyle\int_K f dx\right)_{K \in \mathcal{T}_h}$,
the matrix A is given by:

$$A_{(K,e),(K',e')} = \left\{ \begin{array}{ll} \displaystyle\int_K \mathbf{K}^{-1} \mathbf{w}_{K,e}.\mathbf{w}_{K,e'} & \text{if} \quad K = K' \\ 0 & \text{otherwise,} \end{array} \right.$$

the matrix B is defined by:

$$B_{K,(K',e)} = \left\{ \begin{array}{ll} 1 & \text{if} \quad K = K' \quad \text{and} \quad e \subset K \\ 0 & \text{otherwise,} \end{array} \right.$$

and the matrix D has the following expression:

$$D_{e,(K,e')} = \left\{ \begin{array}{ll} 1 \text{ or } -1 & \text{if} \quad e = e' \\ 0 & \text{otherwise.} \end{array} \right.$$

The matrix

$$S := \begin{pmatrix} A & B^T & D^T \\ B & 0 & 0 \\ D & 0 & 0 \end{pmatrix}$$

is symmetric, non-singular but fails to be positive definite. However, A is a block-diagonal matrix, each block being a 6×6 matrix easy to invert. We can therefore eliminate $\mathbf{u}$ in (8) finding

$$\begin{cases} BA^{-1}B^T p + BA^{-1}D^T \mu &= \mathbf{F} \\ DA^{-1}B^T p + DA^{-1}D^T \mu &= 0, \end{cases} \tag{9}$$

i.e., a linear system associated to a symmetric and positive definite matrix. The unknown p_h is not continuous, therefore another simple elimination procedure leads to a system where the only unknown is μ. It reads

$$R\mu = \tilde{\mathbf{F}}, \tag{10}$$

where

$$R := DA^{-1}D^T - DA^{-1}B^T(BA^{-1}B^T)^{-1}BA^{-1}D^T,$$

$$\text{and} \qquad \tilde{\mathbf{F}} := -DA^{-1}B^T(BA^{-1}B^T)^{-1}\mathbf{F}.$$

Having determined the solution of system (10) for the Lagrange multiplier μ, the mixed-Lagrangian algorithm furnishes p through (9) and $\mathbf{u}$ through (8).
For the numerical computation, the symmetric definite positive system (10) is first solved by a preconditionned conjugate gradient method to compute the trace of the pressure on the faces on the elements; next the pressure and the velocity are recovered by a local procedure from the system (7). This yields a reduction of the number of equations that have to be solved globally. We give the principal steps of the MHFE algorithm.

1. Initialize geometry and physical parameters of the problem.
2. Create the Schur complement matrix at the element level.
3. Find μ (trace of the pressure) by solving (10) via a preconditionned conjugate gradient method.
4. Loop on the number of cells.
   (a) Evaluate and invert $A_K = \displaystyle\int_K \mathbf{K}^{-1}\mathbf{w}_{K,e}.\mathbf{w}_{K,e'}$.
   (b) Calculate the flux $\mathbf{u}_K$ and the pressure p_K by solving (7).
   (c) Write the outputs p_K and U_K.

Remark 2.2 *For the numerical calculation of the matrixs A_K, B_K and D_K on the reference elements, we use the Piola transformation: let $\hat{K}$ be the reference element. For each $K \in \mathcal{T}_h$, there exist a transformation*

$\hat{K} \xrightarrow{T_a} K = T_a(\hat{K})$, bijective from $\hat{K}$ to K. We denote by DT_a the deformation gradient and by J the determinant of DT_a. Here, to each vector function $\hat{\mathbf{u}} \in H(div;\hat{K})$ we associate the function $\mathbf{u} \in H(div;K)$, defined by

$$\mathbf{u}(x) = \frac{1}{|J|} DT_a.\hat{\mathbf{u}}(\hat{x}) \quad \textit{for each} \quad x = F(\hat{x}) \in K. \tag{11}$$

The transformation (11) was constructed in such a way that

$$\int_K \mathbf{u}.\nabla p \; dx = \int_{\hat{K}} \hat{\mathbf{u}}.\nabla \hat{p} \; d\hat{x}$$

Using Green's formula we deduce, cf. *[96], that*

$$\int_K p div \; \mathbf{u} \; dx = \int_{\hat{K}} \hat{p} div \; \hat{\mathbf{u}} \; d\hat{x},$$

and we have, with $\hat{\mathbf{n}}_K$ denoting the exterior unit normal of $\partial\hat{K}$,

$$\int_{\partial K} p \; \mathbf{u}.\mathbf{n}_K \; d\sigma = \int_{\partial\hat{K}} \hat{p} \; \hat{\mathbf{u}}.\hat{\mathbf{n}}_K \; d\hat{\sigma}$$

2.2 Numerical examples

2.2.1 First example:

In this experiment, we impose a pressure drop between two opposite faces of a unit cube. The permeability tensor is equal to the identity. Figure 4.2 shows the pressure.

2.2.2 Second example:

In this experiment, we impose the same Dirichlet condition on the 6 faces of a unit cube (Dirichlet condition equal to xyz). The permeability tensor is equal to the identity. Figure 4.3 shows the the velocity and the pressure.

2.2.3 Third example

In this experiment, the tensor of permeability is given by

$$\boldsymbol{K}(x_1) = \boldsymbol{R}(x_1)\boldsymbol{K}_0\boldsymbol{R}^{-1}(x_1), \tag{12}$$

with

$$\boldsymbol{R}(x_1) = \begin{bmatrix} 1 & 0 & 0 \\ 0 & \cos\gamma(x_1) & -\sin\gamma(x_1) \\ 0 & \sin\gamma(x_1) & \cos\gamma(x_1) \end{bmatrix}$$

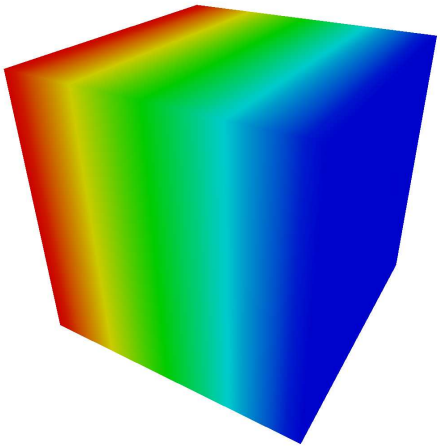

Figure 4.2: The pressure.

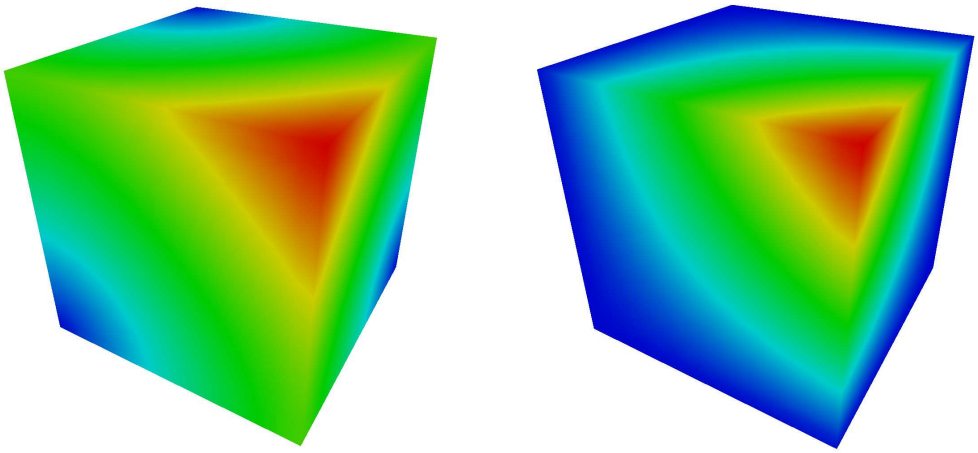

Figure 4.3: Velocity (at left) and pressure (at right).

and

$$\boldsymbol{K}_0 = \frac{1}{|\mathcal{Y}|} \begin{bmatrix} \int_{\mathcal{Y}_F} U_1^1 & 0 & \int_{\mathcal{Y}_F} U_1^2 \\ 0 & \int_{\mathcal{Y}_F} V & 0 \\ \int_{\mathcal{Y}_F} U_2^1 & 0 & \int_{\mathcal{Y}_F} U_2^2 \end{bmatrix} \tag{13}$$

where the coefficients of $\boldsymbol{K}_0$ are the solutions of the two generic problems (Stokes/Poisson) given in the chapter 3.
We impose a pressure drop between two opposite faces of a unit cube, The angle between the fibers and Ox_2 is variable ($\gamma(x_1) = 2\pi x_1$). Figure 4.4 shows the influence of the orientation of the fibers on the velocity vectors. Figure 4.5 show an isometric view and views along Ox_1, Ox_2, Ox_3 of some streamlines.

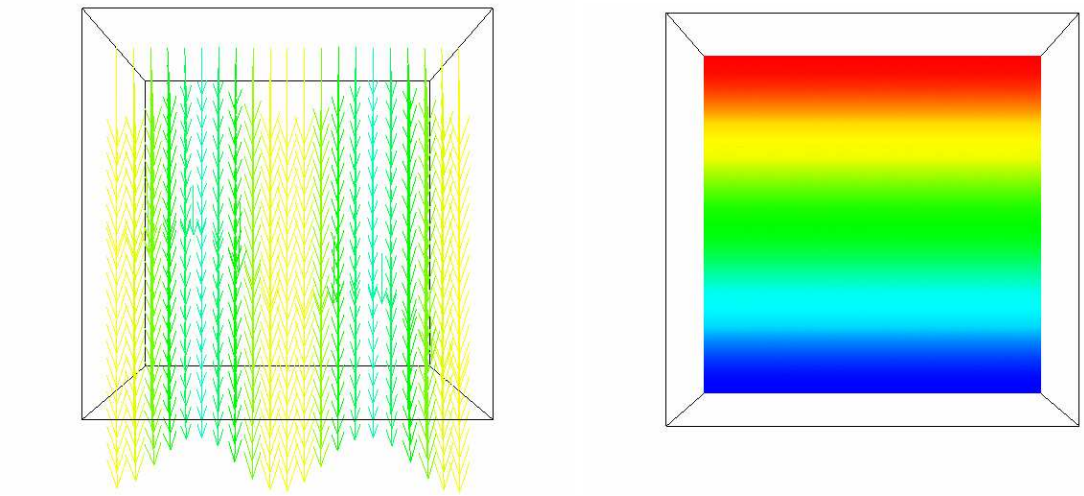

Figure 4.4: Velocity and pressure obtained with fibers making an angle $\gamma(x_1) = 2\pi x_1$ with Ox_2 (on this picture Ox_1 is horizontal and Ox_2 vertical).

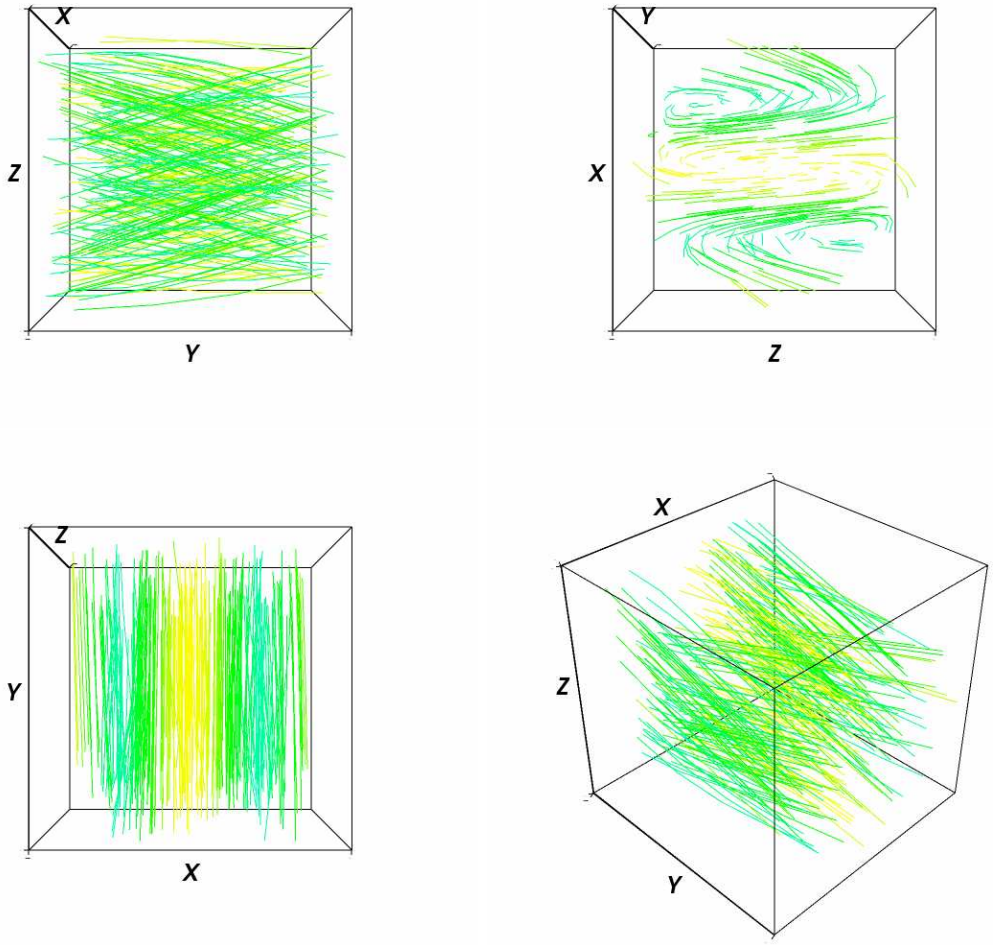

Figure 4.5: Streamlines obtained with fibers making an angle $\gamma(x_1) = 2\pi x_1$ with Ox_2 (x_1, x_2, x_3 are denoted by X, Y, Z on these pictures)

3 Numerical approximation of colloid transport equation

3.1 Introduction

We consider the advection-diffusion-reaction equations:

$$\frac{\partial c}{\partial t} + \operatorname{div}(\mathbf{u}c - \mathbf{D}(\mathbf{u})\nabla c) = -k\, c\, s, \quad \text{in} \quad \Omega, \tag{14}$$

$$\frac{\partial s}{\partial t} = -k\, c\, s, \quad \text{in} \quad \Omega. \tag{15}$$

In our case, the reaction term models the adhesion and the diffusion models the so-called dispersion of the porous medium.
When (14)-(15) is advection dominated, conventional numerical methods exhibit some combination of difficulties, ranging from non-physical oscillations (central difference/ Galerkin schemes) to excessive numerical diffusion (upwind schemes) at steep fronts.
One powerful approach for such problems are operator splitting techniques, which involve decoupling the full model into single physics components, employing specialized numerical methods to solve each component, and coupling the resulting solutions togother. Indeed, a natural strategy is to split the equation into a hyperbolic conservation law modelling advection and a parabolic equation modelling diffusion and lower-order terms, and then try to reproduce the solution using these simpler equations as building blocks. Variations on this operator splitting approach have indeed been taken by several authors; we mention Demkowitz & Oden [38], Douglas & Russel [39], Espedal & Ewing [43], Dahle [32], and Arbogast & Wheeler [10]. A more general approach is that of the Eulerian-Lagrangian localized adjoint methods of Celia et al. [26], and Wang et al. [99].
A number of methods for advection-dominated diffusion equations have been based on the above splitting. For example, Douglas and Russell developped the Modified Method of Characteristics [39] based on combining a characteristic method for advection equation with a Galerkin finite element method for diffusion equation.

In [34, 35, 36], Dawson examined Upwind-Mixed methods to explicitly approximate the advective terms using an upwind method and implicitly approximate diffusive terms using a mixed finite element method. Recently, Dawson and Aizinger [37] extended this analysis by applying the Discontinuous Galerkin method developed by Cockburn and Shu [30] and the Enhanced Mixed finite element method developped by Arbogast et al [9] to the transport equation. They analyzed the standard transport equation utilizing higher order approximating spaces, a positive semi-definite diffusion coefficient, and physically realistic boundary conditions.

The purpose here, is to approximate (14)-(15) by employing the splitting techniques. Indeed, we will explicitly approximate the advective-reactive terms using an upwind technique based on the finite volume scheme and we will implicitly approximate diffusive term using a mixed hybrid finite element method.

3.2 Construction of approximate solutions

Here we describe time-splitting techniques which can be applied to the system given by (14)-(15), whereby advection/reaction and diffusion are approximated by different solution procedures. Therefore, before giving the splitting algorithm, we introduce numerical schemes for solving these two equations.

3.2.1 The advection-reaction system

In this section, we consider the following advection-reaction system

$$\frac{\partial c}{\partial t} + \mathrm{div}\,(c\ \mathbf{u}) = -k\ c\ s, \tag{16}$$

$$\frac{\partial s}{\partial t} = -k\ c\ s. \tag{17}$$

We will employ a cell-centered finite volume scheme for the spatial discretization of (16) and (17). Note that this finite volume scheme can be derived from the mixed finite element method *cf.* [13]. It is well known that the finite volume method is well-suited to treat numerically hyperbolic systems of conservation laws, it is robust and presents the advantage to be conservative (we refer to [44] for a survey of its properties).

Formulation of the method: Integrating (16) over a cell $K \in \mathcal{T}_h$ and applying the divergence theorem yields the following equation for all $K \in \mathcal{T}_h$:

$$\frac{1}{|K|}\int_K \frac{\partial c}{\partial t} = -\frac{1}{|K|}\int_{\partial K} c\ \mathbf{u}.\mathbf{n}_K\ d\sigma - \frac{k}{|K|}\int_K c\ s\ dx, \tag{18}$$

where $|K|$ is the measure of K.
We subdivide the time interval $[0,T]$ into a finite number of sub-interval $[t^n, t^{n+1}]$. Let $\Delta t = t^{n+1} - t^n$ denote the time step. Writing equation (18) at time t^n and discretizing the time partial derivative by the Euler explicit scheme suggests to find an approximation $c^n(x)$ of the solution c at time t^n which satisfies the following semi-discretized equation:

$$\frac{1}{|K|}\int_K \frac{c^{n+1} - c^n}{\Delta t} = -\frac{1}{|K|}\int_{\partial K} c^n\ \mathbf{u}.\mathbf{n}_K\ d\sigma - \frac{k}{|K|}\int_K c^n\ s^n\ dx. \tag{19}$$

Now, if we apply the cell-centered finite volume method, each discrete unknown is associated with a control volume. Let $\left(c_K^n, s_K^n\right)_{K\in\mathcal{T}_h}$ denote the discrete unknowns.
In order to define the upwind technique [58], we need to split the boundary ∂K of a discretized element K into an inflow part ∂K^{in} and an outflow part ∂K^{out} defined by

$$\begin{aligned} \partial K^{in} &= \{x \in \partial K : \mathbf{u}.\mathbf{n}_K(x) \geq 0\}, \\ \partial K^{out} &= \{x \in \partial K : \mathbf{u}.\mathbf{n}_K(x) < 0\}, \end{aligned}$$

where $\mathbf{n}_K(x)$ denotes the unit outward normal to ∂K.
Let E be a common edge between any two adjacent elements K and K'. Since discontinuity for any function $c \in Q_h$ is allowed acrooss interelemnet boundaries, we need to define the jump discontinuity of c across E. We introduce the notation c^{in} and c^{out} to denote respectively the inner and the outer values of c over E with respect to K, that is,

$$\begin{aligned} c^{\text{in}}(x) &= \lim_{\varepsilon\to 0^-} c(x+\varepsilon\beta), \\ c^{\text{out}}(x) &= \lim_{\varepsilon\to 0^+} c(x+\varepsilon\beta). \end{aligned}$$

Define the upwind value c^u on an element boundary as follows:

$$c^u = \begin{cases} c^{\text{in}}, \text{ if } \mathbf{u}.\mathbf{n} \geq 0, \\ c^{\text{out}}, \text{ if } \mathbf{u}.\mathbf{n} < 0. \end{cases}$$

We have therefore derived the following finite volume scheme for the discretization of (16)

$$\boxed{c_K^{n+1} = c_K^n - \Delta t\Big[\frac{1}{|K|}c^{\text{in}}\int_{\partial K^{\text{in}}} \mathbf{u}.\mathbf{n}\, d\sigma + \frac{1}{|K|}c^{\text{out}}\int_{\partial K^{\text{out}}} \mathbf{u}.\mathbf{n}\, d\sigma + k\, c_K^n\, s_K^n\Big]} \quad (20)$$

For the discretization of (17), we obtain

$$\boxed{s_K^{n+1} = s_K^n - k\,\Delta t\, c_K^n\, s_K^n} \quad (21)$$

Remark 3.1 *This upwind scheme is known to be too diffusive. We propose in section 4 a simple technics which reduces the numerical diffusion while preserving the maximum principle.*

3.2.2 The diffusion equation

As pointed out earlier, the diffusion is modelled by writing an equation of the form

$$\frac{\partial c}{\partial t} - \operatorname{div}(\mathbf{D}\nabla c) = 0, \quad \text{in} \quad \Omega. \tag{22}$$

$$\tag{23}$$

Here we will employ an implicit mixed-hybrid finite element scheme. Therefore, we introduce a new variable ϕ defined by

$$\phi = -\mathbf{D}.\nabla c. \tag{24}$$

Consequently, we obtain the following system

$$\begin{cases} \phi = -\mathbf{D}\nabla c, & \text{in} \quad \Omega, \\ \dfrac{\partial c}{\partial t} + \operatorname{div}\phi = 0, & \text{in} \quad \Omega. \end{cases} \tag{25}$$

Time integration: Here, we use the Euler implicit time discretization, and so we obtain the following scheme

$$\begin{cases} \phi^{n+1} = -\mathbf{D}\nabla c^{n+1}, & \text{in} \quad \Omega, \\ \dfrac{c^{n+1}-c^n}{\Delta t} + \operatorname{div}\phi^{n+1} = 0, & \text{in} \quad \Omega. \end{cases} \tag{26}$$

The mixed formulation of the semi-discrete problem (26) reads as: Find $\phi^{n+1} \in H(\operatorname{div};\Omega)$, $c^{n+1} \in L^2(\Omega)$ such that for all $(\psi, q) \in H_{0,N}(\operatorname{div};\Omega) \times L^2(\Omega)$, we have

$$\begin{cases} \displaystyle\int_\Omega \mathbf{D}^{-1}\phi^{n+1}.\psi = \int_\Omega c^{n+1}\operatorname{div}\psi - \int_{\Gamma_d} c_d(\psi.\mathbf{n}), \\ \displaystyle\int_\Omega (\frac{c^{n+1}-c^n}{\Delta t})q + \int_\Omega \operatorname{div}\phi^{n+1} q = 0. \end{cases}$$

space integration: Again here, for the spatial discretization, we will employ the mixed hybrid finite element method.
The hybridized mixed formulation reads: Find $(\phi_h^{n+1}, c_h^{n+1}, \mu_h^{n+1}) \in W_h^{u_b,\Gamma_N} \times Q_h \times \Lambda_h^{p_b,\Gamma_D}$, such that for every $(\psi_h, q_h, \lambda_h) \in W_h^{0,\Gamma_N} \times Q_h \times \Lambda_h^{0,\partial\Omega}$

$$\left\{\begin{array}{lcll} a(\phi_h^{n+1},\psi_h)-\displaystyle\sum_{K\in\mathcal{T}_h} b_K(\psi_h,c_h^{n+1})+\sum_{K\in\mathcal{T}_h} d_K(\mu_h^{n+1},\psi_h) & = & 0, & \\ M(\dfrac{c_h^{n+1}-c_h^n}{\Delta t},q_h)+\displaystyle\sum_{K\in\mathcal{T}_h} b_K(\phi_h^{n+1},q_h) & = & f(q_h), & (27)\\ \displaystyle\sum_{K\in\mathcal{T}_h} d_K(\lambda_h,\phi_h^{n+1}) & = & 0. & \end{array}\right.$$

where the operators d_K, a and b_K are the same as in the section (2). The operator M is defined by $M(c_h^{n+1},q_h)=\dfrac{1}{\Delta t}\displaystyle\int_\Omega c_h^{n+1}q_h dx$.
Employing the basis function in (27) as test functions, i.e., $\psi_h=\mathbf{w}_{K,\overline{e}}$ for $(K,\overline{e})\in\mathcal{T}_h\times\varepsilon_h^N$ with $\overline{e}\subset\partial K$, $q_h=\chi_K$ for $K\in\mathcal{T}_h$ and $\lambda_h=\chi_{\overline{e}}$ for $\overline{e}\in\varepsilon_h^I$, we obtain the following system of algebraic equations:

$$\left\{\begin{array}{lcll} a(\phi_K^{n+1},\mathbf{w}_{K,\overline{e}})-c_K^{n+1}+\mu_{\overline{e}}^{n+1} & = & 0, \quad K\in\mathcal{T}_h,\ \overline{e}\subset\partial K, & \\ \dfrac{c_K^{n+1}}{\Delta t}+\displaystyle\sum_{e\in\partial K}\phi_{K,e}^{n+1} & = & \displaystyle\int_K f dx+\frac{c_K^n}{\Delta t}, \quad K\in\mathcal{T}_h, & (28)\\ \phi_{K,\overline{e}}^{n+1}+\phi_{K',\overline{e}}^{n+1} & = & 0, \quad \overline{e}\in\varepsilon_h^I,\ \overline{e}=\partial K\cap\partial K'. & \end{array}\right.$$

Here $\phi_K^{n+1}\in RT_0(K)$ is defined by $\phi_K^{n+1}=\displaystyle\sum_{e\in\partial K}\phi_{K,e}^{n+1}\mathbf{w}_{K,e}$.

3.2.3 The splitting algorithm

One particular splitting for the transport equation, results, at each time step, in the approximation of a hyperbolic-reaction system and a parabolic equation: given $(C^n=C(t^n),\ S^n=S(t^n))\in Q_h\times Q_h\subset L^2(\Omega)\times L^2(\Omega)$, solve the hyperbolic-reaction system

$$\begin{aligned} \frac{\partial\hat{C}}{\partial t}+\operatorname{div}(\hat{C}\ \mathbf{u}) &= -k\ \hat{C}\ \hat{S} \quad \text{on} \quad \Omega\times(t^n,t^{n+1}],\\ \frac{\partial\hat{S}}{\partial t} &= -k\ \hat{C}\ \hat{S} \quad \text{on} \quad \Omega\times(t^n,t^{n+1}]. \end{aligned}$$

The solution generated at this step, $\hat{C}$, is the initial condition for the parabolic equation

$$\left\{\begin{array}{lcl} \dfrac{\partial C^*}{\partial t}+\operatorname{div}\phi^* & = & 0, \quad \text{on} \quad \Omega\times(t^n,t^{n+1}],\\ \phi^* & = & -\mathbf{D}\nabla C^* \quad \text{on} \quad \Omega\times(t^n,t^{n+1}]. \end{array}\right.$$

The solution generated here will approximate $c^{n+1}=c(t^{n+1})$ and $s^{n+1}=s(t^{n+1})$.

4 Modified method of upwinding (M2U)

4.1 Notation and Definitions

Here we define the notation we use throughout this section. Let α be a common edge between any two adjacent elements Q and Q'. Let c_Q^n (resp. $c_{Q'}^n$) the concentration in Q (resp. in Q') at the instant n. (We suppose that c_Q^n and $c_{Q'}^n$ are positives).

We define q_α as: $q_\alpha = \int_\alpha \mathbf{u}.n$ where n denotes the unit outward normal to Q. Define the upwind value c_D^n on an element boundary as follows:

$$c_D^n = \begin{cases} c_Q^n & \text{if} \quad q_\alpha \geq 0 \\ c_{Q'}^n & \text{if} \quad q_\alpha \leq 0 \end{cases}$$

Let $\theta \in [0,1]$ and let c_α^n the value of the concentration on the interface α. We define c_α^n as follows:

$$c_\alpha^n = \theta \frac{(c_Q^n + c_{Q'}^n)}{2} + (1-\theta) c_D^n \tag{29}$$

Let $|Q|$ be the measure of the element Q and let δt be the time step. Then we define β_α by

$$\boxed{\beta_\alpha = \frac{6\ \delta t\ q_\alpha}{|Q|}} \tag{30}$$

We suppose that $|\beta_\alpha| \leq 1$.

Finally, we define $c_{\max}^{Q,n}$ (resp. $c_{\max}^{Q',n}$) as the maximum of the values c_K^n where K go over Q (resp. Q') and its neighbouring.

4.2 Numerical Method

We consider the transport equation of the form

$$\partial_t c + \text{div}\,(c\mathbf{u}) = 0 \quad \text{in} \quad \Omega \times (0,T), \tag{31}$$

with the initial condition

$$c(x,0) = c^0(x) \quad \text{in} \quad \Omega, \tag{32}$$

and appropriate boundary conditions. Here $\mathbf{u}$ is given, and it verifies div $\mathbf{u} = 0$. The discretization of the advection problem will be performed by a cell-centered finite volume method. It is well known that when using constant cell approximations the numerical diffusion due to upwinding is big enough

to keep the scheme stable. However, by using higher order approximation spaces the scheme produces non physical oscillations near shocks. In this chapter, we introduce modified upwinding techniques, namely modified upwind finite volume scheme, in order to have a non-oscillatory shock capturing method for the approximation of hyperbolic conservative laws without adding excessive numerical diffusion and without using more sophisticated and well known flux limiters *cf.*[59]

4.2.1 Discretization

We integrate (31) over each control volume Q between two instants t^n and t^{n+1} and by using the Green's formula we get

$$c_Q^{n+1} = c_Q^n - \sum_{\alpha \subset \partial Q} \frac{\delta t q_\alpha}{|Q|} c_\alpha^n \tag{33}$$

we introduce a new variable $\overline{c}_\alpha^{n+1}$ defined by:

$$\overline{c}_\alpha^{n+1} = c_Q^n - \beta(c_\alpha^n - c_{\max}^{Q,n}), \tag{34}$$

and thanks to the relation $\sum_{\alpha \subset \partial Q} q_\alpha = 0$, we deduce that

$$c_Q^{n+1} = \frac{1}{6} \sum_{\alpha \subset \partial Q} \overline{c}_\alpha^{n+1} \tag{35}$$

We want to impose, for each $\alpha \in \partial Q$,

$$\overline{c}_\alpha^{n+1} \leq c_{\max}^{Q,n}, \tag{36}$$

(the same property can be deduced for c_Q^{n+1}).
For the positivity, we write

$$\tilde{c}_\alpha^{n+1} = c_Q^n - \beta c_\alpha^n \tag{37}$$

and we want to impose $\tilde{c}_\alpha^{n+1} \geq 0$ (the same property can be deduced for c_Q^{n+1}).

Two cases can arise:

First Case : $q_\alpha \geq 0$: In this case $c_D = c_Q$ and $\beta \geq 0$

For the maximum principle, we write

$$\overline{c}_\alpha^{n+1} - c_{\max}^{Q,n} = c_Q^n - c_{\max}^{Q,n} - \beta\Big[\frac{\theta}{2}(c_{Q'}^n - c_{\max}^{Q,n}) + (1 - \frac{\theta}{2})(c_Q^n - c_{\max}^{Q,n})\Big]$$

By using (36), we obtain:

$$\Big(c_Q^n - c_{\max}^{Q,n}\Big)\Big(1-\beta(1-\frac{\theta}{2})\Big) \leq \frac{\beta}{2}\theta\Big(c_{Q'}^n - c_{\max}^{Q,n}\Big)$$

and also

$$0 \leq \frac{\beta}{2}\theta\Big(c_{Q'}^n - c_Q^n\Big) + \Big(1-\beta\Big)\Big(c_{\max}^{Q,n} - c_Q^n\Big)$$

We come to a choice

- if $c_{Q'}^n \geq c_Q^n$, we take $\theta_1^+ = 1$.
- otherwise, we choose $\theta_1^+ = \min\Big(\dfrac{(1-\beta)(c_{\max}^{Q,n} - c_Q^n)}{\dfrac{\beta}{2}(c_Q^n - c_{Q'}^n)}, 1\Big)$

for the positivity, we write

$$\tilde{c}_\alpha^{n+1} = c_Q^n - \beta\Big(\frac{\theta}{2}c_{Q'}^n + (1-\frac{\theta}{2})c_Q^n\Big) \tag{38}$$

Due to the relation $0 \leq \tilde{c}_\alpha^{n+1}$, we will have

$$0 \leq \frac{\beta}{2}\theta(c_Q^n - c_{Q'}^n) + (1-\beta)c_Q^n \tag{39}$$

and again we have to choose:

- if $c_Q^n \geq c_{Q'}^n$, we take θ_2^+ as 1.
- otherwise, we choose $\theta_2^+ = \min\Big(\dfrac{(1-\beta)c_Q^n}{\dfrac{\beta}{2}(c_{Q'}^n - c_Q^n)}, 1\Big)$

This way, the value of θ is given by

$$\boxed{\theta_Q^+ = \min(\theta_1^+, \theta_2^+)} \tag{40}$$

Second Case : $q_\alpha \leq 0$: In this case $c_D = c_{Q'}^n$ et $\beta \leq 0$.

For the maximum principle, we write

$$\overline{c}_\alpha^{n+1} - c_{\max}^{Q,n} = c_Q^n - c_{\max}^{Q,n} - \beta\Big[\frac{\theta}{2}(c_Q^n - c_{\max}^{Q,n}) + (1-\frac{\theta}{2})(c_{Q'}^n - c_{\max}^{Q,n})\Big]$$

By using the relation (36), we obtain

$$(1-\beta\frac{\theta}{2})(c_Q^n - c_{\max}^{Q,n}) \leq \beta(1-\frac{\theta}{2})(c_{Q'}^n - c_{\max}^{Q,n})$$

Rewriting the equation above, we obtain

$$0 \leq \frac{\beta}{2}\theta(c_Q^n - c_{Q'}^n) + \beta(c_{Q'}^n - c_{\max}^{Q,n}) + (c_{\max}^{Q,n} - c_Q^n)$$

we come to a choice

- if $c_{Q'}^n \geq c_Q^n$, we take θ_1^- as 1.
- otherwise, we choose $\theta_1^- = \min\Big(\dfrac{\beta(c_{Q'}^n - c_{\max}^{Q,n}) + (c_{\max}^{Q,n} - c_Q^n)}{\dfrac{\beta}{2}(c_{Q'}^n - c_Q^n)}, 1\Big)$

For the positivity, we write $\tilde{c}_\alpha^{n+1} = c_Q^n - \beta c_\alpha^n$.
From $0 \leq \tilde{c}_\alpha^{n+1}$, we will have

$$0 \leq c_Q^n - \beta\Big(\frac{\theta}{2}c_Q^n + (1-\frac{\theta}{2})c_{Q'}^n\Big)$$

and also

$$0 \leq \frac{\beta}{2}\theta(c_{Q'}^n - c_Q^n) + c_Q^n - \beta c_{Q'}^n$$

and again we have to choose

- if $c_Q^n \geq c_{Q'}^n$, we take $\theta_2^- = 1$.
- otherwise, we choose $\theta_2^- = \min\Big(\dfrac{c_Q^n - \beta c_{Q'}^n}{\dfrac{\beta}{2}(c_Q^n - c_{Q'}^n)}, 1\Big)$

This way, the value of θ is given by

$$\boxed{\theta_Q^- = \min(\theta_1^-, \theta_2^-)} \tag{41}$$

Now, in order to preserve the balance of mass, the flux should be locally conserved.
Analogously, we choose a value of θ see by Q'.
Two cases are considered:

- if $q_\alpha \geq 0$ see by (Q) then $q_\alpha \leq 0$ see by (Q').
  In this case θ is chosen as: $\theta_{fin} = \min(\theta_Q^+, \theta_{Q'}^-)$, with θ_Q^+ is given by (40) and $\theta_{Q'}^-$ is given by (41) by substitute respectively c_Q^n with $c_{Q'}^n$, $c_{Q'}^n$ with c_Q^n, $c_{\max}^{Q,n}$ with $c_{\max}^{Q',n}$ and β with $-\beta$.

- if $q_\alpha \leq 0$ see by (Q) then $q_\alpha \geq 0$ see by (Q').
  In this case θ is chosen as: $\theta_{fin} = \min(\theta_Q^-, \theta_{Q'}^+)$, with θ_Q^- is given by (41) and $\theta_{Q'}^+$ is given by (40) by substitute respectively c_Q^n with $c_{Q'}^n$, $c_{Q'}^n$ with c_Q^n, $c_{\max}^{Q,n}$ with $c_{\max}^{Q',n}$ and β with $-\beta$.

5 Numerical examples

5.1 1D simulation

We consider a one dimensional advection-diffusion-reaction equations:

$$\frac{\partial c}{\partial t} + a\, c_x - \mu\, c_{xx} = -k\, c\, s, \quad \text{in} \quad \Omega, \tag{42}$$

$$\frac{\partial s}{\partial t} = -k\, c\, s, \quad \text{in} \quad \Omega. \tag{43}$$

We proceed using an explicit finite-difference method. The reaction term $(-k\, c\, s)$ will be treated implicitely in order to deal with large k. Let (C_i^n, S_i^n) denote the discrete approximation to the exact solution $(c(x_i, t_n), s(x_i, t_k))$ at the lattice point (x_i, t_n), where $x_i = i\Delta x$ and $t_n = n\Delta t$ are the denote i^{th} spatial and n^{th} time steps, respectively, and Δt and Δx are the time and spatial increments. We take the later to satisfy a stability condition $\Delta t < \frac{\Delta x^2}{\mu}$. The spatial derivatives c_{xx} and c_x are approximated with a second-order centered difference and an upstream first-order difference, respectively. Then, replacing the time partial derivative $(\frac{\partial c}{\partial t})$ and $\frac{\partial s}{\partial t}$ by the Euler explicit scheme. Therefore, we obtain the following discretized system

$$\frac{C_i^{n+1} - C_i^n}{\Delta t} + a\, \frac{C_i^n - C_{i-1}^n}{\Delta x} - \mu\, \frac{C_{i+1}^n - 2C_i^n + C_{i-1}^n}{(\Delta x)^2} = -k\, C_i^{n+1}\, S_i^{n+1},$$

$$\frac{S_i^{n+1} - S_i^n}{\Delta t} = -k\, C_i^{n+1}\, S_i^{n+1}.$$

This results in the quadratic equation (for the unknown C_i^{n+1})

$$A1\ (C_i^{n+1})^2 + A2\ C_i^{n+1} + A3 = 0. \tag{44}$$

where

$$A1 = k\Delta t,$$

$$A2 = 1 - A1\ C_i^n + A1\frac{a\Delta t}{\Delta x}(C_i^n - C_{i-1}^n) - A1\frac{\mu\Delta t}{(\Delta x)^2}(C_{i+1}^n - 2C_i^n + C_{i-1}^n) + A1\ S_i^n,$$

$$A3 = -C_i^n + \frac{a\Delta t}{\Delta x}(C_i^n - C_{i-1}^n) - \frac{\mu\Delta t}{(\Delta x)^2}(C_{i+1}^n - 2C_i^n + C_{i-1}^n)$$

The equation (44) is then solved explicitly to obtain the approximation C_i^{n+1} at the subsequent time step. The the approximation S_i^{n+1} is then given by

$$S_i^{n+1} = \frac{S_i^n}{1 + k\ \Delta t\ C_i^{n+1}}$$

We see here that for all value of k, the scheme that we have proposed is stable.
The Figure 4.6 shows the values of c and s obtained numerically with $k = 10^4$, $\mu = 4\,10^{-3}$ and $a = 0.1$. We notice the presence of propagation front across which s presents a discontinuity. (as shown in chapter 2)

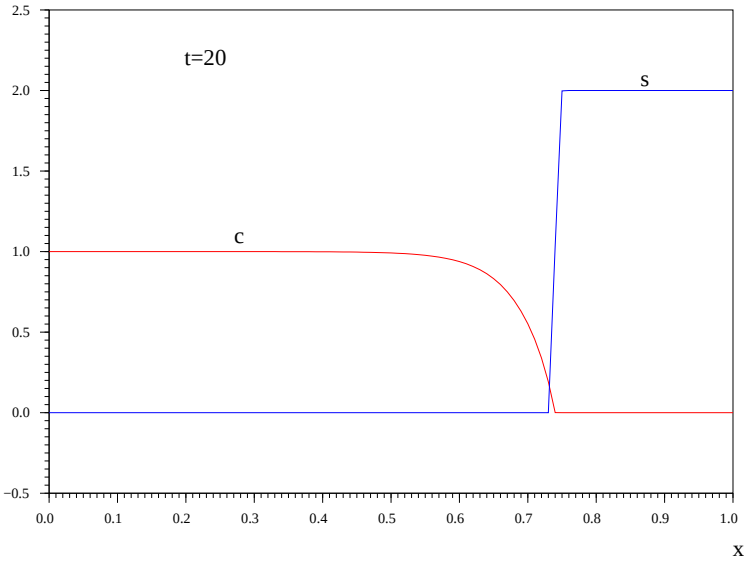

Figure 4.6: Simulation in $1D$ with $\mu = 10^{-3}$ and $k = 10^4$

5.2 2D simulation

We have developped a code (based on A .Marrocco's code (INRIA)) permitting the simulation of the 2D version of the advection-diffusion-reaction equations introduced in section 3. We proceed using a finite volume scheme with inflow and outflow Dirichlet conditions.
One type of result that can be obtained is as follows. we impose a pressure drop between two opposite edges of a unit square. More precisely, the inflow is at the top left while the outflow is at the bottom right.
The figure 4.7 shows the isovalues of c (at left) and s (at right) during the process. The figure 4.8 illustrates the same quantities at the end of filtration process. It is observed that the zones of the filter situated on the right and at the bottom, do not play any role in the filtration process.
In this experiment, the dispersion has not taken into account.

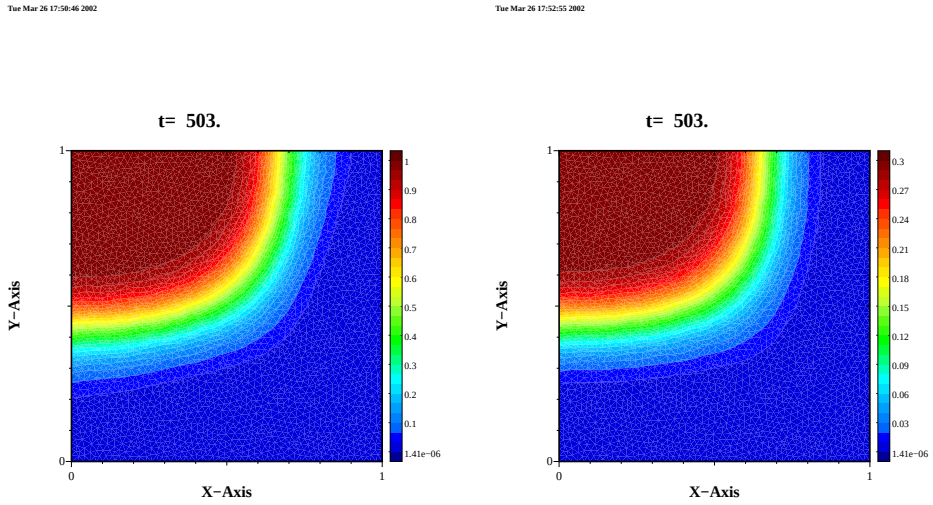

Figure 4.7: Isovalue of c and s during the filtration process

5.3 3D simulation

Here, for the simulation we consider the advection-dispersion-reaction system proposed in the chapter 1 in the section 3.2.2.
First example:
In this experiment, we impose a concentration drop between two opposite faces of a unit cube. This is the $3D$ counterpart of the $1D$ experiment presented in the figure 4.6. Figure 4.9 shows the the concentrations c and s.

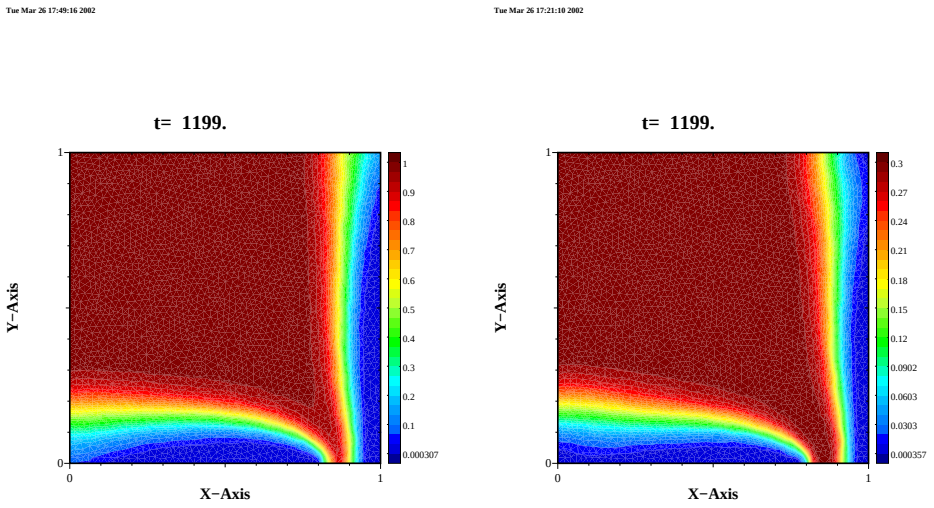

Figure 4.8: Isovalue of c and s at the end of the filtration process

Second example: ***The filter***
In this experiment, we impose an inflow and outflow Dirichlet conditions on the filter. Figure 4.10 shows the the concentrations c and s.

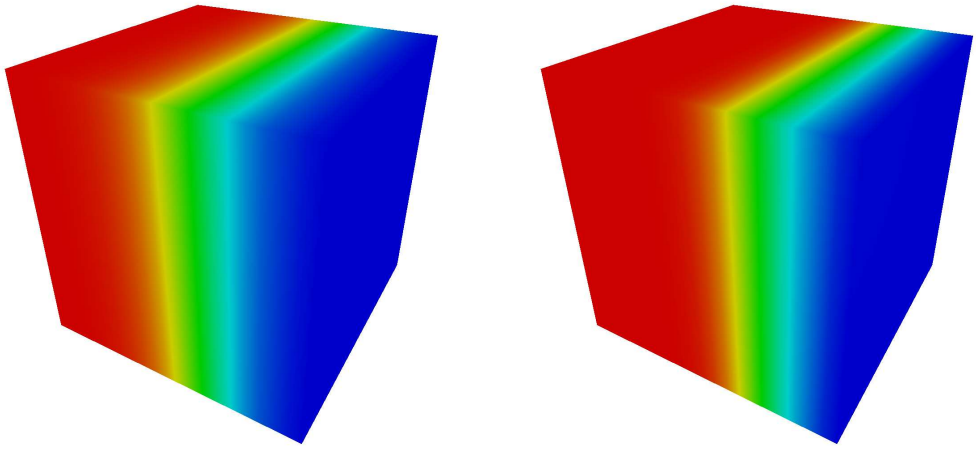

Figure 4.9: c (at left) and s (at right).

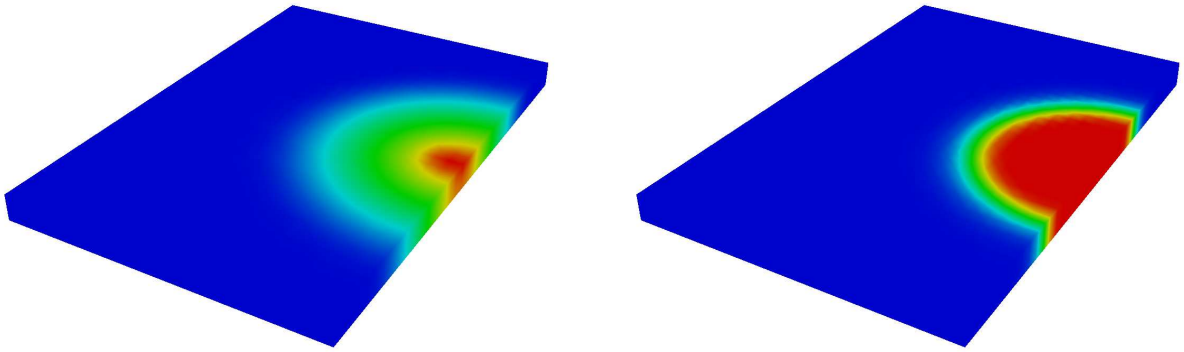

Figure 4.10: c (at left) and s (at right).

Third example:
In this experiment, we impose a concentration drop between two opposite faces of a unit cube. The Figure 4.11 shows that the modified method of upwinding is less diffusive than the method of upwinding.

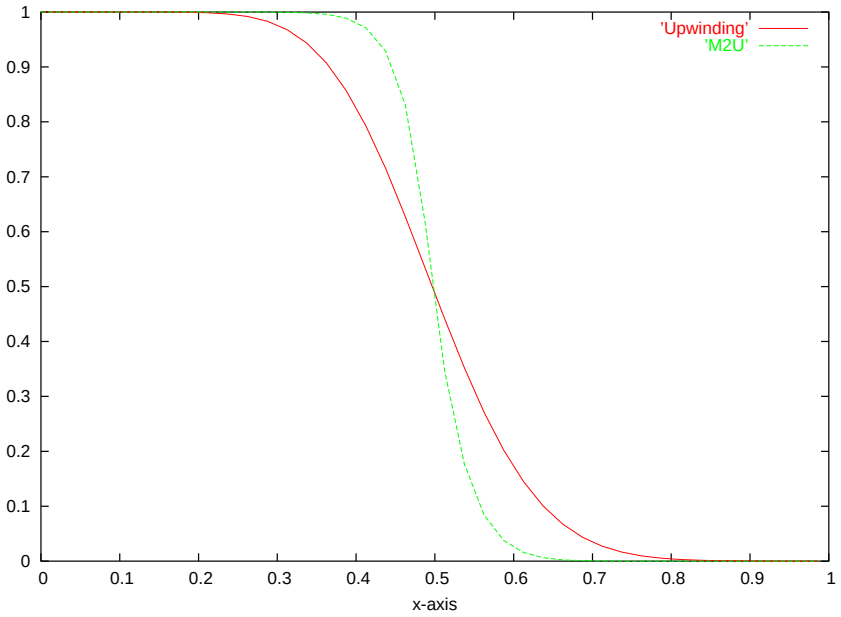

Figure 4.11: A comparison between the method of upwinding and the modified method of upwinding

General bibliography

[1] Y. Achdou and M. Avellaneda. Influence of pore roughness and pore-size dispersion in estimating the permeability of a porous medium from electrical measurements. *Phys. Fluids A.*, 4(12) :2651–2673, 1992.

[2] P. Ackerer, G. Chavent, R. Mosé and P. Siegel. Application of the mixed hybrid finite element approximation in a groundwater flow model : Luxury or necessity ? *Water Resources Research*, 30(11) :3001–3012, 1994.

[3] G. Allaire. Homogenization of the Stokes flow in a connected porous medium, *Asymptotic Analysis*, 2 :203–222, 1989.

[4] G. Allaire. Homogenization of the Navier-Stokes equations in open sets perforated with tiny holes. I. Abstract framework, a volume distribution of holes. *Arch. Rational Mech. Anal.*, 113(3) :209–259, 1990.

[5] G. Allaire. Homogenization of the Navier-Stokes equations in open sets perforated with tiny holes. II. Noncritical sizes of the holes for a volume distribution and a surface distribution of holes. *Arch. Rational Mech. Anal.*, 113(3) :261–298, 1990.

[6] G. Allaire. Continuity of the Darcy's law in the low-volume fraction limit. *Ann. Scuola Norm. Sup. Pisa Cl. Sci. (4)*, 18(4) :475–499, 1991.

[7] G. Allaire. Homogenization of the Navier-Stokes equations with a slip boundary condition. *Comm. Pure Appl. Math.*, 44(6) :605–641, 1991.

[8] G. Allaire. One-Phase Newtonian Flow, *in Homogenization and Porous Media, U. Hornung, ed. , Interdisciplinary Applied Mathematics Series*, Vol. 6, Springer, New York, 1997, pp. 45-68.

[9] T. Arbogast, C. N. Dawson, P. T. Keenan, M. F. Wheeler and I. Yotov. Enhanced cell-centered finite differences for elliptic equations on general geometry. *SIAM J. Sci. Comput.,* 19(2) :404–425, 1998.

[10] T. Arbogast and M. F. Wheeler. A characteristic-mixed finite element method for advection-dominated transport problems. *SIAM J. Numer. Anal.* 32 :404–424, 1995.

[11] D.N. Arnold, F. Brezzi. Mixed and non-conforming finite element methods : implementation, post-processing and error estimates. *M2AN* 19 :7–35, 1985.

[12] B. Bang and D. Lukkassen. Application of homogenization theory related to Stokes flow in porous media. *Appl. Math.*, 44(4) :309–319, 1999.

[13] J. Baranger, J.-F. Maitre and F. Oudin. Connection between finite volume and mixed finite element methods. *RAIRO Math. Mod. Num. Anal.*, 30 :445–465, 1996.

[14] L. Barbe. *Mécanismes d'adhérence des leucocytes aux fibres synthétiques. Application à la filtration du sang.* Thèse, Université Paris VII, 2001.

[15] M. Belhadj. Modelling and simulation of white blood cells filtration. Thesis, University Paris 6 and ENIT, in preparation.

[16] A. Yu. Beliaev and S. M. Kozlov. Darcy equation for random porous media. *Comm. Pure Appl. Math.*, 49(1) :1–34, 1996.

[17] A. Bensoussan, J.-L. Lions, and G. Papanicolaou. *Asymptotic analysis for periodic structures*, volume 5 of *Studies in Mathematics and its Applications*. North-Holland Publishing Co., Amsterdam, 1978.

[18] C.H. Bolster, A.L. Mills, G. M. Hornberger, and J.S. Herman. Effect of surface coatings, grain size, and ionic strength on the maximum attainable coverage of bacteria on sand surfaces. *Journal of Contaminant Hydrology*, 50 :287–305, 2001.

[19] H. Brezis. *Analyse fonctionnelle, Théorie et applications.* Masson, 1983.

[20] F. Brezzi, M. Fortin. Mixed and hybride finite element methods. *Springer series in computational mathematics*, vol. 15, Springer-Verlag, Berlin, Heidelberg, New York, 1991.

[21] M. Briane. *Homogénéisation de matériaux fibrés et multi-couches.* PhD thesis, Université Paris VI, 1990.

[22] M. Briane. Three models of nonperiodic fibrous materials obtained by homogenization. *RAIRO Modél. Math. Anal. Numér.*, 27(6) :759–775, 1993.

[23] M. Briane. Homogenization of a nonperiodic material. *J. Math. Pures Appl. (9)*, 73(1) :47–66, 1994.

[24] A. Bruil, T. Beugeling, J. Feijen, and W. G. van Aken. The mechanisms of leukocyte removal by filtration. *Transfusion Medicine Reviews*, 9(2) :145–166, 1995.

[25] J. Carrillo. *Arch. Rational Mech. Anal.*, 147 :269–361, 1999.

[26] M. A. Celia, T. F. Russell, I. Herrera and R. E. Ewing. An Eulerian-Lagrangian localized adjoint method for the advection-diffusion equation. *Adv. Water Resources.*13 :187–205, 1990.

[27] G.Q. Chen and B. Perthame. Well-posedness for non-isotropic degenerate parabolic-hyperbolic equation. Ann. Inst. H. Poincaré (Anal. non linéaire), to appear.

[28] R. Cimrman and E. Rohan. Modelling heart tissue using a composite muscle model with blood perfusion. *In K.J. Bathe, editor*, Computational Fluid and Solid Mechanics 2003, pp. 1642–1646. Elsevier Science, 2003. Proceedings of the second MIT conference.

[29] D. S. Clague and R. J. Phillips. A numerical calculation of the hydraulic permeability of the three-dimensional disordered fibrous media. *Phys. Fluid*, 9(6) :1562–1572, 1997.

[30] B. Cockburn and C. W. Shu. Tvb runge-kutta local projection discontinuous galerkin finite element method for scalar conservation laws iv : the multidimensional case. *Math. Comp.,* 54 :545–581, 1990.

[31] Cordes and Kinzelbach. Comment on Application of the mixed-hybrid finite approximation in a groundwater flow model : luxury or necessity. *Water Resourc.,* 32(6) :1905–1909, 1996.

[32] H. K. Dahle. Adaptive characteristic operator splitting techniques for convection-dominated diffusion problems in one and two space dimensions. *PhD Thesis, Department of Mathematics, University of Bergen*, 1988.

[33] J. Dausset and F.-T. Rapaport. Transplantation antigen activity of human blood platelets. *Transplantation*, 4(2) :182–193, 1966.

[34] C. N. Dawson. Godunov-mixed methods for advective flow problems in one space dimension. *SIAM J. Num. Anal.,* 28 :1282–1309, 1991.

[35] C. N. Dawson. Godunov-mixed methods for advection-diffusion equations in multidimensions. *SIAM J. Num. Anal.,* 30 :1315–1332, 1993.

[36] C. N. Dawson. High resolution upwind-mixed finite element methods for advection-diffusion equations with variable time-stepping. *Num. Meth. for PDEs,* 11 :525–538, 1995.

[37] C. N. Dawson and V. Aizinger. Upwind-mixed methods for transport equations. *TICAM Report 98-18*, 1998.

[38] L. Demkowitz and J. T. Oden. An adaptive characteristic Petrov-Galerkin finite element method for convection-dominated linear and nonlinear parabolic problems in two space variables. *Comput. Methods Appl. Mech. Eng.* 55 :63–87, 1986.

[39] J. Douglas and T. F. Russell. Numerical methods for convection-dominated diffusion problems based on combining the method of characteristics with finite element or finite difference procedures. *SIAM J. Numer. Anal.* 19 :871–885, 1982.

[40] J. E. Drummond and M. I. Tahir. Laminar viscous flow through regular arrays of parallel solid cylinders. *Intl J. Multiphase Flow*, 10 :515–540, 1984.

[41] S. Dzik. Leukodepletion blood filter : Filter design and mechanism of leukocyte removal. *Transfus. Med. Rev.*, 7(2) :65–77, 1993.

[42] H.I. Ene and E. Sanchez-Palencia. Equations et phénomènes de surface pour l'écoulement dans un modèle de milieu poreux. *J. Mécan.*, 14 :73–108, 1975.

[43] M. S. Espedal and R. E. Ewing. Characteristic Petrov-Galerkin subdomain methods for two phase immiscible flow. *Comput. Methods Appl. Mech. Eng.* 64 :113–135, 1987.

[44] R. Eymard, T. Gallouët and R. Herbin. Finite volume methods, *Handbook of numerical analysis*, vol. VIII, P.-G. Ciarlet and J.-L. Lions editors, Amsterdam, North-Holland, 2000.

[45] R. Eymard, D. Hilhorst, R. van der Hout, and L. A. Peletier. A reaction-diffusion system approximation of a one-phase Stefan problem. *Optimal Control and Partial differential Equations, J.L. Menaldi et al. (Eds.)*, IOS Press, 2001.

[46] R. Eymard, T. Gallouët, R. Herbin, and A. Michel. Convergence of a finite volume scheme for nonlinear degenerate parabolic equations. *Numer. Math.*, 92(1) :41–82, 2002.

[47] K. Fenmori, D. G. Covell, J. E. Fletcher, and J. N. Weinstein. Modeling analysis of the global and microscopic distribution of immunoglobulin G, $F(ab')_2$ and Fab in tumors. *Cancer Research*, 49 :5656–5663, 1989.

[48] A. Fleming. A simple method of removing leucocytes from blood. *Br J Exp Pathol*, 7 :281–286, 1926.

[49] C.K. Ghaddar. On the permeability of unidirectional fibrous media : A parallel computational approach. *Phys. Fluids*, 7(11) : 2563-2587, 1995.

[50] V. Girault and P.-A. Raviart. *Finite element methods for Navier-Stokes equations.* Springer-Verlag, 1986.

[51] T. Greenwalt, M. Gajewski and J. McKenna. A new method for preparing buffy coat-poor blood. *Transfusion*, 2 :221–229, 1962.

[52] J. Happel. Viscous flow relative to arrays of cylinders. *AIChE J.*, 5 :174–177, 1959.

[53] H. Hasimoto. On the periodic fundamental solutions of the Stokes equations and their application to viscous flow past a cubic array of spheres. *J. Fluid Mech.*, 5 :174–177, 1959.

[54] J. J. L. Higdon and G. D. Ford. Permeability of three-dimensional models of fibrous porous media. *J. Fluid Mech.*, 308 :341–361, 1996.

[55] D. Hilhorst, R. van der Hout, and L. A. Peletier. The fast reaction limit for a reaction-diffusion system. *J. Math. Anal. Appl.*, 199(2) :349–373, 1996.

[56] D. Hilhorst, R. van der Hout, and L. A. Peletier. Diffusion in the presence of fast reaction : the case of a general monotone reaction term. *J. Math. Sci. Univ. Tokyo*, 4(3) :469–517, 1997.

[57] D. Hilhorst, R. van der Hout, and L. A. Peletier. Nonlinear diffusion in the presence of fast reaction. *Nonlinear Anal.*, 41(5-6, Ser. A : Theory Meth. Appl.) :803–823, 2000.

[58] C. Hirsch. Numerical computation of internal and external flows. *A Wiley Interscience Publication,* New York, 1990.

[59] H. Hoteit, P. Ackerer, R. Mosé, J. Erhel, and B. Philippe. New two-dimensional slope limiters for discontinuous Galerkin methods on arbitrary meshes. *Rapport de recherche de l'INRIA-Rennes* No 4491, 2002.

[60] I. D. Howells. Drag due to the motion of a Newtonian fluid through a sparse random array of small fixed rigid objects. *J. Fluid Mech.*, 64 :449–475, 1974.

[61] I. D. Howells. Drag on fixed beds of fibres in slow flow. *J. Fluid Mech.*, 355 :163–192, 1998.

[62] P. S. Huyakorn, B. H. Lester and J. W. Mercer. An efficient finite element technique for modeling transport in fractured porous media, 1. single species transport. *Water Resources Research*, 19(3) :841–854, June 1993.

[63] G.W. Jackson and D.F. James. The hydrodynamic resistance of hyaluronic acid and its contribution to tissue permeability. *Biorheology*, 19 :317–330, 1982.

[64] G.W. Jackson and D.F. James. The permeability of fibrous porous media. *The Canadian Journal of Chemical Engineering*, 64 :364–374, 1986.

[65] W. Jäger and A. Mikelić. On the boundary conditions at the contact interface between a porous medium and a free fluid, *Ann. Sc. Norm. Super. Pisa, Cl. Sci.*- Ser. IV, Vol. XXIII (1996), Fasc. 3, p. 403–465.

[66] W. Jäger and A. Mikelić. On the boundary conditions at the contact interface between two porous media, *in Partial differential equations, Theory and numerical solution, eds. W. Jäger, J. Nečas, O. John, K. Najzar, et J. Stará, π Chapman and Hall/CRC Research Notes in Mathematics n^o* 406, 1999. pp. 175–186.

[67] V. V. Jikov, S. M. Kozlov, and O. A. Oleĭnik. *Homogenization of differential operators and integral functionals.* Springer-Verlag, Berlin, 1994.

[68] K. H. Karlsen and N. H. Risebro. On convergence of finite difference schemes for viscous and inviscid conservation laws with rough coefficients. M^2AN, 35(2) :239–270, 2001.

[69] M. Kaviany. Principles of Heat Transfer in Porous Media, 2nd edition, Springer, New York, 1995.

[70] J.A. Kolodziej, R. Dzięcielak, and Z. Kończak. Permeability tensor for heterogeneous porous medium of fibre type. *Transport in Porous Media*, 32 :1–19, 1998.

[71] S. Kozlov. Geometric aspects of homogenization. *Russian Math. Surveys*, 40 :79–120, 1989.

[72] S. Kruzhkov. First order quasilinear equations with several space variables. *Mat. Sbornik*, 123 :228–255, 1970. Engl. Transl. *Math. USSR Sb.* **10** (1970), 217–273.

[73] S. Kuwabara. The force experienced by randomly distributed parallel circular cylinders or spheres in a viscous flow at small Reynolds number. *J. Phys. Soc. Japan*, 14 :527–532, 1959.

[74] O.A. Ladyzenskaja, V.A. Solonnikov, and N.N. Ural'ceva. *Linear and Quasilinear Equations of parabolic type*, volume 23 of *Translations of Mathematical Monographs*. American Mathematical Society, 1968.

[75] R. E. Larson and J. J. L. Higdon. Microscopic flow near the surface of two-dimensional porous media. Part 1. Axial flow. *J. Fluid Mech.*, 166 : 449–472, 1986.

[76] R. E. Larson and J. J. L. Higdon. Microscopic flow near the surface of two-dimensional porous media. Part 2. Transverse flow. *J. Fluid Mech.*, 178 : 119–136, 1987.

[77] J. D. Logan. Transport modeling in hydrogeochemical systems. Springer-Verlag, 2001.

[78] P. Marcati. Weak solutions to a nonlinear partial differential equation of mixed type. *Diff. and Int. Eq.*, 9(4) :827–848, 1996.

[79] E. Marušić- Paloka and A. Mikelić. An error estimate for correctors in the homogenization of the Stokes and Navier-Stokes equations in a porous medium. *Boll. Unione Mat. Ital.*, (7) 10-A, n^o 3, p. 661–671, 1996.

[80] A. Mikelić. Homogenization theory and applications to filtration through porous media. In *Filtration in porous media and industrial application (Cetraro, 1998)*, volume 1734 of *Lecture Notes in Math.*, pages 127–214. Springer, Berlin, 2000.

[81] R. Natalini. Recent results on hyperbolic relaxation problems. In Chapman & Hall/CRC, editor, *Analysis of systems of conservation laws*, pages 128–198. Boca Raton, FL, 1999.

[82] G. Neale, H. Anaka and D. Hampel. Transport phenomena in non-homogeneous porous media. *Can. J. Chem. Eng.*, 53 :691–694, 1975.

[83] R. Pietersz, I. Steneker, H. Reesink. Comparison of five different filters for the removal of leukocytes from red cell concentrates. Vox Sang, 62 :76–81, 1992.

[84] B. Perthame. *Kinetic formulation of conservation laws.* Oxford Univ. Press. to appear.

[85] J. E. Roberts and J.-M. Thomas. *Handbook of numerical analysis*, Vol. II, chapter Mixed and hybrid methods, pages 523–639. North-Holland, 1991.

[86] E. Sanchez-Palencia. Non-homogeneous media and vibrations theory. *Lecture Notes in Physics* 127, Springer-Verlag, Berlin, 1980.

[87] A. S. Sangani and A. Acrivos. Slow flow past periodic arrays of cylinders with application to heat transfer. *Intl J. Multiphase Flow*, 8 :193–206, 1982.

[88] A. S. Sangani and C. Yao. Transport processes in random arrays of cylinders. I. Thermal conduction. *Phys. Fluids*, 31 :2426–2434, 1988.

[89] A. S. Sangani and C. Yao. Transport processes in random arrays of cylinders. II. Viscous flow. *Phys. Fluids*, 31 :2435–2444, 1988.

[90] E. M. Sparrow and A. L. Loeffler. Longitudinal laminar flow between cylinders arranged in a regular array. *AIChE J.*, 5 :325–330, 1959.

[91] L. Spielman and S. L. Goren. Model for predicting pressure drop and filtration efficiency in fibrous media. *Environ. Sci. Technol.*, 2 :279–287, 1968.

[92] I. Steneker, J. Biewenga. Histologic and immunohistochemical studies on the preparation of white cell-poor red cell concentrates : the filtration processes using three different polyester filters. *Transfusion*, 31(1) :40–46, 1991.

[93] N. Sun, N.-Z. Sun, M. Elimelech, and J. N. Ryan. Sensitivity analysis and parameter identifiability for colloid transport in geochemically heterogeneous porous media. *Water resources research*, 37(2) :209–222, 2001.

[94] L. Tartar. Convergence of the homogenization process, appendix in the book [86].

[95] M.E. Taylor. *Partial Differential Equations III. Nonlinear equations.* Springer, 1996.

[96] J.-M. Thomas. Méthodes des éléments finis hybrides duaux pour les problèmes du second ordre. *RAIRO Anal. Numér.*, 10 :51–79, 1976.

[97] K.E. Thompson. Pore-scale modeling of fluid transport in disorded fibrous materials, *Fluid Mech. and Transp. Phenomena*, 48(7), 1369-1389, 2002.

[98] A. E. Tzavaras. On the mathematical theory of fluid dynamic limits to conservation laws. In J. Malek, J. Necas, and M. Rokyta, editors, *Advances in Math. Fluid Mechanics*, pages 192–222. Springer, 2000.

[99] H. Wang, H. K. Dahle, M. S. Espedal, R. E. Ewing, R. C. Sharpley and S. Man. An ELLAM scheme for advection-dispersion equations in two dimensions. *SIAM J. Sci. Comput. (to appear).*

[100] S. Whitaker. Flow in porous media I : A theoretical derivation of Darcy's law. *Transport in Porous Media*, 1(2) : 3-25, 1986.